CHALMERS
UNIVERSITY OF TECHNOLOGY

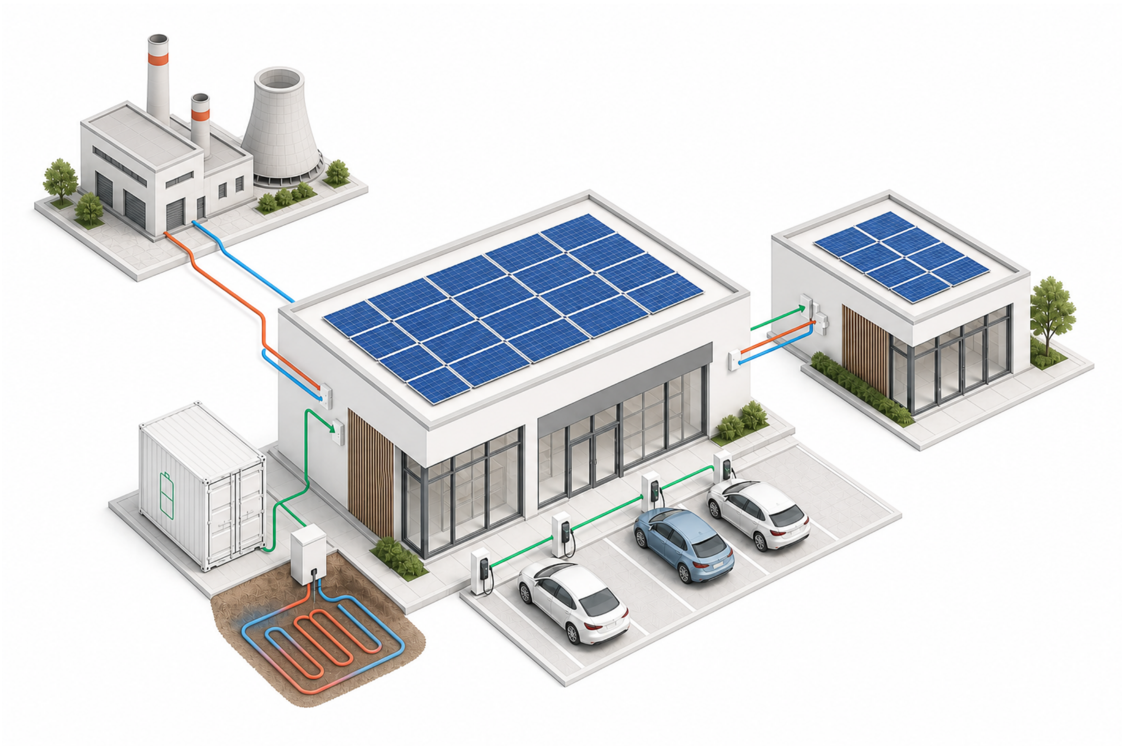

Turning Retail Stores into Energy Assets

A MILP-Based Optimisation of Integrated Flexibility in a Swedish Local Energy Community

Master's thesis in Sustainable Energy Systems

MURILO COSSOVAN MARQUES

DEPARTMENT OF ELECTRICAL ENGINEERING
CHALMERS UNIVERSITY OF TECHNOLOGY
Gothenburg, Sweden 2026
www.chalmers.se

Master's thesis 2026

Turning Retail Stores into Energy Assets

A MILP-Based Optimisation of Integrated Flexibility in a Swedish Local Energy Community

MURILO COSSOVAN MARQUES

CHALMERS
UNIVERSITY OF TECHNOLOGY

Department of Electrical Engineering
Division of Power Grid and Components
Chalmers University of Technology
Gothenburg, Sweden 2026

Turning Retail Stores into Energy Assets
A MILP-Based Optimisation of Integrated Flexibility in a Swedish Local Energy Community
MURILO COSSOVAN MARQUES

Co-Supervisor: Araavind Sridhar, Department of Electrical Engineering
Co-Supervisor: Elena Malakhatka, Chalmers Next Labs AB
Examiner: David Steen, Department of Electrical Engineering

Master's Thesis 2026
Department of Electrical Engineering
Division of Power Grid and Components
Chalmers University of Technology
SE-412 96 Gothenburg
Telephone +46 31 772 1000

Cover: Representation of the proposed system, comprising of the main store connected to the secondary store and the flexibility measures covered in this work. Image generated with AI.

Typeset in LaTeX
Printed by Chalmers Reproservice
Gothenburg, Sweden 2026

Turning Retail Stores into Energy Assets
A MILP-Based Optimisation of Integrated Flexibility in a Swedish Local Energy Community
MURILO COSSOVAN MARQUES
Department of Electrical Engineering
Chalmers University of Technology

Abstract

The decarbonisation of commercial buildings presents one of Europe's most pressing energy transition challenges. Retail stores, operating continuously and consuming energy intensively, occupy a unique position at the intersection of building flexibility, on-site renewable generation, and transport electrification. Realising this potential demands coordinated operational strategies that jointly optimise distributed assets against volatile electricity markets, capacity-based grid tariffs, and the emerging opportunity of energy sharing in local energy communities (LECs). This thesis develops and applies a Mixed-Integer Linear Programming model to evaluate the techno-economic and environmental performance of integrated flexibility solutions at a two-building retail LEC case study site in Sweden. The model optimises the cost-optimal dispatch of solar photovoltaic (PV) generation, battery energy storage systems (BESS), ground-source heat pump (GSHP) thermal supply, and electric vehicle (EV) charging covering direct, smart, and vehicle-to-grid modes, over a three-year simulation period across 34 scenarios of progressive technology integration, evaluated against energy, financial, and environmental key performance indicators. Results identify a cost-efficient PV and BESS configuration at the 500 kWp solar production tax threshold that simultaneously maximises self-consumption. GSHP integration proves to be the most impactful single addition, reducing total energy cost by 14%, avoiding 66.7% of baseline CO_2 emissions, and yielding an net present value of 3.2 MSEK with a payback period of approximately 9.6 years. The full two-building LEC configuration (S-24) extends this through community-level energy sharing, reaching annual savings of 1.25 MSEK. EV charging adds net electricity cost under all modes, though smart and vehicle-to-grid modes limit this significantly compared to uncontrolled direct charging, which reduces annual savings by up to 23%. Sensitivity analysis identifies spot price level and volatility as the dominant drivers of economic performance, followed by GSHP coefficient of performance. This work addresses a clear gap in the existing literature by providing the first techno-economic optimisation of a retail LEC under Swedish market conditions with simultaneous integration of PV, BESS, GSHP, and three modes of EV flexibility. A two-horizon investment strategy is proposed: immediate deployment of PV, BESS, and GSHP at single-store scale, with full LEC formalisation deferred pending regulatory clarification of energy-sharing arrangements.

Keywords: local energy community, mixed-integer linear programming, energy flexibility, battery energy storage system, vehicle-to-grid, solar photovoltaic, ground-source heat pump, retail stores

Acknowledgements

Studying at Chalmers has been a journey, one that led through straight-forward trails and up steep cliffs, through open meadows and into fog. A journey that taught me, above all, that the more one learns, the less one knows. And a journey that shaped me, quietly and persistently, into the person I am today.

This thesis marks the end of that trail, but it was never walked alone. It would not have been possible without my family, whose roots kept me grounded across the distance; the friends I left behind, who reminded me of where I came from; and the friends I met along the way, who reminded me of where I was going.

To Annika, my partner and my anchor. Thank you for your unconditional support, your patience, and your willingness to listen to more about energy systems than anyone outside this field should ever have to endure. I love you dearly.

To Hailan and Juan, those two constants on an otherwise unpredictable trail. You made the hardest, coldest, and darkest stretches feel like a walk through the park. I could not have asked for better companions.

Finally, to Araavind and Elena, thank you for your guidance through the steep final climb. Your support made all the difference when the summit felt furthest away.

Murilo Cossovan Marques, Gothenburg, June 2026

Acknowledgement of AI Use

Generative AI tools, including Claude (Anthropic), were used in the preparation of this thesis in a supporting capacity. Specifically, these tools assisted with grammar and syntax checking of written content, the generation and formatting of figures graphic assets for the system boundary diagram) and tables, and debugging of Python code, including syntax corrections and performance improvements. All technical content, analysis, interpretation of results, and conclusions are the sole work of the author. AI-generated suggestions were reviewed critically and adapted as appropriate throughout the writing and development process. The author bears responsibility of all the contents within this report.

Confidentiality Notice

This thesis was conducted in collaboration with an industrial partner. To preserve the confidentiality of commercially sensitive information, the following data have been anonymised or withheld throughout this report:

- The identity of the distribution system operator (DSO) and any references that would allow its identification.
- Site-specific operational parameters, including contracted electricity and district heating capacity subscriptions.
- Metered electricity and district heating consumption data, which have been scaled by an undisclosed constant multiplier prior to presentation. all relative patterns, seasonal variation, and ratios between buildings are preserved.
- The geographical location of the case study site.
- Baseline scenario results.

All withheld values are marked with an asterisk (*) in the relevant tables. Findings, trends, and conclusions are not affected by these measures.

Contents

List of Acronyms

Below is the list of acronyms that have been used throughout this thesis listed in alphabetical order:

BESS	Battery Energy Storage System
CAPEX	Capital Expenditure
COP	Coefficient of Performance
CP	Charging Point
DC	Direct Charging
DH	District Heating
DoD	Depth-of-Discharge
DSM	Demand-Side Management
DSO	Distribution System Operator
EV	Electric Vehicle
GSHP	Ground Source Heat Pump
HVAC	Heating, Ventilation and Air Conditioning
KPI	Key Performance Indicator
LDC	Load Duration Curve
LEC	Local Energy Community
MILP	Mixed-Integer Linear Programming
NPV	Net Present Value
O&M	Operation and Maintenance
PBP	Payback Period
PV	Photovoltaic
PVGIS	Photovoltaic Geographical Information System
SC	Self Consumption
SEK	Swedish Crown
SoC	State-of-Charge
SS	Self Sufficiency
TES	Thermal Energy Storage
UTC	Coordinated Universal Time
VAT	Value Added Tax
V1G	Smart Charging
V2G	Vehicle-to-Grid

List of Figures

List of Tables

1
Introduction

The decarbonisation of commercial buildings has emerged as a central challenge in Europe's energy transition. Retail stores, operating continuously, consuming energy intensively, and increasingly equipped with solar photovoltaic (PV) generation, battery energy storage systems (BESS), and electric vehicle (EV) charging infrastructure, are uniquely positioned at the intersection of building flexibility, distributed generation, and transport electrification. Yet realising this potential requires more than installing individual technologies: it demands integrated operational strategies that coordinate these assets against volatile electricity markets, rising capacity tariffs, and the emerging opportunity of energy sharing between neighbouring buildings. This thesis investigates exactly that challenge, through the lens of a real retail case study in Sweden.

1.1 Context & Background

The services sector accounts for a substantial and growing share of final electricity consumption in Sweden, as illustrated in Figure 1.1, with retail representing one of its most energy-intensive subsectors.

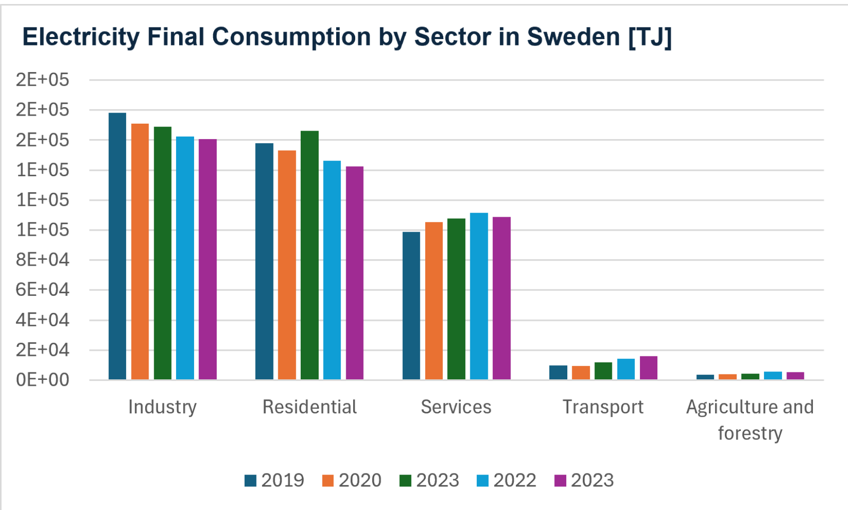

Figure 1.1: Final electricity consumption in Sweden by sector, 2019–2023 [1].

Retail stores are among the most energy-intensive segments of the commercial building stock, with European food retail typically consuming 330–430 $\mathrm{kWh/m^2/yr}$ and non-food retail 130–180 $\mathrm{kWh/m^2/yr}$ [2]. Their high energy demand is driven by a few dominant end uses: in food retail, refrigeration accounts for approximately 40% of total electricity consumption, with lighting contributing 12–20% and heating, ventilation and air conditioning (HVAC) making up the remainder. In non-food retail, HVAC and lighting dominate at roughly 50% and 30% respectively [2].

This flexibility potential in commercial buildings has received growing attention as electricity systems become more variable with the expansion of renewable generation. Energy flexibility in buildings is commonly defined as their capability to adjust electricity demand and on-site generation over time in response to external signals (such as prices or grid constraints) mainly by shifting loads, shaving peaks, and better aligning local renewable production and consumption without interfering with the activity of occupants [3, 4]. In commercial and retail buildings, this flexibility is typically provided by controllable end-uses such as HVAC systems, refrigerated display cases, and on-site thermal or electrical storage [5, 6]. This role of buildings as flexible resources is increasingly reflected in European policy through the revision of the Energy Performance of Buildings Directive and the Smart Readiness Indicator, which emphasise demand-side flexibility, smart controls, and storage in non-residential buildings [7].

Beyond operational measures, stationary battery energy storage systems (BESS) are increasingly deployed behind the meter in commercial and retail buildings to reduce contracted peak demand charges, perform electricity price arbitrage, and increase on-site PV self-consumption (SC) [8, 9]. Techno-economic analyses for Northern Europe demonstrate that when BESS dispatch is optimally scheduled within an energy management system (EMS), storage can substantially enhance building energy flexibility and deliver noticeable reductions in electricity costs under capacity-based tariffs. Simulations of a Swedish commercial facility, for instance, showed that a Li-ion BESS reduced annual demand charges by approximately 40%, saving ~47 kSEK/year relative to the baseline, with peak shaving delivering roughly five times more savings than increased SC [9]. Similarly, for Belgian low-voltage enterprises, modelled peak reductions ranged from 6–27% with a moderately sized battery up to 20–44% with a larger system, with several users exceeding the economic profitability threshold under current capacity tariffs [10]. More broadly, EMS-optimized battery dispatch has been shown to reduce daily average peak demand by 18–38% depending on the tariff structure, a significant lever given that peak demand charges can represent up to 30% of total electricity costs despite being applicable to less than 1% of total operational hours [11]. Nevertheless, high upfront capital expenditure, complex tariff and tax structures, and battery degradation make the business case highly sensitive to system sizing and operational strategy, underscoring the need for careful techno-economic design in retail building BESS deployments [9–11].

A complementary source of flexibility comes from the electrification of transport. vehicle-to-grid (V2G) refers to bidirectional charging in which EVs can both draw power from and supply power back to buildings or the grid, so that their batteries function as controllable, mobile storage providing demand-response and other grid services [12]. Most operational V2G projects to date are concentrated in fleet depots and residential or office buildings, where vehicles are parked for long periods and can be aggregated as a flexible resource [12–14]. Shopping centres and retail parking lots have been highlighted as attractive locations for public charging and potential future V2G services, yet current studies still focus far more on fleets and residential contexts, making large retail car parks a particularly promising but underexplored setting for EV based flexibility [13, 15].

The flexibility technologies discussed above are not limited to single-building applications. When multiple buildings, prosumers, and distributed energy resources in geographical proximity coordinate their production, consumption, and storage, they form a local energy community (LEC). Broadly speaking, an LEC is a collective of households, businesses, or public authorities that jointly produce, share, store, and manage energy, primarily from renewable sources, with the goal of delivering environmental, economic, and social benefits to members [16, 17]. The European Parliament's Clean Energy for All Europeans Package introduced two legal frameworks for such entities: Renewable Energy Communities under the revised Renewable Energy Directive [18], which focus on renewable energy and require proximity to the community's assets; and Citizen Energy Communities under the Internal Electricity Market Directive [19], limited to the electricity sector without geographic restrictions [16, 20]. From a technical standpoint, LECs benefit from the complementarity of members' load profiles: the non-simultaneity of energy needs across different building types increases the capacity factor of shared assets and reduces peak grid consumption, with empirical evidence suggesting cost reductions of up to 26% compared to business-as-usual and up to 46% relative to individual prosumers acting alone [20, 21]. In Sweden, electricity sharing between neighbouring properties was formally authorised from January 2022 onwards [20, 22], yet the academic literature remains heavily focused on residential contexts, with large commercial prosumers receiving little attention as potential anchors for LEC formation [22, 23].

The extent to which a retail operator can capture value from flexibility through BESS, V2G, and demand-side management[1] (DSM) depends critically on the structure of the local electricity market. Sweden is part of the Nord Pool power exchange, where day-ahead electricity prices are calculated for four bidding zones (SE1–SE4) to account for regional transmission constraints between northern production and southern consumption [24]. Prices vary sharply across zones and over time, with the SE3 zone (where this study's case study is located) exposed to both low-price periods during high renewable generation and significant price spikes [25]. The Single Day-Ahead Coupling adopted 15-minute resolution for official prices by late September 2025, enabling finer-grained price signals that better reward demand-side flexibility [26]. Retail customers can choose hourly or variable contracts that pass through Nord Pool's zonal day-ahead spot prices plus a small supplier margin, directly incentivising demand-side flexibility [27]. This market exposure was expected to be reinforced structurally from 1 January 2027 through the planned introduction of mandatory

[1]Demand-side management refers to strategies that encourage electricity consumers to adjust their consumption in response to market price signals. For example, reducing or shifting loads away from peak-price periods and increasing consumption when prices are low.

power tariffs, although the timing and final design remain uncertain [28]. Taken together, these features make Sweden a relevant context for investigating how retail stores can leverage local generation, BESS, and V2G to reduce both emissions and operational energy costs.

1.2 Aim and Objectives

This thesis aims to evaluate the techno-economic and environmental performance of integrated energy flexibility solutions; comprising solar PV, BESS, ground-source heat pumps (GSHP), and EV charging, within a two-building LEC at a retail case study site in Sweden, using a cost-optimal mixed-integer linear programming (MILP) model.

The research pursues five progressive objectives:

1. Establish an empirical baseline by processing metered electrical and thermal load data for both buildings and validating a cost-reconciliation model against historical energy bills for 2023–2025.
2. Develop a MILP-based energy management model of increasing complexity across three nested system levels: building-internal resources (S1: solar PV, BESS, and GSHP at the main store), mobile flexibility (S2: EV charging with direct, smart, and V2G-capable modes), and shared community operation (S3: two-building LEC with pooled generation, storage, and EV flexibility), optimising joint dispatch against the full Swedish electricity cost stack on a 24-hour rolling horizon.
3. Assess the incremental techno-economic value of each technology layer (from solar-only to full LEC operation with V2G), evaluated across economic, self-sufficiency (SS), and environmental performance metrics.
4. Quantify the effect of LEC formation on collective grid costs and peak demand by comparing isolated single-building operation against coordinated community-level dispatch of generation, storage, and EV flexibility across participating buildings.
5. Evaluate the economic and environmental trade-offs of replacing the existing district heating (DH) supply with a GSHP, including sensitivity analysis across electricity tariffs, spot price level and volatility, and GSHP coefficient of performance (COP).

1.3 Research Gap

The literature on LECs and building-level energy optimization is predominantly anchored in residential settings. Of the 30 studies reviewed, 7 address exclusively residential contexts, and while 18 include commercial buildings in some form, only 7 treat commercial settings as the primary focus, with none of these specifically addressing large-format retail environments. Studies that do include commercial buildings typically do so as one member type within a broader mixed-use community alongside households. The distinct load profile of large retail stores (dominated by refrigeration, HVAC systems, and parking lot EV infrastructure) is therefore absent from the existing literature, representing a clear domain-specific gap.

While solar PV is the most ubiquitous resource in the reviewed literature, appearing in 26 of 30 studies, BESS and V2G receive far less attention, featured in 15 and 3 studies respectively. Only two works simultaneously consider the full PV—BESS–V2G combination [29, 30], and the V2G studies that touch on commercial settings apply it within mixed residential–commercial communities rather than retail-specific contexts [29, 31]. Several studies evaluate smart charging (V1G) or demand response as proxies for flexibility [30, 32, 33], but these fall short of the bidirectional grid interaction that V2G enables. The joint integration of stationary storage and vehicle-based flexibility within a cost-optimization framework for commercial energy systems therefore remains largely unexplored.

From a methodological standpoint, 12 of the 30 reviewed studies rely solely on simulation approaches, including dynamic building energy simulation (DBES), quasi-static time-series simulation (QSTS), and rule-based dispatch models (RB) [32, 34–43], without a formal optimization component. While the 18 optimization-based studies employ methods ranging from linear programming (LP) and MILP to mixed-integer non-linear programming (MINLP) and evolutionary algorithms, only one combines optimization with a detailed simulation model [44], limiting the cross-validation of results.

Geographically, 19 of the 30 studies are situated in Southern Europe (Italy, Spain, Portugal), regions characterized by high solar irradiance and specific regulatory frameworks. The Nordic context, with its low-carbon electricity mix, spot-price exposure, and demand-shaping incentives, is represented by only five studies [29, 39, 44–46], none of which address retail settings.

Table 1.1 summarizes the reviewed literature across these dimensions discussed above, highlighting the collective absence of studies that simultaneously target a commercial retail setting, integrate PV, BESS, and V2G within a formal optimisation framework, and operate under Nordic electricity market conditions, which is what this work aims to cover.

While the gaps identified above concern the electrical flexibility and LEC dimensions of retail energy systems, the thermal supply side remains similarly unaddressed in the reviewed literature. Although one study [47] in the review examines geothermal heat supply in a commercial context, it does so through simulation rather than optimisation, and none of the optimisation-based studies incorporate thermal supply switching as a decision dimension. No study therefore evaluates the replacement of DH with a GSHP within a formal cost-optimisation framework for a retail setting. This thesis addresses the GSHP question as a complementary and parallel investigation, modelled as a building-internal asset at the main store, independent of the shared LEC dispatch.

Table 1.1: Coverage of core research dimensions across reviewed LEC studies.

Reference	Year	Location	Resources					Energy Carriers			Setting			Method		Decision Variables					Objectives
			Solar PV	BESS	V2G	Geothermal	Other	Electricity	Heat	Other	Residential	Commercial	Industrial	Optimization	Simulation	Generation	Consumption	Storage	Demand Shifting	Arbitrage	
[34]	2015	IT					x	x	x		x	x			DBES						Evaluate primary energy savings, avoided carbon emissions and PBP of using MCHP vs baseline
[48]	2017	CH	x				x	x	x		x			MILP		x				x	Minimize annualized life-cycle costs and life-cycle GHG emissions
[49]	2017	IT	x	x			x	x					x	BILP					x		Minimize net exported energy
[35]	2018	ES					x	x	x		x	x	x		DBES						Quantify energy, environmental and economic benefits of a MCHP compared to baseline
[32]	2020	IT	x				x	x			x				RB						Demonstrate that combining smart metering with V1G increases SC and economic benefits
[50]	2021	FR	x					x			x	x	x	NLP		x					Minimize total energy exchanged with grid; minimize standard deviation of ramp rates; maximize NPV over 30 years
[36]	2021	IT	x				x	x				x			DBES						Quantify the energy-sharing benefit of a LEC vs individual buildings
[47]	2021	IT				x	x	x	x			x			QSTS						Quantify primary energy consumption and carbon emissions avoided of grid based system vs geothermal system
[51]	2021	PT	x					x			x		x	LP		x					Minimize total system cost
[37]	2022	IT	x					x	x		x	x			QSTS						Benchmark SC, carbon emissions and OPEX among regulatory scenarios
[33]	2022	IT	x	x			x	x			x	x		LP/MILP		x	x	x		x	Minimize total energy costs; maximize minimum relative profit increase
[52]	2022	IT	x	x			x	x	x		x	x		MIQP/MILP			x	x	x	x	MIQP: minimize total cost and GHG emissions; MILP: minimize electricity cost from the grid
[38]	2022	AT	x					x			x				RB						Assess economic viability and allocation mechanisms of REC; validates a simple estimation tool
[39]	2022	SE	x					x							ABM						Evaluate energy and economic performance across four PV scenarios, under present and future climate conditions
[40]	2022	IT	x	x				x				x			DBES						Assess SC, grid imports, carbon emissions and NPV over 21 pre-defined scenarios
[42]	2023	IT	x					x				x	x		QSTS						Evaluate SC, SS, energy savings, carbon emissions and costs among system configurations
[53]	2023	CH	x	x			x	x	x		x	x	x	MILP		x		x			Minimize total cost and carbon emissions
[41]	2023	ES	x	x				x			x	x	x		QSTS						Maximize SS and SC through scenario comparison
[31]	2023	PT	x		x		x	x				x		MILP			x	x	x	x	Minimize total aggregator energy balance cost
[29]	2024	DK	x	x	x			x			x	x		LP				x		x	Minimize total net electricity cost
[45]	2025	NO	x	x			x	x	x		x		x	MINLP				x	x	x	Minimize total annualized cost
[43]	2025	IE	x					x			x				RB						Quantify economic outcomes of SC vs LEC
[54]	2025	IR		x			x	x				x		R-MIQP		x	x	x	x	x	Minimize total daily energy procurement costs
[30]	2025	IT	x	x	x		x	x			x	x		MILP			x	x	x	x	Minimize total energy costs
[55]	2025	PT	x	x				x			x			MILP				x		x	Minimize total electricity cost and grid dependency
[44]	2026	SE	x	x				x	x		x	x		MILP	UBEM	x		x		x	Minimize total lifecycle costs and total lifecycle carbon emissions
[46]	2026	SE	x	x				x			x	x		MILP				x		x	Minimize daily total cost of the LEC
[56]	2026	IT	x					x	x		x			LP			x		x		Minimize electricity cost, thermal discomfort and maximize shared electricity incentive
[57]	2026	IT	x	x			x	x	x	x	x	x		MILP		x	x	x	x		Minimize annual cost; minimize annual primary energy use; minimize annual carbon emissions
[58]	2026	IT	x	x				x				x		NSGA-II		x		x			Maximize NPV and SC; maximize community NPV and shared energy
This Work	2026	SE	x	x	x	x		x	x			x		MILP		x	x	x			Minimize system electricity and heat costs; find optimal investment combination

Note: "Other resources" includes CHP units, TES, heat pumps, biomass boilers, and hydrogen systems. "Other energy carriers" refers to hydrogen [57] and thermal energy in trigeneration or district heating systems [34, 35, 47].The last row summarizes the focus of this study, compared with previous literature. ISO country codes are disclosed in Appendix C.

1.3.1 Research Questions

This thesis addresses a central challenge facing modern retail environments:

'How can the integration of renewable energy and energy flexibility measures be optimally designed and economically justified to reduce operational energy costs within a retail local energy community setting?'

To answer this overarching question, the research unfolds through three interconnected investigations:

1. To what extent does integrating a stationary BESS with on-site solar PV and EV charging flexibility (across direct charging - DC, V1G and V2G modes) deliver economic and operational benefits at the main store, and how are these benefits influenced by participation in a local energy community with the neighbouring secondary store?
2. To what extent do the installed flexibility measures enhance energy self-sufficiency and reduce grid imports across the two-building community?
3. Is replacing the existing DH supply with a GSHP economically attractive when evaluated against total energy costs and avoided carbon emissions, under the Swedish electricity market and DH tariff conditions of the case study site?

1.4 Scope & Limitations

This section defines the boundaries and simplifications underlying the optimisation model and analysis. The system boundaries establish which technologies and resources are included in the study, while the key simplifications outline deliberate methodological choices that maintain analytical tractability while ensuring practical relevance to the case study context.

1.4.1 System Boundaries

The model encompasses three nested levels of increasing technical complexity (Figure 1.2):

- **S1 – Building internal resources**: On-site solar PV, BESS, and GSHP heat supply, implemented only at the main store.
- **S2 - Mobile flexibility**: EV charging featuring DC, V1G and V2G capable charging with power exchange and dynamic session management.
- **S3 - Shared community resources**: A two-building LEC where solar generation, BESS, and EV flexibility are pooled to reduce collective grid imports and associated tariff penalties.

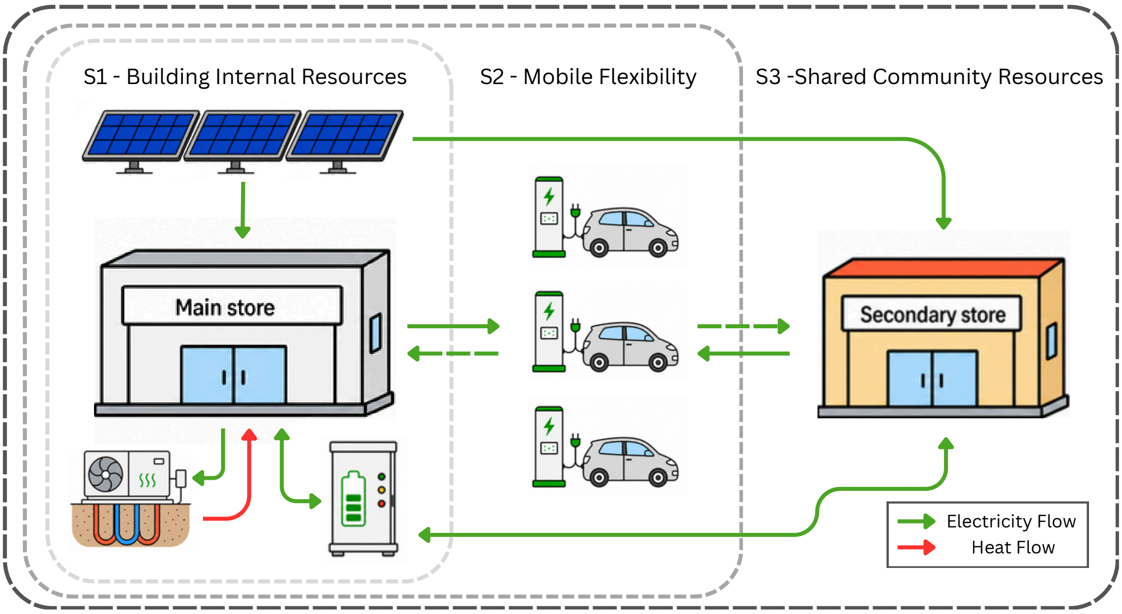

Figure 1.2: System boundary structure and energy flows across the three nested levels.

The LEC is formed by the main retail store together with a neighbouring secondary store located on the same site. The two buildings differ in size, load profile, and asset configuration: flexibility resources comprising solar PV, BESS, and EV charging are installed at the main store, while the secondary store participates as a load-only member contributing its demand profile to the shared community balance. Electricity can be exchanged between the two buildings behind the shared grid connection point, reducing collective peak imports and the associated capacity tariff charges. Full details of both buildings, including their metered load profiles and operational characteristics are presented in Section 3.2.

The analysis is limited to these predefined technologies and resources. Other emerging technologies (e.g. thermal storage, advanced demand-side flexibility, power-to-gas) are excluded.

1.4.2 Key Simplifications

The model operates under the following principal simplifications relative to real-world conditions:

1. **Rolling Horizon Optimisation**: The model operates on a 24-hour rolling horizon with 36-hour foresight, re-optimised daily. This bounds achievable savings to an upper-limit estimate relative to real-time implementations with shorter look-ahead, see Appendix A.1.2.
2. **Aggregated Demand**: Electrical and thermal loads are aggregated to building level from meter data. Component-level control (e.g., individual HVAC zones, refrigeration circuits) and advanced demand-side management are not modelled.
3. **Lossless Community Power Distribution**: Electrical losses within the LEC are neglected, conservatively overstating the economic value of inter-building power exchange (Appendix A.1.2).
4. **GSHP Representation**: GSHP output is modelled using a Carnot-based COP with a linear heating curve. This approximation is not validated against measured performance data. Thermal demand is treated as a hard constraint at every time-step. See Appendix A.1.1 and Appendix A.4.3.
5. **Electricity-Side Emissions Exclusion**: Electricity-related CO_2 emissions are excluded from the environmental assessment. The case study subject holds offset mechanisms that effectively achieve carbon neutrality on the electricity side, so emissions avoidance is quantified solely on the basis of displaced district heating consumption.
6. **EV Fleet Characterisation**: EV sessions are treated as deterministic and known in advance, derived from a synthetic data generator constrained to store operating hours. Stochastic driver behaviour and vehicle heterogeneity are not captured. See Appendix A.1.3 and Appendix A.4.4 for operating hours and session generation details.
7. **Battery and Equipment Dynamics**: All asset performance parameters are held constant over 2023–2025. Battery degradation is represented through a minimum state-of-charge (SoC) floor (20%) and a linear cycling cost. Calendar ageing, temperature effects, and non-linear wear are not modelled. See Appendix A.1.1.
8. **Linear Cost Structure**: Most tariff components are linear functions of power or energy, with two explicitly modelled exceptions: a step-function solar production tax and two-tier DH pricing. See Appendix A.1.2 for full details and implications.
9. **Grid Boundary Conditions**: Upstream grid constraints (transmission/distribution capacity, voltage stability, frequency support) are not modelled.

1.4.3 Data Scope and Constraints

Historical weather data (2023–2025) from measured records and reanalysis are used to represent climatic conditions. Long-term climate variability beyond this period is not captured. Solar generation data, obtained from the Photovoltaic Geographical Information System (PVGIS) [59] is available up to 2023, therefore, 2023 data are looped for subsequent years in the simulation. Electricity and heat demand profiles are based on metered data. EV charging sessions are synthetically generated.

Electricity market prices (NordPool SE3 spot prices), regulatory parameters (solar tax threshold: 500 kWp, transmission rates, distribution system operator - DSO charges), and tariff structures are assumed static over the simulation horizon.

1.4.4 Geographical Scope

Results are specific to the case study locations in Sweden, reflecting Swedish climatic conditions and the structure of the electricity market (SE3 bidding zone). Findings are not directly transferable to other regions without methodological adaptation. Legal, governance, and organisational barriers to LEC formation are not addressed.

2 Theoretical Framework

This chapter establishes the conceptual foundations needed to follow the modelling approach and scenario design presented in Chapter 3, as well as the results presented in Chapter 4. Rather than providing a broad technology review, it introduces only the ideas and definitions directly invoked by the optimisation framework: the mechanisms by which energy flexibility arises in retail buildings and its economic value under Swedish market conditions, the role of each modelled asset in delivering that flexibility, and the MILP formulation used to capture these interactions within a cost-minimisation objective. The chapter closes with a brief description of the techno-economic indicators used to compare scenarios.

2.1 Energy Flexibility in Retail Buildings

Energy flexibility in buildings is commonly understood as the capability to adjust electricity demand and on-site generation over time in response to external signals (prices or grid constraints), mainly by shifting loads, shaving peaks, and better aligning local renewable production with consumption while maintaining core services and comfort [60]. As discussed in Section 1.1, commercial and retail buildings offer significant flexibility potential because their electricity use is dominated by a small number of controllable end-uses (HVAC, refrigeration, and lighting) operating on relatively stable daily and weekly schedules [2]. In food retail, refrigeration alone typically accounts for around 40% of total electricity consumption, with lighting contributing 12–20% and HVAC making up the remainder; in non-food retail, HVAC and lighting dominate at roughly 50% and 30% respectively, with negligible refrigeration loads [2].

In the Swedish context, the economic value of flexibility is shaped by two factors: volatile zonal day-ahead spot prices on Nord Pool, and an increasingly capacity-based grid cost structure at the distribution level. Capacity-based tariffs, already applied by many Swedish DSOs to commercial customers and subject to a regulatory mandate towards universal adoption, charge for the annual peak import of each building rather than total energy alone [28]. Operational strategies that suppress short-duration power peaks and shift demand away from high-price periods can therefore substantially reduce total electricity costs, even without changing annual energy consumption. This link between building flexibility and tariff structure provides the conceptual foundation for including all four modelled assets: BESS, EV charging, GSHP, and LEC energy sharing in the optimisation framework described in Section 3.1.

2.2 Flexibility Resources

2.2.1 On-Site Generation and Storage

The main source of renewable electricity in the system is solar PV installed on-site. PV generation is modelled as a non-dispatchable, exogenous time series at 15-minute resolution. Historical PV production data are derived from PVGIS based on the site's geographical location and system configuration, then scaled to the installed capacity for each scenario (see Appendix A.2.2). Within the optimisation, PV power is either self-consumed within the LEC or exported to the grid, subject to the Swedish solar production tax applied above the 500 kWp threshold (see Appendix A.2.3).

Stationary BESS serve as the primary internal electrical flexibility resource for the system. This system is characterised by its usable energy capacity, rated charge/discharge power, round-trip efficiency, and a SoC that is tracked at each time-step and constrained between a minimum floor, imposed to protect battery longevity, and the full usable capacity. Complementarity constraints prevent simultaneous charging and discharging, and a linear cycling cost term approximates degradation-related wear. Within this representation, the BESS can be exploited for both intra-day price arbitrage and peak import reduction to mitigate capacity-based grid charges (see Section 3.1.7.2 and Appendix A.4 for the full modelling and formulation).

On the thermal side, the main flexible asset is a GSHP installed at the main store in selected scenarios. A GSHP operates by extracting low-grade heat from a borehole field and upgrading it to useful supply temperature via a vapour-compression cycle. Its thermal efficiency is characterised by the COP, i.e. the ratio of heat output to electrical input, which varies over time with outdoor air temperature and the required supply temperature to the building's heating circuit. In pre-processing, a time-varying COP curve is computed from outdoor air temperature, a fixed ground temperature, and a heating curve that determines supply temperature as a function of outdoor conditions, all combined into a Carnot-based efficiency estimate corrected by an empirical factor (see Appendix A.4.3). An auxiliary consumption factor accounts for circulation pumps and ancillary equipment. The resulting time-varying electrical intensity (the electrical power required per unit of heat delivered) is then passed to the optimisation as an exogenous parameter, preserving the linearity of the MILP. The GSHP operates in parallel with the existing district heating connection, where the optimiser determines the least-cost heat supply split at each time-step, subject to the GSHP's rated thermal capacity and the hard constraint that total heat supply meets the building's demand at all times.

2.2.2 Electric Vehicles and Charging Flexibility

The EV fleet at the retail site is represented as a set of individual charging sessions at each charging point. From an energy system perspective, each EV battery acts as a small mobile storage unit whose availability is bounded by the vehicle's arrival and departure times. Within this window, the model tracks each session's state of charge, constrained by a minimum SoC floor for battery health, and requires that the SoC reaches a driver-specified departure target. As no economic value accrues from surplus SoC at departure, the optimiser naturally charges each vehicle to exactly its required level. Full mathematical details are provided in Appendix A.4.4 and Section 3.1.7.1.

Three charging modes are modelled, corresponding to increasing levels of flexibility utilisation:

1. **Direct charging, DC**: EVs charge immediately upon arrival at a fixed power rate until the departure SoC requirement is satisfied. No scheduling flexibility is available so the EV fleet behaves as an uncontrolled, inflexible load and serves as the baseline for EV-related scenarios.
2. **Smart charging, V1G**: Charging remains unidirectional, but the optimisation can distribute charging power freely within the arrival–departure window while respecting power limits and the departure SoC target. This enables shifting of EV demand away from high-price or high-peak periods without feeding power back to the grid.
3. **Vehicle-to-grid, V2G**: Charging becomes bidirectional. When connected, EVs can both draw from and inject power to the building or grid within the availability window, subject to the same SoC floor and departure requirement. This effectively turns the aggregated EV fleet into a controllable mobile storage resource that can support peak shaving and arbitrage alongside the stationary BESS.

In all modes, EV sessions are treated as deterministic and known in advance. The model therefore establishes an upper bound on cost savings and flexibility utilisation under idealised behaviour; effects such as stochastic arrivals, driver non-compliance, and EV battery degradation from V2G cycling are outside the scope of this study (see Section 1.4).

2.2.3 Local Energy Communities

A LEC is a collective of co-located prosumers that jointly produce, share, store, and manage energy, typically with a focus on renewable sources and local environmental and economic benefits [16, 20, 21]. In the EU, Renewable Energy Communities and Citizen Energy Communities are defined under the revised Renewable Energy Directive (RED II) [18] and the Internal Electricity Market Directive [19]. Participation grant members rights to generate, consume, store, sell, and share energy, and to participate in demand response and aggregation [16, 21].

In this thesis, the LEC is instantiated at the S3 system boundary as a two-building community comprising the main and secondary retail stores, as described in Section 1.4. Within this boundary, PV generation, BESS capacity, and EV charging flexibility can be pooled and reallocated between buildings via modelled inter-building power transfers, allowing the optimiser to exploit complementary load profiles and unused capacity in one building to reduce collective peak demand and grid imports. The analysis treats the LEC from a strictly techno-economic perspective; legal, governance, and organisational aspects of its formation are not modelled.

2.3 Optimization Modelling

2.3.1 MILP for Energy System Problems

The operational planning problem for the two-building LEC is formulated as a mixed-integer linear program (MILP), detailed in Section 3.1. A MILP minimises (or maximises) a linear objective function subject to linear constraints, with decision variables that are either continuous (e.g., power flows and SoC levels) or binary (e.g., charge/discharge mode selection, import/export direction). This structure is well-suited to energy dispatch problems that involve mutual-exclusion logic such as no simultaneous charging and discharging of a storage device, and piecewise-linear tariff structures, while remaining solvable at practical scale with commercial solvers.

All investment decisions (PV, BESS, and GSHP capacities) are treated as fixed, scenario-specific parameters rather than decision variables, so the MILP solves a pure operational cost minimisation for a given technology portfolio. The objective function represents the total system energy cost over the simulation horizon, covering electricity procurement at day-ahead spot prices (plus applicable Swedish network charges and taxes), DSO subscription and peak power penalty fees, district heating tariff components, BESS cycling costs, and revenues from electricity export and transmission health incentives (see Section 3.1.6). Binary variables and Big-M linearisation are applied to enforce logical constraints: import/export exclusivity at each metering point, charge/discharge exclusivity for BESS and EVs, and the computation of running peak maxima for capacity tariff tracking, as detailed in Section 3.1.7.5. The problem is solved on a rolling 24-hour horizon with a 36-hour look-ahead window, as described in Section 3.1.2.

2.4 Techno-Economic Assessment

2.4.1 Cost Metrics

The economic assessment compares scenarios on the basis of annualised total system cost, combining capital expenditure (CAPEX) annualised over each asset's lifetime via a capital recovery factor, with annual operating expenditure (OPEX) derived from the optimisation results. Scenarios are ranked by annual cost savings relative to a baseline without flexibility measures. NPV and payback period (PBP) are reported as indicators of financial viability over the investment horizon (see Section 3.4.2).

2.4.2 Performance Indicators

Operational performance is characterised by the PV SC ratio: the fraction of total PV production consumed within the LEC, and the SS ratio: the fraction of total electricity demand met by local PV, directly or via storage. Reductions in annual grid imports and annual peak demand relative to the baseline are also reported to quantify the combined flexibility effect of all modelled assets. On the environmental side, the analysis focuses on avoided CO_2 emissions from district heating, comparing the baseline DH supply against scenarios where part of the heat load is shifted to the GSHP. Electric-side emissions are not accounted for explicitly, as the company operates a corporate offsetting mechanism that brings electricity consumption to net-zero CO_2, making district heating the only unmitigated source of carbon in the system, as it depends on the local DSO's fuel mix. Full key performance indicator (KPI) definitions and parameter choices are given in Section 3.4.

3
Methodology

Assessing the value of integrated energy flexibility solutions requires a modelling framework that captures both the operational dynamics of individual assets and the economic signals that govern their dispatch. This chapter presents such a framework: a MILP-based energy management model applied to a main retail store and adjacent retail building operating as a LEC in Sweden. The model is solved on a rolling 24-hour horizon over a three-year simulation period, optimising the joint dispatch of solar PV, BESS, GSHP, and EVs against a full Swedish electricity cost stack. The chapter proceeds from scope and assumptions through data, component models, and the formal optimisation formulation, before describing the validation procedure, performance metrics, and the 34-scenario matrix used to evaluate technology combinations.

3.1 Optimisation Model Formulation

The energy management problem for the LEC is formulated as a MILP. The model determines the cost-optimal operation of all controllable assets, (i.e. EV charging and discharging, BESS dispatch, GSHP dispatch, and grid import and export flows) subject to technical feasibility constraints and the applicable Swedish electricity market tariffs.

The optimisation problem is solved on a rolling-horizon basis: a 36-hour look-ahead window is optimised at the start of each day (see Section 3.1.2). This approach balances computational tractability with the long-horizon dependencies introduced by peak power tariffs and battery state management.

The model is implemented in Python using the Pyomo algebraic modelling framework [61, 62] and solved with the Gurobi solver [63].

3.1.1 Software Framework

The optimisation model is implemented entirely in Python, using the following software stack:

Pyomo (Python Optimization Modelling Objects)

An open-source algebraic modelling language for mathematical programming embedded in Python. Pyomo is used to declare sets, parameters, decision variables, constraints, and objective functions in a symbolic, solver-agnostic manner. The `ConcreteModel` class is used, meaning all data are bound at model instantiation time. Each daily optimisation is solved on a freshly rebuilt Pyomo model to avoid residual state between days.

Gurobi

A commercial MILP solver, accessed through Pyomo's `SolverFactory` interface. The following solver options are applied to all solves:

- `MIPGap = 0.001`: The solver terminates when the incumbent solution is within 0.1% of the computed lower bound. Because many tariff components (e.g., the transmission fee of 0.04 SEK/kWh) are small relative to spot prices, numerous near-equivalent solutions exist; a strict convergence criterion would result in excessive branch-and-bound exploration for negligible practical gain.
- `NumericFocus = 1`: Activates increased numerical precision in floating-point arithmetic, improving robustness when coefficient magnitudes differ by several orders of magnitude (e.g., the large peak penalty vs. small per-kWh fees).

pandas

All time-series input data (spot prices, load profiles, solar generation, EV session parameters, temperature) are managed as `DataFrame` objects, within pandas [64] and sliced to the appropriate time window prior to each daily solve. Results are extracted from the solved Pyomo model and written to a `DataFrame` for post-processing and KPI calculation.

PyYAML

Scenario and system configuration (tariff values, component ratings, solver settings) are stored in YAML files and loaded at runtime, separating model parameters from source code.

The overall simulation workflow and post-processing of results is coordinated by a Jupyter notebook, which iterates over the simulation period day by day, calls the optimization model class, and accumulates results. Pre-processing and scenario comparison are handled by dedicated notebooks.

3.1.2 Rolling Horizon Implementation

The model is solved on a rolling 24-hour horizon with 36 hours of foresight, re-optimised daily over the full three-year simulation period, as illustrated in Figure 3.1.

At each iteration, the MILP is solved over a 36-hour window (144 time-steps), but only the first 24 hours (96 time-steps) are committed as the operational schedule. The remaining 12 hours serve as a foresight buffer, preventing short-sighted end-of-day decisions such as excessive BESS discharge with no recovery window, and are discarded before the next iteration. End-of-day BESS state of charge and the running annual peak power record are propagated as initial conditions to the following day.

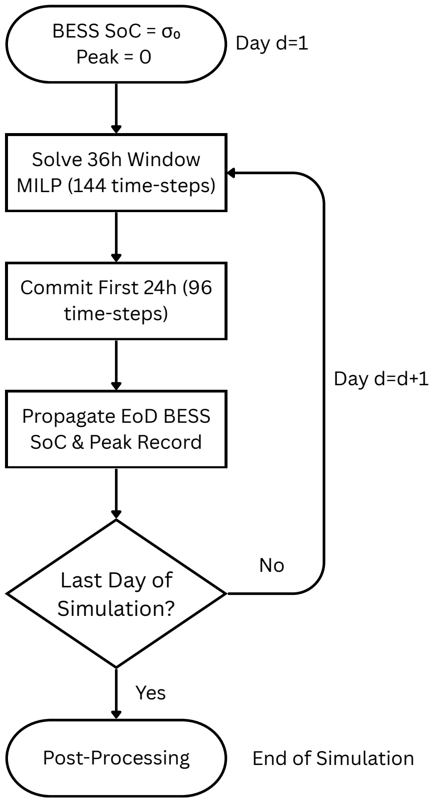

Figure 3.1: Rolling horizon optimisation flow.

This design represents an upper bound on achievable cost savings, so real-time implementations with forecast-driven inputs and shorter look-ahead would incur additional costs due to prediction errors (see Section A.1).

3.1.3 Sets

The model operates over a discrete time horizon partitioned into equal 15-minute intervals. In addition to the time index, separate index sets are defined for buildings and EV charging infrastructure to allow the formulation to scale transparently with the size of the community. Table 3.1 summarises all index sets used.

Table 3.1: Index sets used in the optimisation model.

Symbol	**Description**
$\mathcal{T}$	Set of discrete time steps, $t = 0, 1, \ldots, T-1$. At 15-minute resolution, $\lvert\mathcal{T}\rvert = 144$ for the 36-hour optimisation horizon.
$\mathcal{B}$	Set of buildings in the community, indexed by b.
$\mathcal{C}$	Set of EV charging points, indexed by c.
$\mathcal{E}(c)$	Set of EV charging sessions at charging point c, indexed by e.
$\mathcal{B}^H \subseteq \mathcal{B}$	Subset of buildings with a thermal demand, connected to the district heating network and/or GSHP.

3.1.4 Parameters

All parameters are treated as fixed, known inputs to the optimisation problem. Time-varying parameters are provided as profiles indexed over $\mathcal{T}$; scalar parameters represent constant tariff or physical values. All monetary quantities are denominated in SEK. Numerical values for tariff rates, subscribed power capacities, and component ratings are reported in Appendix A.2; only parameters whose values constitute intrinsic modelling or computational choices are stated explicitly below.

3.1.4.1 Time Resolution

The model operates at a fixed 15-minute time step. Table 3.2 defines the corresponding duration parameter used throughout the formulation to convert power to energy.

Table 3.2: Time resolution parameter.

Symbol	Value	Description
Δt	0.25 h	Duration of each time step

3.1.4.2 Asset Parameters

Building Electrical Load and Solar PV

Table 3.3 defines the exogenous time-series inputs representing each building's electrical load and solar PV generation, which appear directly in the building power balance constraints.

Table 3.3: Building load and generation parameters (per building b).

Symbol	Value	Description
$L_{b,t}$*	kW, per t	Measured electrical load at time step t; excludes GSHP consumption, which is computed endogenously
$G_{b,t}$	kW, per t	Solar PV generation at time step t

* Values not disclosed, see Confidentiality Notice

Battery Energy Storage System Parameters

Table 3.4 lists the parameters characterising the battery storage system at each building, including capacity, power rating, and the efficiency and depth-of-discharge (DoD) limits used in the SoC dynamics.

Table 3.4: BESS parameters (per building b).

Symbol	Value	Description
E_b^{bess}	257–771 kWh	Usable BESS energy capacity
$P_b^{\text{bess,max}}$	125–257 kW	Rated charge/discharge power
$\sigma_b^{\text{bess,0}}$	-	Initial state of charge at the start of the optimisation horizon
η^2	86.5 %	Round-trip charge/discharge efficiency; applied as η on the charging side and $1/\eta$ on the discharging side (see Appendix A.2.4)
σ^{min}	20 %	Minimum permissible state of charge, enforced to protect battery longevity (see Appendix A.1.1)
c_{cyc}	0.17 SEK/kWh/cycle	BESS cycling cost; captures wear-related degradation

Thermal System Parameters

Table 3.5 lists the parameters governing heat supply at buildings with a thermal demand, covering GSHP capacity and the time-varying electrical intensity coefficient used to compute the heat pump's electricity consumption.

Table 3.5: Thermal system parameters (per building $b \in \mathcal{B}^H$).

Symbol	Value	Description
$H_{b,t}$*	kW, per t	Space heating demand at time step t
$Q_b^{\text{gshp,max}}$	0–700 kW	Rated GSHP thermal output capacity; set to 0 for district-heating-only buildings
$\alpha_{b,t}$	[kW_{el} / kW_{th}], per t	GSHP electrical intensity, defined in Appendix A.4.3

3.1.4.3 EV and Charging Point (CP) Parameters

Table 3.6 lists the parameters describing each EV charging session, including battery characteristics, power limits, the parking time window, and the charging mode indicator. The three charging modes and their respective constraint formulations are described in Appendix A.4.4.

Table 3.6: EV and charging point parameters (per session e at charging point c).

Symbol	Value	Description
$E^{\mathrm{ev}}_{c,e}$	61 kWh	EV battery usable capacity
$P^{\mathrm{ev,max}}_{c,e}$	7.4–50 kW	Maximum bidirectional charging/discharging power
$\sigma^{\mathrm{arr}}_{c,e}$	0–100 %	State of charge at arrival
$\sigma^{\mathrm{dep}}_{c,e}$	0–100 %	Minimum required state of charge at departure
$t^{\mathrm{arr}}_{c,e}$	-	Arrival time step index
$t^{\mathrm{dep}}_{c,e}$	-	Departure time step index
m^{ev}	0–2	EV charging mode: 0 = DC, 1 = V1G, 2 = V2G
$v_{2\mathrm{g}}$	0,1	Derived binary flag: $v_{2\mathrm{g}} = 1$ if $m^{\mathrm{ev}} = 2$, otherwise $v_{2\mathrm{g}} = 0$; gates V2G discharge capability

3.1.4.4 Market and Tariff Parameters

Electricity Market Tariffs

Table 3.7 lists the electricity market tariff and fee parameters that appear in the supplier cost, transmission cost, and tax terms of the objective function.

Table 3.7: Electricity market tariff parameters.

Symbol	Value	Description
$\lambda_{b,t}$	SEK/kWh, per t	Day-ahead spot electricity price for building b at time step t; time-varying
$\bar{\lambda}_t$	SEK/kWh, per t	Community-average spot price at time step t; used to value V2G discharge revenue; time-varying
c_{cert}	0.005 SEK/kWh	Renewable energy certificate fee, levied on grid imports
c_{tx}	0.04 SEK/kWh	Transmission (network utilisation) fee on grid imports
c_{hi}	0.04 SEK/kWh	Transmission health incentive received per kWh exported to the grid
c_{tax}	0.439 SEK/kWh	Swedish national energy tax, levied on grid imports only
c_{solar}	0.439 SEK/kWh	Solar production tax on self-consumed PV energy; equals zero for installed capacity $\leq$ 500 kWp and the full energy tax rate otherwise (see Appendix A.4.1)

DSO Power Tariffs

The DSO applies a capacity-based annual tariff consisting of a fixed subscription charge and a penalty surcharge triggered whenever a building's annual peak power demand exceeds its contracted baseline. This tariff structure creates a persistent optimisation incentive to suppress demand peaks throughout the simulated period. The tariff parameters are listed in Table 3.8.

Table 3.8: DSO tariff parameters.

Symbol	Value	Description
P_b^{sub}	500-2,500* kW	Contracted power capacity for building b
c_{sub}	3,000 SEK/day	Fixed DSO grid subscription fee, prorated from the monthly charge
$c_{\text{pk,mo}}$	35.84 SEK/kW/month	Monthly subscribed power fee per kW of contracted capacity
$c_{\text{pk,yr}}$	430 SEK/kW/year	Annualised subscribed power fee rate: $c_{\text{pk,yr}} = 12\, c_{\text{pk,mo}}$
$c_{\text{pen,yr}}$	860 SEK/kW/year	Annual penalty rate for each kW by which the annual peak exceeds P_b^{sub}; set at twice the subscribed power fee: $c_{\text{pen,yr}} = 2\, c_{\text{pk,yr}}$
$\hat{P}_b^{\text{prev}}$	$\mathbb{R} \geq 0\,\text{kW}$	Annual peak state carried in from prior optimisation periods (rolling-horizon state variable)

The model internalises the peak power penalty cost, providing an economic incentive to deploy BESS and V2G discharge at peak-risk time steps.

District Heating Tariff Parameters

The district heating tariff applied by the DSO comprises time-varying energy charges structured into two tiers (base and peak), plus three fixed daily capacity charges. The corresponding parameters are listed in Table 3.9. All district heating demand up to $P^{\text{dh,base}}$ is billed at the base-tier rate $c_t^{\text{dh,base}}$; any demand exceeding this threshold is billed at the higher peak-tier rate $c_t^{\text{dh,spets}}$. The two-tier structure creates a cost incentive to restrict heat demand below $P^{\text{dh,base}}$ during high-rate periods.

Table 3.9: District heating tariff parameters.

Symbol	Units	Description
$c_t^{\mathrm{dh,base}}$	0.188–0.458 SEK/kWh	Base-tier district heating energy rate at time step t; time-varying
$c_t^{\mathrm{dh,spets}}$	1.2 SEK/kWh	Peak-tier district heating energy rate at time step t; time-varying
$c_{\mathrm{cap}}^{\mathrm{dh,base}}$	441 SEK/kW/year	Annual base capacity charge rate
$c_{\mathrm{cap}}^{\mathrm{dh,max}}$	685 SEK/kW/year	Annual maximum capacity charge rate
$P^{\mathrm{dh,base}}$	499-1,000* kW	Power threshold separating base-tier from peak-tier billing
$P^{\mathrm{dh,max}}$	499-1,000* kW	Contracted maximum demand used for peak capacity charge computation
κ_{fa}	465 SEK/day	Fixed daily charge: subscription fee, derived from the yearly fee
κ_{be}	700 SEK/day	Fixed daily charge: base capacity component, derived as $P^{\mathrm{dh,base}} \cdot c_{\mathrm{cap}}^{\mathrm{dh,base}}/365$
κ_{me}	356 SEK/day	Fixed daily charge: peak capacity component, derived as $(P^{\mathrm{dh,max}} - P^{\mathrm{dh,base}}) \cdot c_{\mathrm{cap}}^{\mathrm{dh,max}}/365$

3.1.4.5 Big-M Linearisation Constant

The Big-M method requires a scalar constant M large enough to dominate all physically plausible power flows in the system. The value used throughout the model is given in Table 3.10.

Table 3.10: Big-M constant.

Symbol	Value	Description
M	10,000	Large constant used in Big-M linearisation of binary mutual-exclusion constraints

3.1.5 Decision Variables

The following decision variables are optimised by the solver. They are classified as either continuous or binary (integer-valued), the latter being the source of the mixed-integer character of the problem.

Building Variables

Table 3.11 lists the decision variables associated with each building's electrical systems, including BESS dispatch, net power, and the binary import/export decomposition used for per-building cost accounting.

Table 3.11: Building decision variables (per building $b \in \mathcal{B}$, per time step $t \in \mathcal{T}$).

Variable	Units	Type	Bounds	Description
$p_{b,t}^{\mathrm{ch,b}}$	kW	Continuous	$[0,\ P_b^{\mathrm{bess,max}}]$	BESS charging power
$p_{b,t}^{\mathrm{ds,b}}$	kW	Continuous	$[0,\ P_b^{\mathrm{bess,max}}]$	BESS discharging power
$\sigma_{b,t}^{\mathrm{bess}}$	-	Continuous	$[0, 1]$	BESS state of charge [dimensionless]
$B_{b,t}^{\mathrm{ch,b}}$	-	Binary	$\{0, 1\}$	BESS charging mode indicator: $B = 1$ denotes charging, $B = 0$ denotes discharging
$P_{b,t}$	kW	Continuous	$\mathbb{R}$	Net electrical power of building b; positive values indicate net import
$P_{b,t}^{\mathrm{im}}$	kW	Continuous	$[0, +\infty)$	Import component of building net power
$P_{b,t}^{\mathrm{ex}}$	kW	Continuous	$[0, +\infty)$	Export component of building net power
$B_{b,t}^{\mathrm{im}}$	-	Binary	$\{0, 1\}$	Import mode indicator: $B = 1$ when the building is a net importer

Thermal Variables (only for $b \in \mathcal{B}^H$)

Table 3.12 lists the thermal dispatch variables applicable to buildings with a heat demand; they determine the cost-optimal split between GSHP output and district heating supply.

Table 3.12: Thermal decision variables.

Variable	Units	Type	Bounds	Description
$Q_{b,t}^{\mathrm{gshp}}$	kW	Continuous	$[0,\ Q_b^{\mathrm{gshp,max}}]$	GSHP thermal output at time step t
$Q_{b,t}^{\mathrm{dh}}$	kW	Continuous	$[0, +\infty)$	District heating supply at time step t

Peak Power Tracking Variables (per building b, scalar)

Table 3.13 lists the scalar variables that track each building's annual peak import and compute the associated penalty surcharge; they are re-solved each day and their values carried forward via the rolling horizon.

Table 3.13: Peak power tracking variables (not time-indexed).

Variable	Units	Type	Bounds	Description
$\hat{P}_b^{\text{day}}$	kW	Continuous	$[0, +\infty)$	Maximum net import power observed during the current optimisation period
$\hat{P}_b^{\text{new}}$	kW	Continuous	$[0, +\infty)$	Updated annual peak: $\max(\hat{P}_b^{\text{prev}},\ \hat{P}_b^{\text{day}})$
δ_b^{pk}	kW	Continuous	$[0, +\infty)$	Excess peak above contracted baseline: $\max(0,\ \hat{P}_b^{\text{new}} - P_b^{\text{sub}})$

Inter-Building Power Transfer Variables (when $|\mathcal{B}| \geq 2$)

In multi-building configurations, the model permits the transfer of electrical energy between buildings at zero marginal cost, representing the sharing of locally generated or stored resources within the community. Three transfer variables are defined between building b_1 and building b_2, as listed in Table 3.14.

Table 3.14: Inter-building transfer variables (per time step t).

Variable	Units	Type	Bounds	Description
X_t^{pv}	kW	Continuous	$[0, +\infty)$	PV generation power transferred from b_1 to b_2
X_t^{bess}	kW	Continuous	$[0, +\infty)$	BESS discharge power transferred from b_1 to b_2
X_t^{b2b1}	kW	Continuous	$[0, +\infty)$	Power transferred from b_2 to b_1 for the purpose of charging b_1's BESS

The transfer variable X_t^{pv} enables surplus solar generation at b_1 to reduce the grid import requirement of b_2. Conversely, X_t^{b2b1} allows b_2 to supply energy to b_1's battery using b_2's available grid capacity, thereby enabling peak demand at b_1 to be managed through pre-emptive BESS charging financed by b_2.

District Heating Variables

Table 3.15 lists the district heating aggregation and tier-split variables used to implement the two-tier billing structure of the DSO tariff.

Table 3.15: District heating decision variables (system-level, per time step $t \in \mathcal{T}$).

Variable	Units	Type	Bounds	Description
$Q_t^{\mathrm{dh,tot}}$	kW	Continuous	$[0, +\infty)$	Aggregate district heating demand across all buildings
$Q_t^{\mathrm{dh,base}}$	kW	Continuous	$[0, +\infty)$	Base-tier district heating consumption
$Q_t^{\mathrm{dh,peak}}$	kW	Continuous	$[0, +\infty)$	Peak-tier district heating consumption
$\hat{Q}^{\mathrm{dh,load}}$	kW	Continuous	$[0, +\infty)$	Maximum DH demand across all time steps
$\hat{Q}^{\mathrm{dh,mo}}$	kW	Continuous	$[0, +\infty)$	Monthly DH peak

Grid-Level Variables

Table 3.16 lists the system-wide variables defined at the community metering point, including aggregate import and export flows, cost auxiliary variables, and the solar self-consumption auxiliary.

Table 3.16: Grid-level decision variables (system-wide, per time step $t \in \mathcal{T}$).

Variable	Units	Type	Bounds	Description
P_t^{im}	kW	Continuous	$[0, 100\,000]$	Total LEC grid import power
P_t^{ex}	kW	Continuous	$[0, 100\,000]$	Total LEC grid export power
B_t^{im}	-	Binary	$\{0, 1\}$	Community import mode indicator
$\hat{P}^{\mathrm{load}}$	kW	Continuous	$[0, +\infty)$	Maximum system-level grid import across all time steps
$\hat{P}^{\mathrm{mo}}$	kW	Continuous	$[0, +\infty)$	Monthly peak for ratchet constraint computation
τ_t	SEK	Continuous	$[0, +\infty)$	Transmission cost incurred at time step t
f_t	SEK	Continuous	$\mathbb{R}$	Aggregate supplier cost at time step t
$f_{b,t}$	SEK	Continuous	$\mathbb{R}$	Per-building supplier cost at time step t
S_t	kW	Continuous	$[0, +\infty)$	Solar energy self-consumed (not exported) at time step t

EV Variables

Table 3.17 lists the decision variables associated with EV charging and discharging, defined per charging session and time step. The binary variable $B_{c,e,t}^{\mathrm{ch,ev}}$ enforces mutual exclusion between charging and discharging.

Table 3.17: EV decision variables (per session $e \in \mathcal{E}(c)$, per time step $t \in \mathcal{T}$).

Variable	Units	Type	Bounds	Description
$p^{\mathrm{ch}}_{c,e,t}$	kW	Continuous	$[0,\, P^{\mathrm{ev,max}}_{c,e}]$	Charging power drawn by EV session e at charging point c
$p^{\mathrm{ds}}_{c,e,t}$	kW	Continuous	$[0,\, v_{2\mathrm{g}} \cdot P^{\mathrm{ev,max}}_{c,e}]$	V2G discharge power from EV session e; identically zero when $v_{2\mathrm{g}} = 0$
$\sigma^{\mathrm{ev}}_{c,e,t}$	-	Continuous	$[0, 1]$	State of charge of EV battery at session e
$B^{\mathrm{ch,ev}}_{c,e,t}$	-	Binary	$\{0, 1\}$	Charging mode indicator: $B = 1$ denotes active charging; $B = 0$ denotes discharge or idle
$P^{\mathrm{cp}}_{c,t}$	kW	Continuous	$\mathbb{R}$	Net power at charging point c at time step t; positive values indicate grid import

CP Power Routing Variables (more than one building)

In a multi-building LEC, the net power of each charging point must be attributed to a specific building's metering point for per-building peak power tracking. Four routing variables per charging point allow the optimiser to assign charging loads and V2G discharge quantities freely between the two buildings, as listed in Table 3.18.

Table 3.18: CP power routing variables (per charging point c, per time step t).

Variable	Units	Type	Bounds	Description
$r^{\mathrm{ch}}_{c,t,b_1}$	kW	Continuous	$[0, +\infty)$	Charging power of CP c attributed to building b_1
$r^{\mathrm{ch}}_{c,t,b_2}$	kW	Continuous	$[0, +\infty)$	Charging power of CP c attributed to building b_2
$r^{\mathrm{ds}}_{c,t,b_1}$	kW	Continuous	$[0, +\infty)$	V2G discharge power of CP c attributed to building b_1
$r^{\mathrm{ds}}_{c,t,b_2}$	kW	Continuous	$[0, +\infty)$	V2G discharge power of CP c attributed to building b_2

The routing variables allow the optimiser to selectively direct V2G discharge towards the building most at risk of exceeding its annual peak record, thereby maximising the cost benefit of vehicle-to-grid operation.

3.1.6 Objective Function

The model minimises total system cost over the optimisation horizon. All cost terms are expressed in SEK and are exclusive of value-added tax (VAT). Capital C denotes aggregated cost terms [SEK]; lower-case c denotes unit rate parameters [SEK/kWh or SEK/kW]. The objective function is:

$$\begin{aligned} \min \quad Z = C_{\mathrm{DSO}} + C_{\mathrm{supplier}} + C_{\mathrm{tax}} + C_{\mathrm{cycling}} + C_{\mathrm{solar}} \\ + C_{\mathrm{DH}} + C_{\mathrm{pk,base}} + C_{\mathrm{pk,penalty}} - R_{\mathrm{hi}} + P_{\mathrm{DC}} \end{aligned} \tag{3.1}$$

The term P_{DC} is a penalty applicable only in the DC charging mode ($m^{\mathrm{ev}} = 0$). it evaluates to zero for V1G and V2G modes and is described in Section 3.1.6.

DSO Cost

The DSO cost (C_{DSO}) comprises a variable transmission fee on imports and a fixed daily subscription charge:

$$C_{\mathrm{DSO}} = C_{\mathrm{tx}} + c_{\mathrm{sub}} \tag{3.2}$$

The variable transmission cost is:

$$C_{\mathrm{tx}} = \sum_{t \in \mathcal{T}} \tau_t = \sum_{t \in \mathcal{T}} c_{\mathrm{tx}} \cdot P_t^{\mathrm{im}} \cdot \Delta t \tag{3.3}$$

The fixed subscription fee c_{sub} is a scalar charge applied once per optimisation day, independent of actual consumption.

Supplier Cost

The supplier cost (C_{supplier}) reflects electricity procurement at spot prices, inclusive of renewable energy certificates, net of export compensation. Each building is billed at its own connection-point electricity price $\lambda_{b,t}$:

$$C_{\mathrm{supplier}} = \sum_{t \in \mathcal{T}} f_t \tag{3.4}$$

where the aggregate supplier cost f_t is defined via the constraint in Section 3.1.7.4. The per-building contribution is:

$$f_{b,t} = \left[P_{b,t}^{\mathrm{im}} \cdot (\lambda_{b,t} + c_{\mathrm{cert}}) - P_{b,t}^{\mathrm{ex}} \cdot (\lambda_{b,t} + c_{\mathrm{cert}}) \right] \cdot \Delta t \tag{3.5}$$

V2G discharge reduces the LEC's aggregate grid import but does not appear in any individual building's $P_{b,t}^{\mathrm{im}}$ variable, since charging points are modelled at the community bus level. To ensure that V2G dispatch is correctly valued in the optimisation, a revenue credit is applied directly in the supplier cost aggregation:

$$f_t = \sum_{b \in \mathcal{B}} f_{b,t} \; - \; \bar{\lambda}_t \cdot \Delta t \sum_{c \in \mathcal{C}} \sum_{e \in \mathcal{E}(c)} p^{\mathrm{ds}}_{c,e,t} \tag{3.6}$$

The V2G credit is evaluated at the community-average spot price $\bar{\lambda}_t$, consistent with the assumption that discharge power is shared among all community members.

Energy Tax

The Swedish national energy tax (C_{tax}) is levied on all electricity imported from the public grid. Exported electricity does not generate a tax refund:

$$C_{\mathrm{tax}} = c_{\mathrm{tax}} \cdot \Delta t \sum_{t \in \mathcal{T}} P^{\mathrm{im}}_t \tag{3.7}$$

Note that the model does not distinguish between electricity exported from locally generated PV and electricity exported after grid-charging a battery, thus, any potential tax refund on grid-charged storage export is not represented here.

BESS Cycling Cost

Battery degradation is captured through a cycling cost (C_{cycling}) term proportional to the total energy throughput of each BESS, normalised by its usable capacity. This penalises excessive cycling relative to the economic benefit and may be set to zero when degradation is not the subject of study:

$$C_{\mathrm{cycling}} = \sum_{\substack{b \in \mathcal{B} \\ E^{\mathrm{bess}}_b > 0}} \frac{c_{\mathrm{cyc}}}{E^{\mathrm{bess}}_b} \cdot \Delta t \sum_{t \in \mathcal{T}} p^{\mathrm{ds,b}}_{b,t} \tag{3.8}$$

Solar Production Tax

Under Swedish law, self-consumed PV electricity is subject to the national energy tax (C_{solar}) for installations exceeding 500 kWp (per building) in rated capacity. For smaller installations the rate is zero. The corresponding cost term is:

$$C_{\mathrm{solar}} = c_{\mathrm{solar}} \cdot \Delta t \sum_{t \in \mathcal{T}} S_t \tag{3.9}$$

where S_t is the self-consumed solar power at time step t, as defined in Section 3.1.7.5.

District Heating Cost

The district heating cost (C_{DH}) comprises three fixed daily charges and two time-varying energy components reflecting the base/peak tier structure:

$$C_{\text{DH}} = \underbrace{(\kappa_{\text{fa}} + \kappa_{\text{be}} + \kappa_{\text{me}}) \cdot \frac{|\mathcal{T}| \cdot \Delta t}{24}}_{\text{total fixed daily charge}} + \underbrace{\Delta t \sum_{t \in \mathcal{T}} c_t^{\text{dh,base}} \cdot Q_t^{\text{dh,base}}}_{\text{base-tier energy cost}} + \underbrace{\Delta t \sum_{t \in \mathcal{T}} c_t^{\text{dh,spets}} \cdot Q_t^{\text{dh,peak}}}_{\text{peak-tier energy cost}} \tag{3.10}$$

The fixed daily charges are prorated by the ratio of the optimisation horizon to 24 hours, ensuring that each daily solve contributes its proportionate share of the daily fixed costs.

Peak Power Base Fee

A fixed daily charge is incurred for each building's contracted power capacity ($C_{\text{pk,base}}$), regardless of actual demand. Expressed as a daily contribution to the annual subscribed-power fee:

$$C_{\text{pk,base}} = \sum_{b \in \mathcal{B}} \frac{P_b^{\text{sub}} \cdot c_{\text{pk,yr}}}{365} \tag{3.11}$$

Peak Power Penalty

When a building's annual peak power record $\hat{P}_b^{\text{new}}$ exceeds its contracted baseline P_b^{sub}, an annual penalty surcharge ($C_{\text{pk,penalty}}$) of $c_{\text{pen,yr}}$ per kW of excess is incurred. Since this cost depends on decision variables, it is endogenous to the optimisation and creates a continuous incentive for peak demand management:

$$C_{\text{pk,penalty}} = \sum_{b \in \mathcal{B}} \delta_b^{\text{pk}} \cdot c_{\text{pen,yr}} \tag{3.12}$$

The excess variable δ_b^{pk} is defined through the constraints in Section 3.1.7.4.

Transmission Health Incentive Income

The DSO reimburses the LEC for each kWh exported to the distribution network under the Nätnytta scheme, which compensates prosumers for voltage support and reduced network loading associated with local generation. This constitutes a revenue item (R_{hi}) and is therefore subtracted from total costs:

$$R_{\text{hi}} = c_{\text{hi}} \cdot \Delta t \sum_{t \in \mathcal{T}} P_t^{\text{ex}} \tag{3.13}$$

Direct Charging Uncontrolled Charging Penalty

The DC scenario ($m^{\text{ev}} = 0$) represents the baseline case of uncontrolled EV charging. In practice, this is modelled as immediate maximum-rate charging upon arrival, rather than as a flexible charging schedule within the parking window. Since a MILP would otherwise schedule charging at cost-optimal (typically off-peak) hours, a large penalty term (P_{DC}) is introduced to enforce maximum-rate charging throughout the parking window:

$$P_{\text{DC}} = w_{\text{DC}} \sum_{c \in \mathcal{C}} \sum_{e \in \mathcal{E}(c)} \sum_{\substack{t \in \mathcal{T} \\ t^{\text{arr}}_{c,e} \leq t < t^{\text{dep}}_{c,e}}} \left(P^{\text{ev,max}}_{c,e} - p^{\text{ch}}_{c,e,t} \right) \tag{3.14}$$

The weight $w_{\text{DC}} = 1\,000$ is chosen to dominate all tariff-related terms, ensuring that the optimiser prioritises immediate full-power charging throughout the parking window. If the battery reaches its capacity or the departure SoC requirement is satisfied earlier, charging naturally stops due to the state-of-charge constraints. This formulation is intended as a transparent approximation of uncontrolled charging and does not represent alternative feasible within-parking charging profiles that may also satisfy the departure requirement. This term evaluates to zero for V1G and V2G modes.

3.1.7 Constraints

3.1.7.1 EV Charging Dynamics

EV State of Charge Dynamics

The state of charge of each EV battery evolves according to a discrete-time energy balance, accounting for charging efficiency losses in both directions. The dynamics are only active during the parking window $[t^{\text{arr}}_{c,e}, t^{\text{dep}}_{c,e}]$; outside this window the SoC variable is fixed to zero, representing the physical absence of the vehicle.

At arrival ($t = t^{\text{arr}}_{c,e}$):

$$\sigma^{\text{ev}}_{c,e,t} = \sigma^{\text{arr}}_{c,e} + \frac{\eta \cdot p^{\text{ch}}_{c,e,t} - p^{\text{ds}}_{c,e,t}/\eta}{E^{\text{ev}}_{c,e}/\Delta t} \tag{3.15}$$

During subsequent parking steps ($t^{\text{arr}}_{c,e} < t \leq t^{\text{dep}}_{c,e}$):

$$\sigma^{\text{ev}}_{c,e,t} = \sigma^{\text{ev}}_{c,e,t-1} + \frac{\eta \cdot p^{\text{ch}}_{c,e,t} - p^{\text{ds}}_{c,e,t}/\eta}{E^{\text{ev}}_{c,e}/\Delta t} \tag{3.16}$$

Outside the parking window ($t < t^{\text{arr}}_{c,e}$ or $t > t^{\text{dep}}_{c,e}$):

$$\sigma^{\text{ev}}_{c,e,t} = 0 \tag{3.17}$$

The asymmetric efficiency formulation (i.e. η applied to charging and $1/\eta$ applied to discharging) yields a round-trip efficiency of η^2, consistent with the symmetric efficiency assumption stated in Section 1.4.

EV Minimum State of Charge

A lower bound on the EV state of charge is enforced throughout the parking window to represent battery health constraints:

$$\sigma^{\mathrm{ev}}_{c,e,t} \geq \sigma^{\min} \quad \forall\, t \in [t^{\mathrm{arr}}_{c,e},\, t^{\mathrm{dep}}_{c,e}] \tag{3.18}$$

EV Charging and Discharging Power Limits

Simultaneous charging and discharging of an EV battery is physically infeasible. This mutual exclusion is enforced via the Big-M method using the binary variable $B^{\mathrm{ch,ev}}_{c,e,t}$:

$$p^{\mathrm{ch}}_{c,e,t} \leq B^{\mathrm{ch,ev}}_{c,e,t} \cdot P^{\mathrm{ev,max}}_{c,e} \quad \forall\, c,\, e,\, t \tag{3.19}$$

$$p^{\mathrm{ds}}_{c,e,t} \leq (1 - B^{\mathrm{ch,ev}}_{c,e,t}) \cdot P^{\mathrm{ev,max}}_{c,e} \quad \forall\, c,\, e,\, t \tag{3.20}$$

When $B^{\mathrm{ch,ev}}_{c,e,t} = 1$ the vehicle is in charging mode and discharging power is bounded to zero; when $B^{\mathrm{ch,ev}}_{c,e,t} = 0$ the reverse applies.

EV Availability Constraints

Charging and discharging are permitted only during the parking window. Outside this interval both power variables are forced to zero:

$$p^{\mathrm{ch}}_{c,e,t} = 0 \quad \text{and} \quad p^{\mathrm{ds}}_{c,e,t} = 0 \quad \forall\, t \notin [t^{\mathrm{arr}}_{c,e},\, t^{\mathrm{dep}}_{c,e}) \tag{3.21}$$

EV Departure State of Charge Requirement

At the scheduled departure time step, the EV state of charge must meet or exceed the user-specified minimum departure SoC, representing the driver's range requirement:

$$\sigma^{\mathrm{ev}}_{c,e,t^{\mathrm{dep}}_{c,e}} \geq \sigma^{\mathrm{dep}}_{c,e} \tag{3.22}$$

This constraint is treated as hard (inviolable), meaning the optimiser must satisfy it regardless of the associated energy cost.

Charging Point Power Balance

The net power at each charging point is defined as the algebraic sum of charging and discharging across all concurrent EV sessions:

$$P^{\mathrm{cp}}_{c,t} = \sum_{e \in \mathcal{E}(c)} \left(p^{\mathrm{ch}}_{c,e,t} - p^{\mathrm{ds}}_{c,e,t} \right) \quad \forall\, c,\, t \tag{3.23}$$

CP Power Routing Conservation Constraints

In multi-building scenarios, the total charging demand and total V2G discharge of each charging point must be fully and exclusively attributed between the two buildings:

$$r^{\mathrm{ch}}_{c,t,b_1} + r^{\mathrm{ch}}_{c,t,b_2} = \sum_{e\in\mathcal{E}(c)} p^{\mathrm{ch}}_{c,e,t} \quad \forall\, c,\, t \tag{3.24}$$

$$r^{\mathrm{ds}}_{c,t,b_1} + r^{\mathrm{ds}}_{c,t,b_2} = \sum_{e\in\mathcal{E}(c)} p^{\mathrm{ds}}_{c,e,t} \quad \forall\, c,\, t \tag{3.25}$$

3.1.7.2 BESS Operation

BESS State of Charge Dynamics

The BESS state of charge evolves according to the same discrete-time energy balance as the EV battery. For buildings without a BESS ($E^{\mathrm{bess}}_b = 0$), the SoC and power variables are fixed to zero.

Initialisation at $t = 0$:

$$\sigma^{\mathrm{bess}}_{b,0} = \sigma^{\mathrm{bess},0}_b + \frac{\eta \cdot p^{\mathrm{ch,b}}_{b,0} - p^{\mathrm{ds,b}}_{b,0}/\eta}{E^{\mathrm{bess}}_b/\Delta t} \tag{3.26}$$

Subsequent time steps ($t > 0$):

$$\sigma^{\mathrm{bess}}_{b,t} = \sigma^{\mathrm{bess}}_{b,t-1} + \frac{\eta \cdot p^{\mathrm{ch,b}}_{b,t} - p^{\mathrm{ds,b}}_{b,t}/\eta}{E^{\mathrm{bess}}_b/\Delta t} \quad \forall\, t > 0 \tag{3.27}$$

BESS Minimum State of Charge

A lower bound on the BESS state of charge is imposed throughout the horizon to protect battery longevity:

$$\sigma^{\mathrm{bess}}_{b,t} \geq \sigma^{\mathrm{min}} \quad \forall\, b \in \mathcal{B},\, t \in \mathcal{T} \quad (E^{\mathrm{bess}}_b > 0) \tag{3.28}$$

BESS Charging and Discharging Power Limits

Simultaneous charging and discharging of the BESS is precluded by the binary variable $B^{\mathrm{ch,b}}_{b,t}$ via the same Big-M formulation:

$$p^{\mathrm{ch,b}}_{b,t} \leq B^{\mathrm{ch,b}}_{b,t} \cdot P^{\mathrm{bess,max}}_b \quad \forall\, b,\, t \tag{3.29}$$

$$p^{\mathrm{ds,b}}_{b,t} \leq (1 - B^{\mathrm{ch,b}}_{b,t}) \cdot P^{\mathrm{bess,max}}_b \quad \forall\, b,\, t \tag{3.30}$$

3.1.7.3 Thermal System

Heat Supply Balance

For all buildings with a thermal demand ($b \in \mathcal{B}^H$), the heat supply constraint requires that the sum of GSHP output and district heating supply equals the exogenous heat demand at each time step:

$$Q^{\mathrm{gshp}}_{b,t} + Q^{\mathrm{dh}}_{b,t} = H_{b,t} \quad \forall\, b \in \mathcal{B}^H,\, t \tag{3.31}$$

The optimiser determines the least-cost split between the two sources. When GSHP is not installed ($Q_b^{\text{gshp,max}} = 0$), the variable $Q_{b,t}^{\text{gshp}}$ is effectively zero and all demand is served by district heating.

District Heating Energy Tier Decomposition

The two-tier billing structure of the district heating tariff requires decomposing total DH consumption into base-tier and peak-tier components.

Aggregate DH demand:

$$Q_t^{\text{dh,tot}} = \sum_{b \in \mathcal{B}^H} Q_{b,t}^{\text{dh}} \quad \forall\, t \tag{3.32}$$

Energy tier balance:

$$Q_t^{\text{dh,base}} + Q_t^{\text{dh,peak}} = Q_t^{\text{dh,tot}} \quad \forall\, t \tag{3.33}$$

Base-tier capacity limit:

$$Q_t^{\text{dh,base}} \leq P^{\text{dh,base}} \quad \forall\, t \tag{3.34}$$

Demand in excess of $P^{\text{dh,base}}$ is automatically assigned to $Q_t^{\text{dh,peak}}$ and billed at the higher rate $c_t^{\text{dh,spets}}$.

DH peak load tracking:

$$\hat{Q}^{\text{dh,load}} \geq Q_t^{\text{dh,tot}} \quad \forall\, t; \qquad \hat{Q}^{\text{dh,mo}} \geq \hat{Q}^{\text{dh,load}} \tag{3.35}$$

3.1.7.4 Grid and Community Power Balances

Community Grid Power Balance

The net power balance at the community metering point requires that grid imports minus exports equal the aggregate demand of all buildings and charging points:

$$P_t^{\text{im}} - P_t^{\text{ex}} = \sum_{b \in \mathcal{B}} P_{b,t} + \sum_{c \in \mathcal{C}} P_{c,t}^{\text{cp}} \quad \forall\, t \tag{3.36}$$

Grid Import/Export Mutual Exclusion

Simultaneous grid import and export at the community metering point is physically impossible and is precluded by the Big-M constraints:

$$P_t^{\text{im}} \leq M \cdot B_t^{\text{im}} \quad \forall\, t \tag{3.37}$$

$$P_t^{\text{ex}} \leq M \cdot (1 - B_t^{\text{im}}) \quad \forall\, t \tag{3.38}$$

The same mutual exclusion is applied at the per-building level using the binary variable $B_{b,t}^{\text{im}}$, with the sign decomposition:

$$P_{b,t} = P_{b,t}^{\text{im}} - P_{b,t}^{\text{ex}} \quad \forall\, b,\, t \tag{3.39}$$

$$P_{b,t}^{\text{im}} \leq M \cdot B_{b,t}^{\text{im}} \quad \forall\, b,\, t \tag{3.40}$$

$$P_{b,t}^{\text{ex}} \leq M \cdot (1 - B_{b,t}^{\text{im}}) \quad \forall\, b,\, t \tag{3.41}$$

This decomposition is necessary to compute per-building supplier costs correctly and to prevent the simultaneous presence of import and export revenues, which would otherwise distort the BESS arbitrage incentive signal.

System Peak Load Tracking

The system peak load variable records the maximum grid import across the optimisation horizon:

$$\hat{P}^{\text{load}} \geq P_t^{\text{im}} \quad \forall\, t \tag{3.42}$$

The monthly ratchet constraint reflects the Swedish DSO convention that the monthly peak charge cannot fall below the peak from the preceding month:

$$\hat{P}^{\text{mo}} \geq \hat{P}^{\text{load}}, \qquad \hat{P}^{\text{mo}} \geq P^{\text{prev,mo}} \tag{3.43}$$

where $P^{\text{prev,mo}}$ is a fixed parameter representing last month's peak. This system-level tracking is retained for reference; the principal peak cost mechanism is the per-building annual tracking in Section 3.1.7.4.

Per-Building Annual Peak Power Tracking

The DSO peak power tariff requires tracking the annual peak import demand for each building. The following constraints implement a state-based linearisation of the running maximum over the simulation period.

Daily peak tracking, the variable $\hat{P}_b^{\text{day}}$ captures the maximum net import observed at building b during the current optimisation period:

Single-building or building index beyond b_2:

$$\hat{P}_b^{\text{day}} \geq P_{b,t} + \sum_{c \in \mathcal{C}} P_{c,t}^{\text{cp}} \quad \forall\, t \tag{3.44}$$

Multi-building, building b_1:

$$\hat{P}_{b_1}^{\text{day}} \geq P_{b_1,t} + \sum_{c \in \mathcal{C}} \left(r_{c,t,b_1}^{\text{ch}} - r_{c,t,b_1}^{\text{ds}} \right) \quad \forall\, t \tag{3.45}$$

Multi-building, building b_2:

$$\hat{P}_{b_2}^{\text{day}} \geq P_{b_2,t} + \sum_{c \in \mathcal{C}} \left(r_{c,t,b_2}^{\text{ch}} - r_{c,t,b_2}^{\text{ds}} \right) \quad \forall\, t \tag{3.46}$$

V2G discharge attributed to a building reduces its effective peak measurement, constituting the primary mechanism by which vehicle-to-grid operation mitigates annual peak power charges.

Annual peak update:

$$\hat{P}_b^{\text{new}} \geq \hat{P}_b^{\text{prev}} \tag{3.47}$$

$$\hat{P}_b^{\text{new}} \geq \hat{P}_b^{\text{day}} \tag{3.48}$$

Penalty increment:

$$\delta_b^{\mathrm{pk}} \geq \hat{P}_b^{\mathrm{new}} - P_b^{\mathrm{sub}} \tag{3.49}$$

Combined with the non-negativity bound on δ_b^{pk}, this yields the effective relationship $\delta_b^{\mathrm{pk}} = \max(0,\, \hat{P}_b^{\mathrm{new}} - P_b^{\mathrm{sub}})$.

Transmission Cost Definition

The per-timestep transmission cost auxiliary variable is defined as:

$$\tau_t = c_{\mathrm{tx}} \cdot P_t^{\mathrm{im}} \cdot \Delta t \quad \forall\, t \tag{3.50}$$

Supplier Cost Aggregation

The per-building supplier cost and its system-level aggregate are defined through the following equality constraints, used in both the objective function and results extraction.

Per-building supplier cost:

$$f_{b,t} = \Big[P_{b,t}^{\mathrm{im}} \cdot (\lambda_{b,t} + c_{\mathrm{cert}}) - P_{b,t}^{\mathrm{ex}} \cdot (\lambda_{b,t} + c_{\mathrm{cert}} + c_{\mathrm{comp}}) \Big] \cdot \Delta t \quad \forall\, b,\, t \tag{3.51}$$

System-level supplier cost (incorporating V2G discharge revenue):

$$f_t = \sum_{b \in \mathcal{B}} f_{b,t} \; - \; \bar{\lambda}_t \cdot \Delta t \sum_{c \in \mathcal{C}} \sum_{e \in \mathcal{E}(c)} p_{c,e,t}^{\mathrm{ds}} \quad \forall\, t \tag{3.52}$$

Building Electrical Power Balance

The net power of each building represents the sum of all local generation and storage offset against demand. A positive value indicates a net import from the community bus; a negative value indicates net export.

Single-building scenario, without GSHP ($b \notin \mathcal{B}^H$):

$$P_{b,t} = L_{b,t} - G_{b,t} - p_{b,t}^{\mathrm{ds,b}} + p_{b,t}^{\mathrm{ch,b}} \quad \forall\, b,\, t \tag{3.53}$$

Single-building scenario, with GSHP ($b \in \mathcal{B}^H$):

$$P_{b,t} = L_{b,t} - G_{b,t} - p_{b,t}^{\mathrm{ds,b}} + p_{b,t}^{\mathrm{ch,b}} + \alpha_{b,t} \cdot Q_{b,t}^{\mathrm{gshp}} \quad \forall\, b,\, t \tag{3.54}$$

The term $\alpha_{b,t} \cdot Q_{b,t}^{\mathrm{gshp}}$ represents the GSHP's electrical demand, computed as the product of the dispatch decision and the time-varying electrical intensity parameter.

Multi-building scenario, for building b_1:

$$P_{b_1,t} = L_{b_1,t} - G_{b_1,t} + X_t^{\mathrm{pv}} + X_t^{\mathrm{bess}} - p_{b_1,t}^{\mathrm{ds,b}} + p_{b_1,t}^{\mathrm{ch,b}} - X_t^{\mathrm{b2b1}} + \alpha_{b_1,t} \cdot Q_{b_1,t}^{\mathrm{gshp}} \quad \forall\, t \tag{3.55}$$

Multi-building scenario, for building b_2:

$$P_{b_2,t} = L_{b_2,t} - G_{b_2,t} - X_t^{\mathrm{pv}} - X_t^{\mathrm{bess}} - p_{b_2,t}^{\mathrm{ds,b}} + p_{b_2,t}^{\mathrm{ch,b}} + X_t^{\mathrm{b2b1}} + \alpha_{b_2,t} \cdot Q_{b_2,t}^{\mathrm{gshp}} \quad \forall\, t \tag{3.56}$$

Transfer variables that increase the supply available to a building appear with a negative sign, reducing that building's net import requirement. Variables representing energy dispatched away from a building appear with a positive sign. The sign convention follows from the definition of $P_{b,t}$ as net import: supplying energy to another building increases the apparent demand at the source and decreases it at the destination.

Inter-Building Transfer Upper Bounds

The following constraints ensure that inter-building power transfers do not exceed the physically available quantities.

PV transfer is bounded by the available solar generation at b_1:

$$X_t^{\text{pv}} \leq G_{b_1,t} \quad \forall\, t \tag{3.57}$$

BESS transfer is bounded by the actual BESS discharge of b_1:

$$X_t^{\text{bess}} \leq p_{b_1,t}^{\text{ds,b}} \quad \forall\, t \tag{3.58}$$

The b_2-to-b_1 transfer is bounded by b_1's maximum BESS charge rate:

$$X_t^{\text{b2b1}} \leq P_{b_1}^{\text{bess,max}} \quad \forall\, t \tag{3.59}$$

3.1.7.5 Linearisation Constraints

Solar Self-Consumption Auxiliary Constraints

The auxiliary variable S_t represents self-consumed solar energy. Its value is bounded below and above to correctly model the relationship between generation, export, and local consumption.

Lower bound, any PV generation not exported must have been consumed locally:

$$S_t \geq \sum_{b \in \mathcal{B}} G_{b,t} - P_t^{\text{ex}} \quad \forall\, t \tag{3.60}$$

Upper bound, self-consumption cannot exceed total PV generation:

$$S_t \leq \sum_{b \in \mathcal{B}} G_{b,t} \quad \forall\, t \tag{3.61}$$

The upper bound is necessary to prevent numerical artefacts when $c_{\text{solar}} = 0$: in the absence of a positive cost coefficient, the solver would otherwise assign an arbitrarily large value to S_t, yielding physically meaningless self-consumption ratios in post-processing.

3.1.8 Linearisation Methods

The model is entirely linear in its decision variables, but several physical realities would otherwise require non-linear expressions. The following standard linearisation techniques are applied throughout.

Big-M Method.

Mutual exclusion between two binary-governed alternatives (e.g., charging vs. discharging, import vs. export) is enforced by pairing a binary variable $B \in \{0,1\}$ with a large constant M. The constraint $x \leq M \cdot B$ forces $x = 0$ when $B = 0$, effectively switching the variable off. The value $M = 10\,000$ is chosen to exceed the maximum physically plausible power flow in the system.

Auxiliary Variable with Bound Constraints.

The max operator is linearised by introducing a new non-negative variable and replacing the original expression with two inequality constraints. For example, the annual peak record update $\hat{P}_b^{\text{new}} = \max(\hat{P}_b^{\text{prev}}, \hat{P}_b^{\text{day}})$ is replaced by:

$$\hat{P}_b^{\text{new}} \geq \hat{P}_b^{\text{prev}} \quad \text{and} \quad \hat{P}_b^{\text{new}} \geq \hat{P}_b^{\text{day}} \tag{3.62}$$

Since $\hat{P}_b^{\text{new}}$ appears in the objective with a non-negative coefficient, the minimiser drives it to the smallest feasible value, which equals the maximum of the two right-hand sides.

Solar Self-Consumption Auxiliary Variable.

The self-consumed PV energy $S_t = \max(0, \sum_b G_{b,t} - P_t^{\text{ex}})$ is expressed through a non-negative auxiliary variable bounded by one inequality from below and one from above, removing the non-linear $\max(\cdot, 0)$ operator while preserving the correct physical relationship.

3.2 Input Data

Building Electrical Load Profiles

Electrical load data for both buildings were obtained from metered records covering the period 2023–2025. To preserve confidentiality, all load values have been scaled by a constant multiplier, maintaining the relative patterns and the ratio between the two buildings.

Figure 3.2 presents the 2025 load duration curves (LDCs) for both stores. The secondary store exhibits a consistently higher load than the main store across the entire year, with noticeably higher peak demand. Despite the difference in scale, the two buildings share broadly similar operating schedules, as evidenced by the comparable shape of their LDCs and the alignment of their high-demand periods.

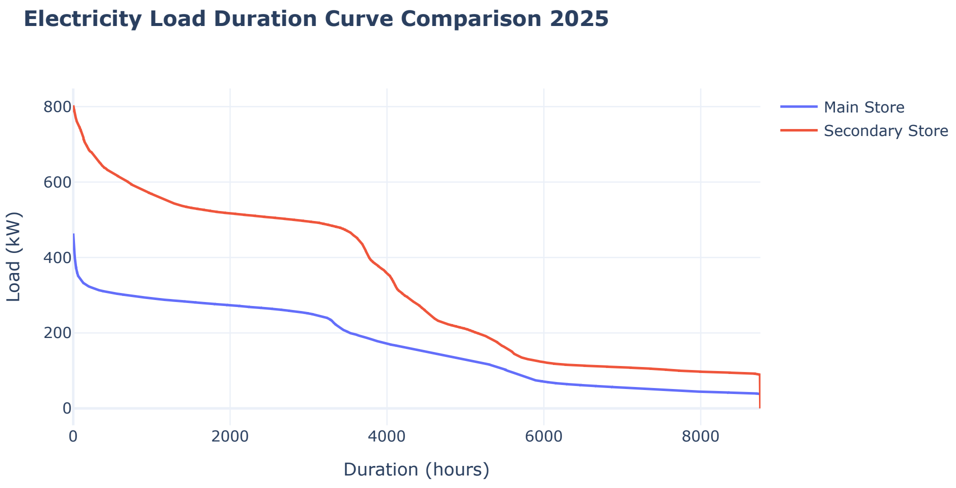

Figure 3.2: Load duration curves for the main and secondary store, 2025.

Figure 3.3 shows a representative week (Monday to Sunday) of electrical load for the main store. The profile illustrates the characteristic daily demand cycle of a retail building, with load rising sharply at store opening, sustaining an elevated plateau through operating hours, and dropping at closing. Weekend patterns follow the same structure, reflecting the continuous operation typical of large-format retailer in Sweden.

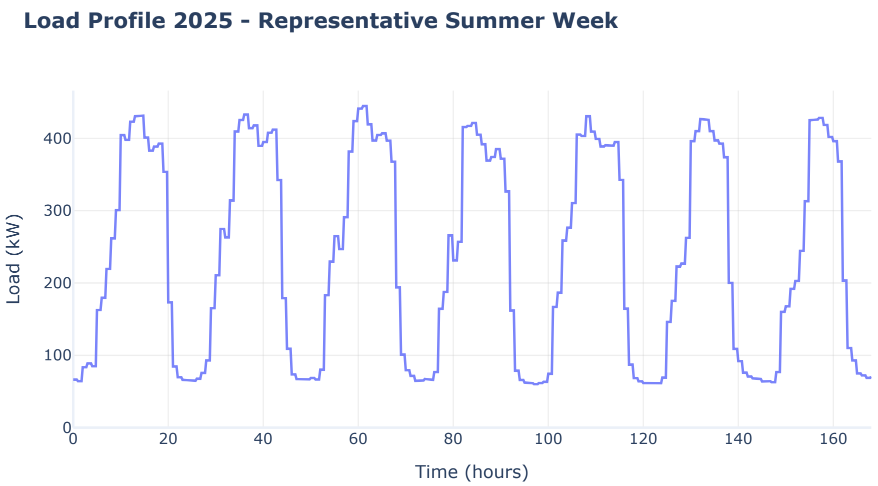

Figure 3.3: Representative weekly electrical load profile for the main store.

3.2.1 Thermal Load Profile

Thermal load data for the main store were obtained from metered DH records covering 2023–2025. All values have been scaled by a constant multiplier to preserve confidentiality.

Figure 3.4 shows a representative winter week (Monday to Sunday) of heat consumption. The profile follows a clear daily cycle, with demand peaking in the morning as the system pre-conditions the building before opening, then declining through the day as internal heat gains from lighting, HVAC, and occupancy partially offset the space heating requirement.

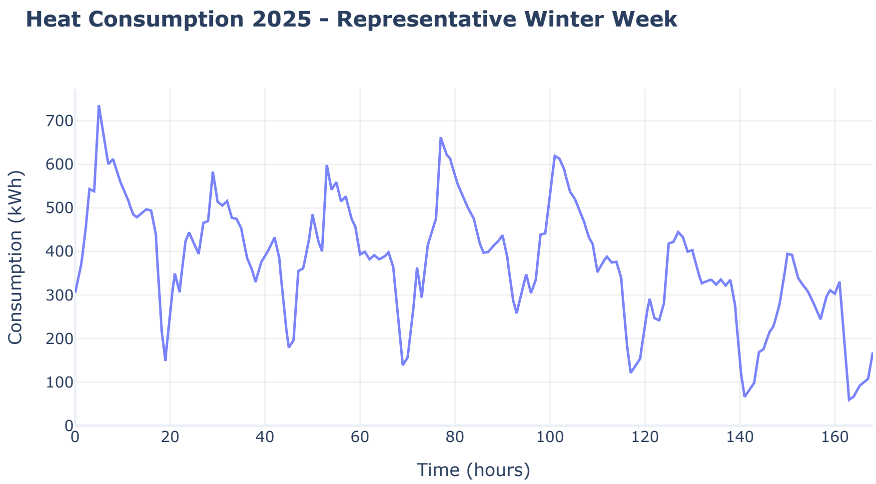

Figure 3.4: Representative winter week of thermal load at the main store, 2025.

3.2.2 Solar PV Generation Profile

Solar PV generation data were obtained from PVGIS, scaled to the installed capacity of each scenario as described in Appendix A.2.2. Figure 3.5 presents representative daily capacity factor profiles for a winter and a summer day, with a PV array of 500 kWp.

The contrast between seasons is pronounced. On the representative summer day, generation begins in the early morning, reaches a broad midday peak with a mean generation output of approximately 35 kW, and sustains meaningful output for roughly 9 hours. On the representative winter day however, the generation window is substantially shorter, approximately 3 hours (with a mean output of approximately 1 kW), with a sharper and lower peak reflecting the reduced solar elevation and shorter days at the case study latitude.

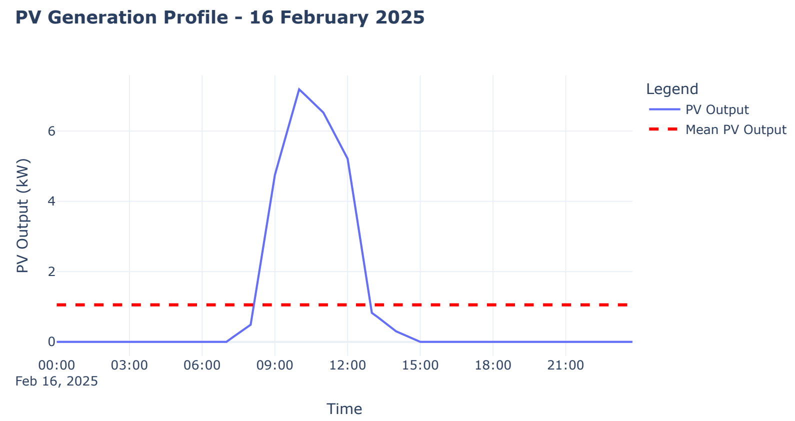

(a) Representative winter day.

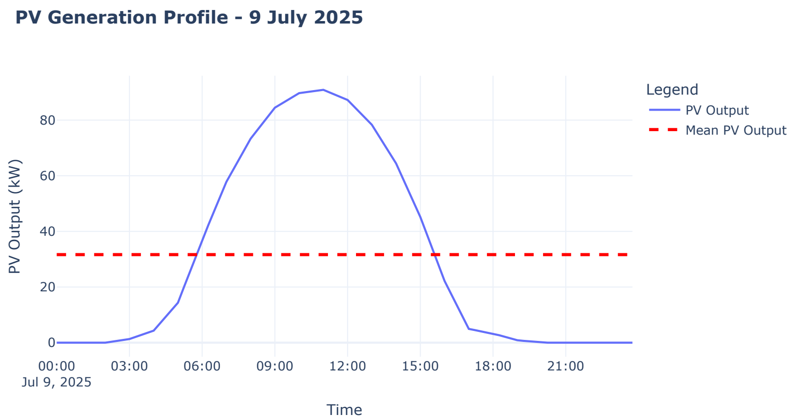

(b) Representative summer day.

Figure 3.5: Solar PV generation profiles for representative winter and summer days at the case study site.

3.3 Results Post-Processing

Upon completion of the rolling horizon optimisation, the committed operational schedules for each day are aggregated and passed to a dedicated post-processing stage, where final cost figures and key performance indicators are computed outside the solver environment. This separation is necessary because several terms in the objective function serve as economic incentives to guide the optimiser towards desirable behaviour, rather than as direct representations of the billing mechanism actually applied by the network operator or supplier.

The most prominent example is the DSO peak power charge. Within the optimisation, peak penalisation is modelled as a running annual maximum, which causes the solver to treat every additional kilowatt of peak demand as incurring a cost for the entire remaining year. In practice, however, peak capacity charges are settled on a monthly basis: the highest 15-minute net import recorded during each calendar month determines the charge for that month alone. Post-processing therefore reconstructs the peak cost by scanning the committed power profiles month by month, identifying the maximum grid import in each period, and multiplying by the applicable DSO rate, yielding the actual billed peak cost rather than the surrogate penalty used during optimisation.

A second incentive term is the BESS cycling cost C_{cycling} (Equation (A.3)), which penalises battery throughput to approximate degradation-related wear and discourage excessive cycling. Because this penalty is a modelling artefact rather than a billing item in an invoice, it is excluded from the reported system costs and treated solely as a penalty. The true degradation impact is instead captured through the BESS capital replacement cost in the NPV and PBP calculations.

For analogous reasons, the direct charging penalty term P_{DC} and the linearisation artefacts introduced by auxiliary variables are stripped from the post-processed cost stream before any financial KPI is computed. The final electricity and heat costs reported for each scenario therefore reflect only tariff components that correspond to real invoice line items: spot-price procurement, transmission fees, the energy tax, the DSO subscription and monthly peak charges, district heating energy and capacity fees, and the solar production tax where applicable. All performance metrics defined in Section 3.4 are derived from this reconciled cost representation.

3.4 Performance Evaluation Framework

The optimisation model outputs are evaluated using a set of KPIs that measure energy efficiency, economic viability, and environmental impact. Each metric is designed to support scenario comparison and technology assessment.

3.4.1 Energy Performance Metrics

Self-Consumption

Self-consumption measures the fraction of locally generated solar energy that is used within the community rather than exported to the grid.

$$\text{SC} = \frac{E_{\text{PV,used locally}}}{E_{\text{PV,generated}}} \tag{3.63}$$

where $E_{\text{PV,used locally}}$ is the annual solar energy consumed by buildings, storage, and CPs (including GSHP), and $E_{\text{PV,generated}}$ is the total annual PV generation. SC is expressed as a percentage; higher values indicate better local utilization of solar generation. SC is constrained to the range $[0, 1]$ and accounts for temporal mismatch between PV generation and demand patterns.

Self-Sufficiency

Self-sufficiency measures the fraction of total electricity demand met by locally generated solar energy.

$$\mathrm{SS} = \frac{E_{\text{PV,used locally}}}{E_{\text{total demand}}} \tag{3.64}$$

where $E_{\text{total demand}}$ is the annual electricity consumed by all buildings, heating systems, and EV CPs. Unlike SC, SS can exceed 1 when seasonal storage (BESS/V2G) enables supply of stored solar to future demand. SS quantifies the community's independence from grid electricity and is used to assess whether installed PV capacity meets strategic energy independence targets.

Grid Import Difference

The reduction in grid electricity imports is measured as the absolute change in annual import energy and the relative percentage reduction compared to the baseline scenario.

$$\Delta E_{\text{import}} = E_{\text{import,baseline}} - E_{\text{import,optimized}} \quad [\text{kWh}] \tag{3.65}$$

$$\text{Import Difference \%} = \frac{\Delta E_{\text{import}}}{E_{\text{import,baseline}}} \times 100 \tag{3.66}$$

Import reduction reflects the combined effect of PV generation, local storage, V2G discharge, and demand-side management. Reduction in imports directly lowers electricity supplier costs and network fees.

3.4.2 Financial Performance Metrics

Annual Savings & Annual Net Benefit

Annual savings represent the cost reduction achieved by the optimized scenario compared to a baseline scenario with no renewable technologies or energy management.

$$\text{Annual Savings} = C_{\text{baseline,annual}} - C_{\text{optimized,annual}} \quad [\text{SEK/year}] \tag{3.67}$$

where $C_{\text{baseline,annual}}$ includes grid electricity imports at spot prices plus all network tariffs (transmission, subscription, peak charges), district heating costs, and taxes (energy tax, VAT). $C_{\text{optimized,annual}}$ includes actual operational costs from the optimized scenario including solar tax (where applicable) and GSHP electricity consumption. Annual savings are calculated on a normalized annual basis even if the simulation covers a different duration (e.g., 3-year rolling horizon).

Annual net benefit is simply obtained by subtracting the additional annualised fixed operation and maintenance (O&M) costs of the new systems from the annual savings.

$$\text{Annual Net Benefit} = \text{Annual Savings} - C_{\text{O\&M}} \quad [\text{SEK/year}] \tag{3.68}$$

Net Present Value

NPV evaluates the long-term economic merit of the investment by discounting all future cash flows to present value.

$$\text{NPV} = -\text{CAPEX}_{\text{total}} + \sum_{t=1}^{T_{\text{lifetime}}} \frac{\text{Annual Net Benefit}_t}{(1+r)^t} - \sum_i \frac{\text{CAPEX}_{\text{replacement},i}}{(1+r)^{t_i}} \tag{3.69}$$

where r is the discount rate (5 %, assumed), T_{lifetime} is the system lifetime (assumed as 30 years for PV and GSHP, and 15 years for BESS), and $\text{CAPEX}_{\text{replacement},i}$ accounts for battery replacement if its technical lifetime is shorter than the system lifetime. NPV > 0 indicates a financially positive investment, while NPV < 0 suggests the investment does not recover its costs under the assumed discount rate and conditions.

Payback Period:

The time required for the annual net benefit to equal the original cost, useful as a reference metric.

$$\text{Simple PBP} = \frac{\text{CAPEX}_{\text{total}}}{\text{Annual Net Benefit}} \quad [\text{years}] \tag{3.70}$$

Values are expressed in years with one decimal place. PBP > system lifetime indicates the investment does not pay for itself; such scenarios are flagged for further review.

3.4.3 Environmental Impact Metrics

CO_2 Emissions Avoidance

Emissions avoidance is calculated by comparing baseline district heating emissions to emissions from a mixed heat supply (district heating and GSHP). The analysis focuses exclusively on heat-related emissions.

$$E_{\text{baseline}} = e_{\text{DH}} \times Q_{\text{heat,total}} \quad [\text{kgCO}_2] \tag{3.71}$$

$$E_{\text{with GSHP}} = e_{\text{DH}} \times Q_{\text{DH}} \quad [\text{kgCO}_2] \tag{3.72}$$

$$\text{Avoided Emissions} = E_{\text{baseline}} - E_{\text{with GSHP}} \quad [\text{kgCO}_2] \tag{3.73}$$

where e_{DH} is the carbon intensity of district heating (see Appendix A.2.3), $Q_{heat,total}$ is the total annual heat demand, and Q_{DH} is the heat supplied by the district heating system in the optimized scenario. Avoided emissions are expressed in kg CO_2 and as a percentage reduction relative to the baseline. This metric is most relevant for scenarios with GSHP enabled; for scenarios with GSHP disabled, avoidance is zero.

3.4.4 Scenario Selection Methodology

Scenarios are evaluated using a multi-criteria trade-off approach in which no single KPI dominates the decision. The evaluation hierarchy prioritizes economic viability while incorporating environmental and operational considerations:

1. **Primary screening**: NPV must be positive and PBP must be feasible (within the system lifetime). Scenarios failing this screen are deprioritized.
2. **Economic optimisation**: Among feasible scenarios, the shortest PBP is preferred, as it indicates faster capital recovery. When two scenarios have similar PBP (within 0.2–0.3 years), the next criterion is used.
3. **Technology balance**: For technology combinations (e.g., PV + BESS, or PV + BESS + GSHP), the “sweet spot” is sought: the minimum installed capacity that achieves the bulk of operational benefits. This avoids over-sizing, which increases CAPEX without proportional gains in annual savings. For example, scenarios with PV capacity below or at the solar tax threshold (500 kWp) are preferred as they avoid solar tax Appendix A.2.3.
4. **Operational performance**: SC, SS, and grid import reduction are secondary criteria used to assess system efficiency and resilience. These metrics guide technology assessment.
5. **Environmental impact**: CO_2 emissions avoidance is considered as a co-benefit rather than a primary objective. When two scenarios have similar economic merit (PBP and NPV within tolerance), the scenario with higher emissions reduction is preferred. Trade-offs are made explicit: for instance, accepting increases in PBP is justified if emissions avoidance improves substantially.

This approach ensures that investments are economically sound (positive NPV, acceptable PBP) while steering toward solutions with lower environmental impact and robust operational performance.

3.5 Scenario Matrix

A comprehensive scenario matrix of 34 scenarios (S-01 through S-33, plus S-01a) evaluates the techno-economic feasibility of a LEC in a retail setting. Scenarios progress from baseline configurations through fully integrated multi-technology systems with alternative EV integration pathways. Table 3.19 presents all technology parameters; detailed phase-specific analysis follows, evaluating total system cost, self-consumption, self-sufficiency, reduced energy imports, CO_2 emissions avoidance, and economic performance metrics.

Table 3.19: Complete scenario matrix: technology parameters for all scenarios.

Scenario	PV [m^2]	BESS [kWh]	BESS [kW]	GSHP [kW_h]	# CP	EV Mode
S-01	0	0	0	0	—	—
S-01a	0	0	0	0	—	—
S-02	2,000	0	0	0	—	—
S-03	2,500	0	0	0	—	—
S-04	4,000	0	0	0	—	—
S-05	6,000	0	0	0	—	—
S-06	8,000	0	0	0	—	—
S-07	2,000	257	125	0	—	—
S-08	2,500	257	125	0	—	—
S-09	2,500	514	125	0	—	—
S-10	4,000	257	125	0	—	—
S-11	4,000	514	125	0	—	—
S-12	6,000	514	125	0	—	—
S-13	6,000	771	125	0	—	—
S-14	8,000	514	125	0	—	—
S-15	8,000	771	125	0	—	—
S-16	2,500	257	125	100	—	—
S-17	2,500	257	125	300	—	—
S-18	2,500	257	125	500	—	—
S-19	2,500	257	125	700	—	—
S-20	2,500	257	125	500	—	—
S-21	3,500	514	125	500	—	—
S-22	5,000	514	257	500	—	—
S-23	3,500	771	125	500	—	—
S-24	5,000	771	257	500	—	—
S-25	5,000	771	257	500	5	DC
S-26	5,000	771	257	500	15	DC
S-27	5,000	771	257	500	30	DC
S-28	5,000	771	257	500	5	V1G
S-29	5,000	771	257	500	15	V1G
S-30	5,000	771	257	500	30	V1G
S-31	5,000	771	257	500	5	V2G
S-32	5,000	771	257	500	15	V2G
S-33	5,000	771	257	500	30	V2G

3.5.1 Baseline Scenarios

Two baseline scenarios establish reference points for comparison. S-01 represents the business-as-usual case with independent facility operation and no renewable energy, storage, or thermal technologies. S-01a extends this baseline to include both buildings of the system, again operating independently with no energy management coordination, serving as the reference point for total system costs. These scenarios establish the cost baseline against which all subsequent technology integration scenarios are evaluated.

3.5.2 Scenario Structure

Phase 1: Solar-Only (S-02 to S-06)

These scenarios investigate the stand-alone value of PV generation without complementary storage or flexibility technologies (Table 3.20).

Table 3.20: Phase 1: Solar-only scenarios.

Scenario	PV [m^2]
S-02	2,000
S-03	2,500
S-04	4,000
S-05	6,000
S-06	8,000

These scenarios establish the potential for PV self-consumption and grid energy reduction independent of storage. Minimal cost reductions on non-summer days due to limited winter solar generation is expected, highlighting the need for complementary storage and other flexibility measures.

Phase 2: Solar with Battery Storage (S-07 to S-15)

This phase examines the combined value of PV and BESS for peak shaving, load shifting, and improved energy self-sufficiency, without thermal decarbonization (Table 3.21).

Table 3.21: Phase 2: solar with BESS scenarios.

Scenario	PV [m^2]	BESS [kWh]	BESS [kW]
S-07	2,000	257	125
S-08	2,500	257	125
S-09	2,500	514	125
S-10	4,000	257	125
S-11	4,000	514	125
S-12	6,000	514	125
S-13	6,000	771	125
S-14	8,000	514	125
S-15	8,000	771	125

These scenarios quantify the value of BESS for peak shaving and SC optimization. Selection of an optimal combination (Combination A) is based on total system cost, SC, SS, as well as economic performance in terms of PBP and NPV.

Phase 3: Ground Source Heat Pump Integration (S-16 to S-19)

This phase explores thermal decarbonization through GSHP technology with fixed electrical and storage components, without LEC coordination (Table 3.22). Phase 3 fixes PV array size at 2,500 m^2 and BESS at 257 kWh (Combination A from Phase 2) and varies GSHP capacity.

Table 3.22: Phase 3: ground source heat pump integration scenarios.

Scenario	**PV [m^2]**	**BESS [kWh]**	**BESS [kW]**	**GSHP [kW_h]**
S-16	2,500	257	125	100
S-17	2,500	257	125	300
S-18	2,500	257	125	500
S-19	2,500	257	125	700

These scenarios assess the stand-alone techno-economic and environmental performance of GSHP technology for heating decarbonization in combination with the PV and BESS baseline. Selection of an optimal GSHP sizing (Combination B) is based on system cost, economic performance, and CO_2 emissions avoidance potential.

Phase 4: Complete LEC Operation (S-20 to S-24)

This phase integrates all three technology pillars; PV, BESS, and GSHP (fixed at 500 kW) within a fully coordinated LEC framework before evaluating EV integration (Table 3.23).

Table 3.23: Phase 4: complete LEC operation scenarios.

Scenario	**PV [m^2]**	**BESS [kWh]**	**BESS [kW]**	**GSHP [kW_h]**
S-20	2,500	257	125	500
S-21	3,500	514	125	500
S-22	5,000	514	257	500
S-23	3,500	771	125	500
S-24	5,000	771	257	500

These scenarios demonstrate the integrated operation of the complete LEC system with joint optimization of renewable generation, storage, and thermal supply across both facilities. When loads are aggregated, additional capacity of both PV and BESS is required to maintain cost-effectiveness. The optimal integrated configuration (Combination C) is selected based on total system cost, SS, SC, and economic performance (NPV and PBP). CO_2 emissions avoidance remains unchanged from Phase 3 as heating is specific to the main building.

Phase 5: EV Integration Pathways (S-25 to S-33)

Three alternative EV integration pathways are examined with increasing charging point densities (Tables 3.24, 3.25, 3.26). These represent technology alternatives overlaid on the complete LEC configuration, Combination C, which fixes the PV array size at 5,000 m^2, BESS at 771 kWh / 257 kW and GSHP at 500 kW.

Table 3.24: Phase 5: direct charging scenarios.

Scenario	PV [m^2]	BESS [kWh]	GSHP [kW$_h$]	# CP	EV Mode
S-25	5,000	771	500	5	DC
S-26	5,000	771	500	15	DC
S-27	5,000	771	500	30	DC

Table 3.25: Phase 5: smart charging scenarios.

Scenario	PV [m^2]	BESS [kWh]	GSHP [kW$_h$]	# CP	EV Mode
S-28	5,000	771	500	5	V1G
S-29	5,000	771	500	15	V1G
S-30	5,000	771	500	30	V1G

Table 3.26: Phase 5: vehicle-to-grid scenarios.

Scenario	PV [m^2]	BESS [kWh]	GSHP [kW$_h$]	# CP	EV Mode
S-31	5,000	771	500	5	V2G
S-32	5,000	771	500	15	V2G
S-33	5,000	771	500	30	V2G

These scenarios investigate the impact of EV integration strategy and charging infrastructure density on system economics and grid interaction.

Notes on Scenario Design

EV integration (S-25 to S-33) is evaluated on top of the complete LEC configuration (S-24) rather than introducing EVs at earlier phases. This approach reflects the practical reality that EV presence increases system-wide electricity demand and associated costs across all charging modes; the cost advantage derives from the charging strategy employed, not from whether EVs are present.

By sequencing LEC optimization before EV integration, we avoid combinatorial scenario explosion while preserving distinct value propositions: LEC coordination optimizes renewable integration, storage utilization, and thermal-electrical synergies for the buildings themselves, while EV charging strategy optimization determines how to manage additional vehicle charging most efficiently within the established LEC framework. Within each charging paradigm, scenarios are evaluated at three charging point densities (5, 15, and 30) to establish the relationship between infrastructure scale and system economics.

3.6 Sensitivity Analysis

Six parameters are tested across S-18 and S-31: electricity tariff level, spot price level, spot price volatility, BESS cycling cost, GSHP COP, and charging point power rating. The first five apply a continuous multiplier in the range 0.6–1.4; the charging point analysis instead uses four discrete power ratings (5, 11, 22, and 50 kW), with 11 kW serving as the reference baseline. Each parameter is varied independently while all others are held at their reference values.

3.6.1 Electricity Tariffs

A uniform multiplier (ranging from 0.60 to 1.40) is applied to consumption-specific tariffs: the electricity transmission fee and transmission health incentive. Fixed, capacity-based, and legislated charges are held constant, as these are independent of consumption level or are regulatory obligations. The analysis is applied to S-18 and S-31, serving as the reference scenarios for SAG1 and SAG2 respectively. Output metrics are total system cost, grid energy imports, and BESS discharge, reported as relative changes. Results pertaining to electricity tariffs are reported in Sections 4.5 and 4.8.

3.6.2 Spot Price Level

A uniform multiplier (ranging from 0.60 to 1.40) is applied to the full spot price profile for the simulation period, scaling all prices proportionally. This represents a scenario in which the overall electricity market price level is higher or lower than the historical 2023–2025 reference period, as may arise from shifts in hydro reservoir levels, cross-border transmission constraints, or fuel price changes. The analysis is applied to both S-18 and S-31, with total system cost, grid energy imports, and BESS discharge as output metrics, all reported as relative changes. Results pertaining to spot price level are reported in Sections 4.5 and 4.8.

3.6.3 Spot Price Volatility

Rather than shifting the mean price level, this analysis tests the sensitivity of results to changes in price volatility while keeping the mean price constant. A volatility factor α is applied to the deviations of spot prices from their temporal mean:

$$\tilde{\lambda}_t = \bar{\lambda} + \alpha \left(\lambda_t - \bar{\lambda} \right), \quad \forall t \in T \tag{3.74}$$

where λ_t is the original spot price at time-step t, $\bar{\lambda}$ is the mean spot price over the simulation period, and $\tilde{\lambda}_t$ is the modified price. A factor $\alpha > 1$ amplifies price peaks and troughs while preserving the mean, increasing the potential arbitrage value of BESS and V2G dispatch; conversely, a factor $\alpha < 1$ compresses the price distribution towards the mean, reducing the spread between high and low price periods and diminishing the incentive for flexible dispatch. Both directions are assessed: factors below unity ($\alpha \in \{0.6, 0.7, 0.8, 0.9\}$) represent a flatter price regime, while factors above ($\alpha \in \{1.1, 1.2, 1.3, 1.4\}$) reflect the expected trend of greater price variability as variable renewable generation penetration rises, with Figure 3.6 showcasing these effects. The analysis is applied to both S-18 and S-31, with total system cost, grid energy imports, and BESS discharge as output metrics, all reported as relative changes. Results pertaining to spot price volatility are reported in Sections 4.5 and 4.8.

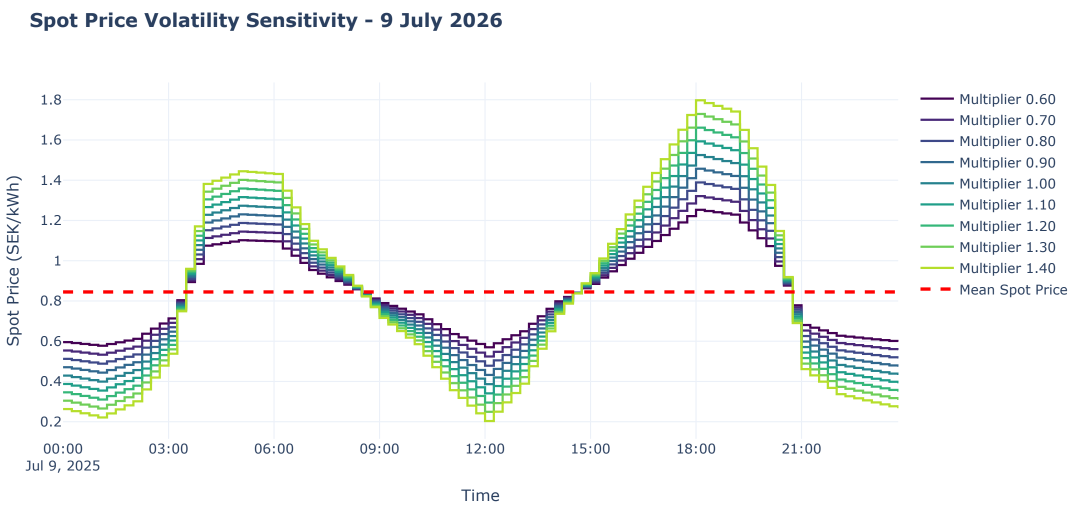

Figure 3.6: Effect of different volatility prices applied to the spot price profile.

3.6.4 BESS Cycling Cost

A multiplier (ranging from 0.60 to 1.40) is applied to the cycling cost parameter c_{cyc}, which penalises BESS throughput in the objective function to represent battery degradation wear. This analysis is applied to S-18 only, as it is the scenario in which BESS dispatch is the primary flexibility mechanism. A higher cycling cost discourages frequent charge–discharge cycles; a lower value incentivises deeper and more frequent utilisation. Total system cost, grid energy imports, and BESS discharge as output relative change are tracked, with results reported in Section 4.5.

3.6.5 GSHP Coefficient of Performance

A multiplier (ranging from 0.60 to 1.40) is applied to the full COP heating curve of the GSHP, scaling electrical-to-thermal conversion efficiency uniformly across all outdoor temperature points, capturing uncertainty in the Carnot-based COP model. A higher COP reduces the electrical consumption required to meet a given heat demand, improving the economic case for GSHP relative to district heating. The analysis is applied to S-18, with total system cost, grid energy imports, GSHP/DH utilisation rate, and avoided emissions as output metrics, all reported as relative changes. Results pertaining to GSHP COP are reported in Section 4.5

3.6.6 Charging Point Power Rating

Rather than a multiplier-based analysis this one evaluates the effect of four discrete CP power ratings (7.4, 11, 22, and 50 kW) on system performance and economics, with 11 kW serving as the reference baseline. The CP rating determines the maximum charging and discharging power per session, directly affecting the speed of EV energy exchange and the magnitude of V2G contributions to the LEC. This analysis is applied to S-31 and is reported separately from the multiplier-based SAG2 parameters. Output metrics are total system cost, grid energy imports, and BESS discharge volume, all reported as relative changes with respect to the 11 kW reference rating. Results pertaining to CP power rating are reported in Section 4.8.

4 Results

This chapter presents the results of the 34-scenario matrix, organised into five progressive phases: solar-only configurations, PV with BESS, GSHP integration, complete two-building LEC operation, and EV charging pathways (see Section 3.5). Each section reports the best-performing scenario within its phase, defined by the selection methodology in Section 3.5, and full KPI tables for all scenarios are provided in Appendix B. Sensitivity analyses on the full single-store configuration (SAG1) and the complete LEC with V2G (SAG2) follow their respective reference sections.

4.1 Model Validation

To ensure the optimisation model produces reliable results for scenario analysis, validation was conducted through energy balance verification, cost reconciliation against real billing data, and feasibility testing across diverse system configurations. It is acknowledged that the technology configurations introduced in Phases 1–5 of the scenario matrix (BESS, GSHP, and EV charging) cannot be validated against measured operational data, as none of these systems are currently installed at the case study sites. Validation is therefore limited to confirming that the model correctly represents the existing system (baseline configuration, S-01 and S-01a) and behaves consistently across the full range of simulated technology portfolios.

Energy Balance Verification

The model enforces energy balance constraints at each 15-minute time step for both electricity and thermal energy. At the electricity level, power supply from grid import, PV generation, and BESS discharge equals power demand from buildings, heating systems, CPs, and battery charging at every time-step. Similarly, thermal energy produced by the district heating system and GSHP equals total building heat demand at every time-step. These constraints are explicitly enforced in the MILP formulation (Section 3.1.7), ensuring conservation of energy across all system boundaries by construction. No post-optimization energy balance check is therefore required as satisfaction of the constraints is a prerequisite for solver feasibility.

Cost Reconciliation

The baseline scenarios (S-01 and S01a) were run using real 2025 operational data: measured load profiles, actual spot prices, and the tariff rates described in Appendix A.2, for both the main store and the secondary building. The simulated annual costs were compared against internal company billing records for the same period. The 2025 period was selected as it offers the most complete overlap between model inputs, billed data, and independently verifiable tariff schedules. Results are reported as relative deviations from billed totals, absolute values are withheld for confidentiality.

Table 4.1 summarises the cost reconciliation results. The model reproduces billed electricity costs for both buildings within 0.76 %, confirming accurate representation of spot price exposure and DSO peak power charges under real operating conditions. District heating costs for the main store show a larger deviation of approximately 10.74 %, attributable to the return water temperature reimbursement mechanism described in Appendix A.1, which is not captured in the model and results in a systematic overestimation of district heating costs. Accounting for this known omission, the total system deviation is 2.75 %, which is considered acceptable given that the same cost structure is applied uniformly across all scenarios, leaving relative comparisons between scenarios unaffected.

Table 4.1: Cost reconciliation results for the 2025 baseline scenarios.

Cost Category	**Building**	**Relative Deviation** [%]
Electricity	Main store	0.76 %
Electricity	Secondary building	0.02 %
District heating	Main store	10.74 %
Total system	**Both buildings**	**2.75 %**

Feasibility Testing and Solver Performance

The model was exercised across the full scenario matrix, varying PV capacity (0–1,000 kWp), BESS energy capacity (0–771 kWh), GSHP thermal capacity (0–700 kW), and the number of active CPs and EV charging modes. All configurations solved successfully, with no infeasible instances recorded across the full three-year simulation horizon (1,095 daily MILP instances per scenario). All daily optimisation instances converged within the specified MIP gap tolerance of 0.1 % (Section 3.1.1), confirming numerical stability across the full range of technology portfolios and operational scales.

4.2 Solar-Only Scenarios

Building on the validated base scenario (S-01), five PV system sizes corresponding to available effective areas at the main store were evaluated. Table 4.2 summarises the economic and energy performance KPIs of S-03, the largest feasible installation at 2,500 m^2 (500 kWp), achieves the best outcome across all metrics, reducing annual electricity costs by 12.8% relative to the base scenario, with a SC ratio of 100% and a PBP of 11.5 years.

Table 4.2: S-03 performance KPIs, Phase 1 best scenario.

KPI	Value	Units
SC	100	%
SS	18	%
Electricity Import Reduction	17.6	%
Electricity Cost Reduction	12.8	%
Annual Savings	429	kSEK
CAPEX	4	MSEK
NPV	1.4	MSEK
PBP	11.5	years

Figure 4.1 illustrates the mechanism behind these savings on a representative summer day. PV generation covers a large share of demand during daytime, reducing net grid import. However, the solar generation window does not coincide with the highest spot price hours, especially the evening peak price, leaving morning and evening demand peaks, which coincide with the highest spot price hours, unaddressed by solar generation alone.

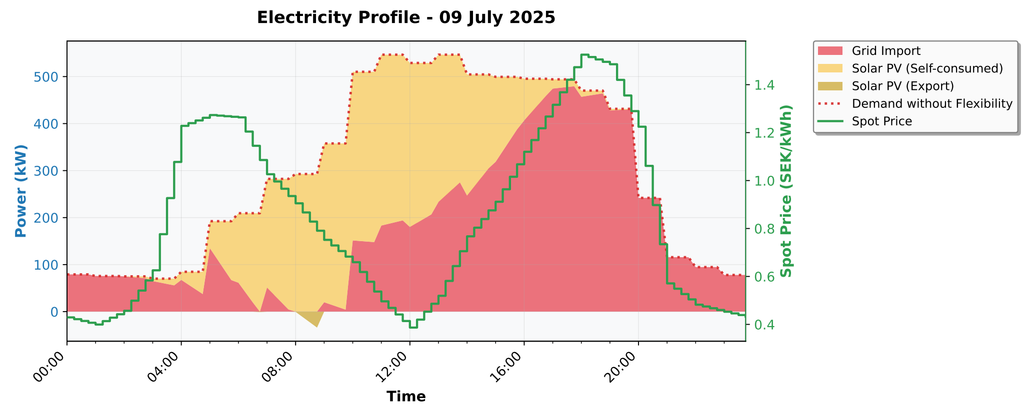

Figure 4.1: Electricity profile on a representative summer day, S-03.

On a representative winter day, however (Figure 4.2), the shortened generation window and lower solar elevation limit PV output to a marginal contribution relative to building demand, leaving the system almost entirely dependent on grid imports throughout the day. This highlights the core limitation of a solar-only configuration. In the absence of storage, the system has no mechanism to shift or buffer energy, and flexibility is effectively zero outside summer daylight hours.

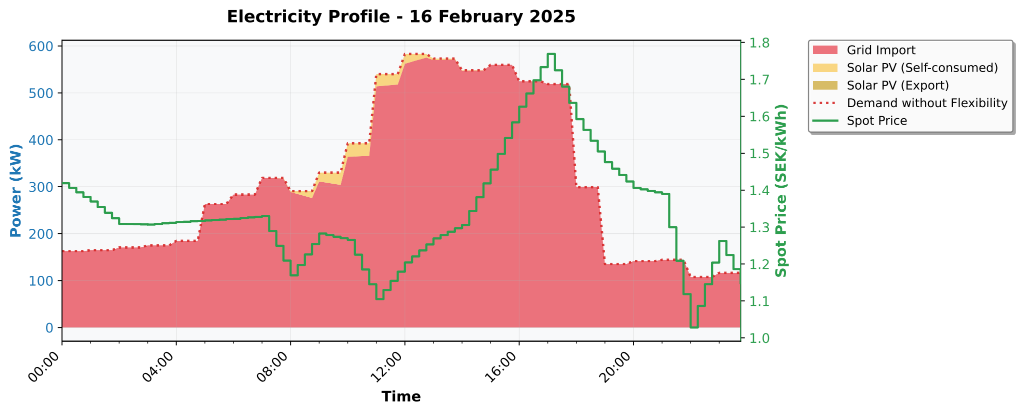

Figure 4.2: Electricity profile on a representative winter day, S-03.

4.3 Solar PV & BESS Scenarios

The solar-only analysis revealed a clear opportunity for BESS integration. While S-03 achieves full SC of on-site generation, the absence of storage means that solar-displaced grid imports are concentrated in midday hours, leaving morning and evening demand peaks (which coincide with the highest spot prices) unaddressed. To exploit this, nine scenarios combining three PV array sizes with three BESS configurations were assessed in Phase 2 of the scenario matrix. Table 4.3 summarises the KPIs for S-08 (the best-performing scenario in this phase) pairing a 2,500 m^2 (500 kWp) PV array with a 257 kWh BESS rated at 125 kW. Relative to the base scenario S-01, S-08 achieves a 14.1 % reduction in total electricity costs and maintains a self-consumption ratio of 100 %, matching S-03. The CAPEX addition of the BESS extends the PBP by approximately one year relative to S-03, with a positive NPV.

Table 4.3: S-08 performance KPIs, Phase 2 best scenario.

KPI	Value	Units
SC	100	%
SS	17.6	%
Electricity Import Reduction	17.6	%
Electricity Cost Reduction	14.1	%
Annual Savings	475	kSEK
CAPEX	4.7	MSEK
NPV	0.8	MSEK
PBP	12.4	years

Figure 4.3 illustrates the BESS dispatch strategy on a representative summer day. During low-price overnight hours, the BESS charges from the grid, building stored energy ahead of the opening of the sore. At store opening, it discharges in complement with solar generation, enabling the building to operate with minimal grid imports for several hours. As solar irradiance peaks around midday and spot prices fall, the BESS recharges from surplus PV generation. It then discharges again into the evening peak period, when spot prices recover and solar generation ceases, the precise interval that the solar-only scenarios were unable to address.

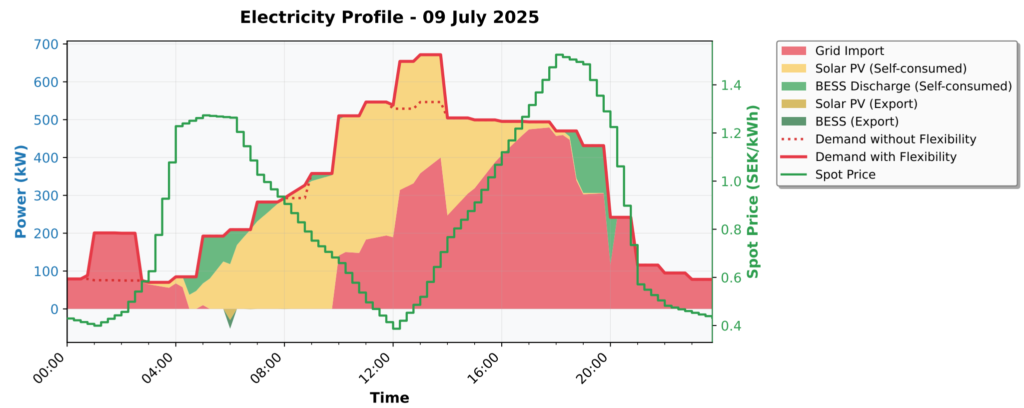

(a) Electricity profile on a representative summer day, showing PV generation, grid imports, and net building demand.

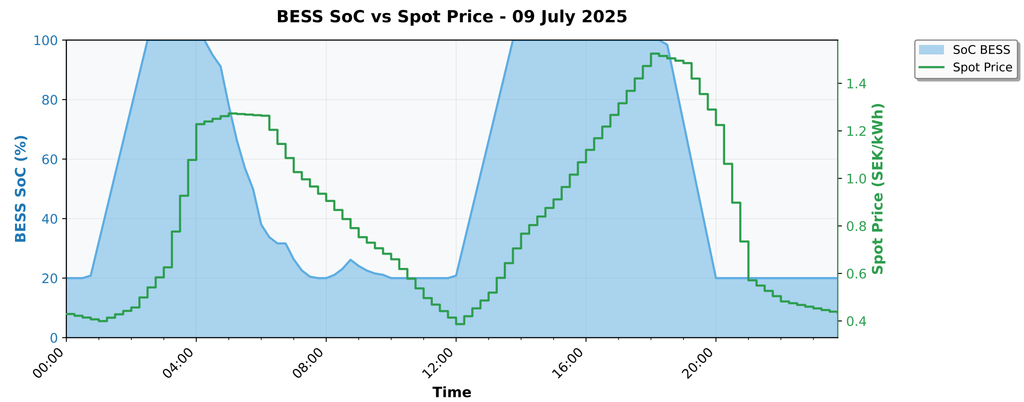

(b) BESS SoC against the spot price profile on a summer day.

Figure 4.3: Operational dispatch of scenario S-08 on a representative summer day, showing the interplay between PV generation, BESS arbitrage, and grid interaction under the Swedish day-ahead spot price signal.

On a representative winter day (Figure 4.4), the absence of meaningful PV generation removes the midday charging opportunity that drives arbitrage in summer. The BESS instead charges during the noon low-price window and only discharges to the single highest-price peak of the day, reflecting a more conservative dispatch regime dictated by the winter price profile.

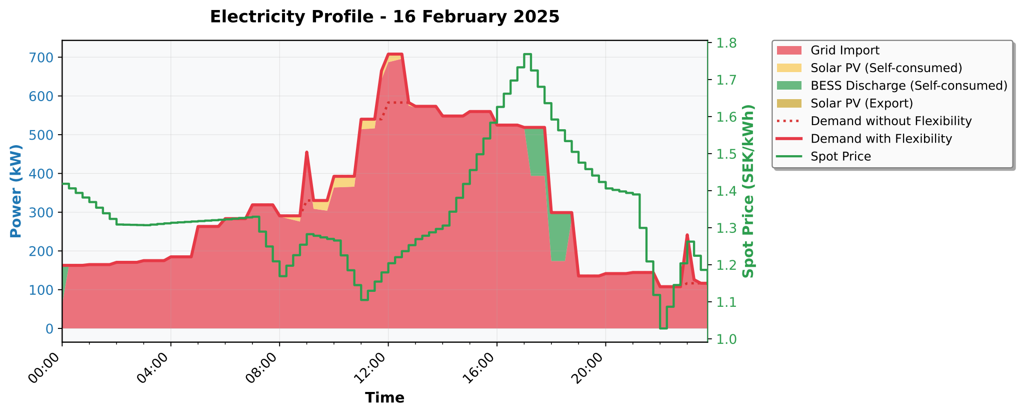

(a) Electricity profile on a representative winter day, showing PV generation, grid imports, and net building demand.

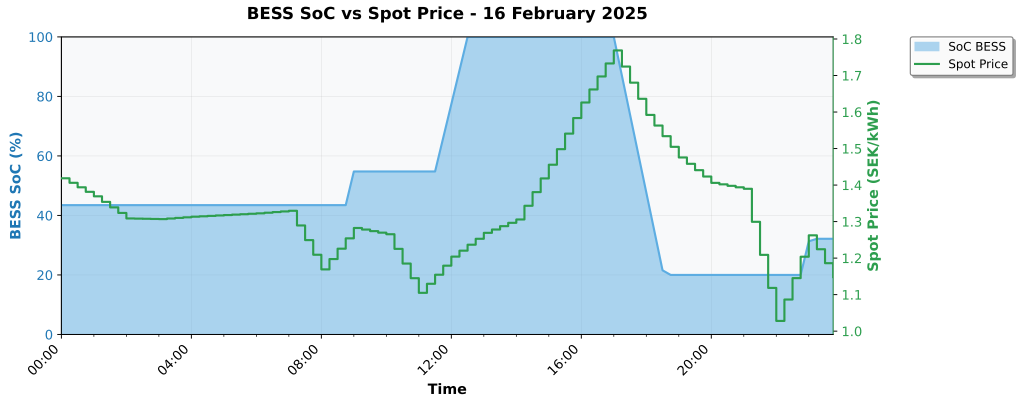

(b) BESS SoC against the spot price profile on a winter day.

Figure 4.4: Operational dispatch of BESS on a representative winter day, showing the interplay between marginal PV generation, BESS arbitrage, and grid interaction under the Swedish day-ahead spot price signal.

4.4 GSHP Integration Scenarios

Four scenarios varying GSHP thermal capacity were assessed on top of S-08 in Phase 3 of the scenario matrix. S-18, equipped with a 500 kW GSHP, delivers the best overall performance across all metrics and is reported in Table 4.4. The GSHP introduces an additional electrical load, increasing grid imports by approximately 15 % relative to S-08. However, by displacing the most expensive tier of the two-part DH tariff structure, it achieves a 14 % reduction in total energy costs compared to S-01 and avoids 67 % of CO_2 emissions, yielding a PBP of 9.6 years and a positive NPV.

Figure 4.5 illustrates the GSHP dispatch on a representative winter day. The DH connection covers the base thermal load continuously, while the GSHP activates to serve demand peaks, operating as a top-up supply. However, this peak-covering operation introduces a constraint: the additional electrical load from the GSHP compressor risks pushing net grid imports above the contracted capacity threshold,

Table 4.4: S-18 performance KPIs, Phase 3 best scenario.

KPI	Value	Units
SC	100	%
SS	17.6	%
CO_2 Avoidance	66.7	%
Electricity Import Reduction	2	%
Electricity Cost Reduction	3	%
Heat Cost Reduction	34	%
Annual Savings	736	kSEK
CAPEX	5.9	MSEK
NPV	3.2	MSEK
PBP	9.6	years

triggering DSO peak penalties. The optimiser therefore balances thermal peak coverage against electrical peak exposure, deploying the GSHP selectively during intervals where the incremental compressor load does not cause a new grid import peak.

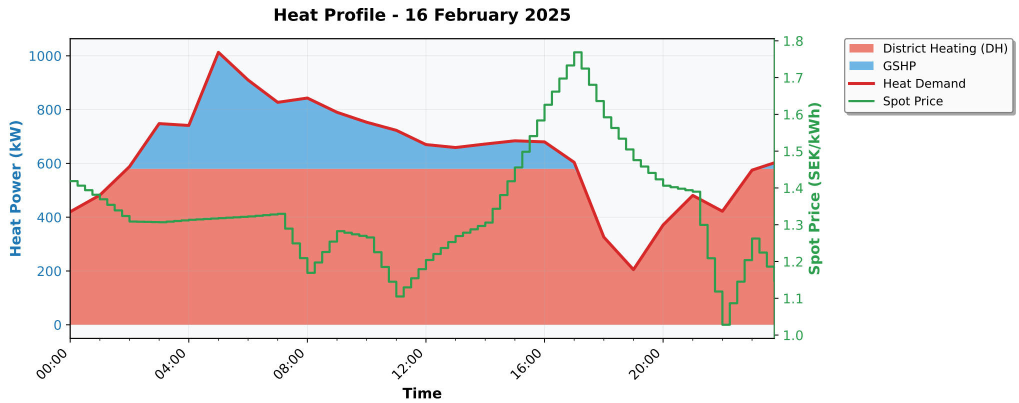

Figure 4.5: Thermal supply profile on a representative winter day, S-18.

4.5 Sensitivity Analysis on Full Store Operation

S-18 represents the most complete single-building configuration modelled, integrating PV, BESS, and GSHP, and serves as the reference point for the first sensitivity analysis group (SAG1). Five parameters are varied independently across the range 0.6×–1.4× their baseline values: electricity tariffs (SA-1), spot price level (SA-2), spot price volatility (SA-2a), BESS cycling cost (SA-3), and GSHP coefficient of performance (SA-5). Figures 4.6 to 4.8 report the relative change in total energy cost, energy imports, and BESS discharge respectively across all five parameters.

Total Energy Cost

Spot price level (SA-2) produces the largest response, with total costs ranging from approximately $-13\,\%$ at 0.6× to $+12\,\%$ at 1.4× relative to the S-18 baseline. The GSHP coefficient of performance (SA-5) yields a moderate effect in the opposing direction, reaching approximately +4 % at 0.6× and −3 % at 1.4×. Electricity tariffs (SA-1), spot price volatility (SA-2a), and BESS cycling cost (SA-3) all remain within ±2 % across the full range.

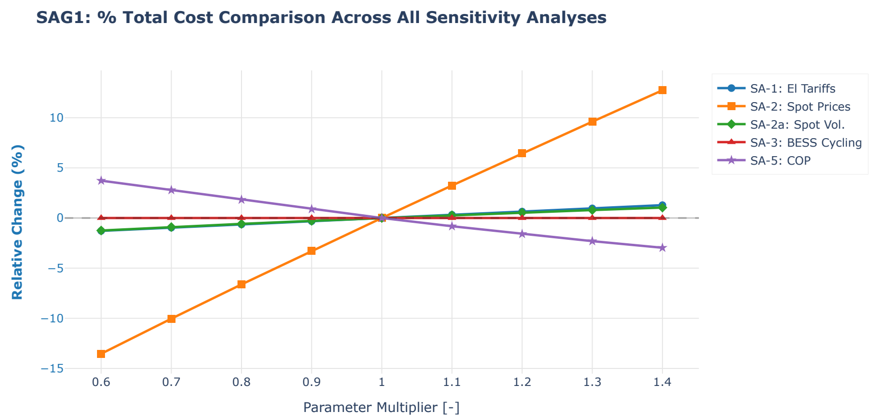

Figure 4.6: SAG1: relative change in total energy cost across all sensitivity parameters. Reference scenario: S-18.

Electricity Imports

All parameters produce changes below ±5 % in energy imports. Spot price level (SA-2) shows a quasi-linear decreasing response, reaching approximately −3 % at 1.4×. The COP sensitivity (SA-5) exhibits a non-linear profile, with imports rising sharply by approximately +3.3 % at 0.6× and flattening above the baseline. Spot price volatility (SA-2a) produces a small symmetric response peaking at ±1 %. Electricity tariffs (SA-1) and BESS cycling cost (SA-3) show negligible variation throughout.

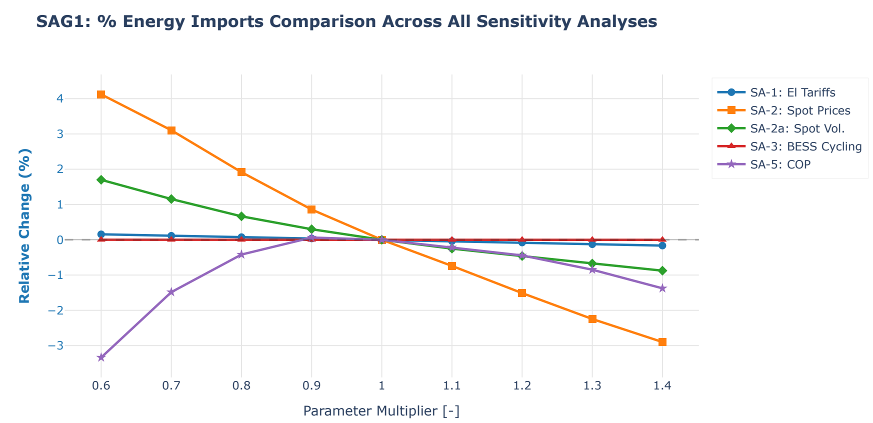

Figure 4.7: SAG1: relative change in electricity imports across all sensitivity parameters. Reference scenario: S-18.

BESS Discharge

Spot price volatility (SA-2a) produces the largest range of any parameter in SAG1, with BESS discharge increasing by approximately +18 % at 1.4× and decreasing by −22 % at 0.6×. Spot price level (SA-2) has a secondary positive effect, reaching approximately +8 % at 1.4×. Electricity tariffs (SA-1), BESS cycling cost (SA-3), and COP (SA-5) all remain within ±1 % across the full parameter range.

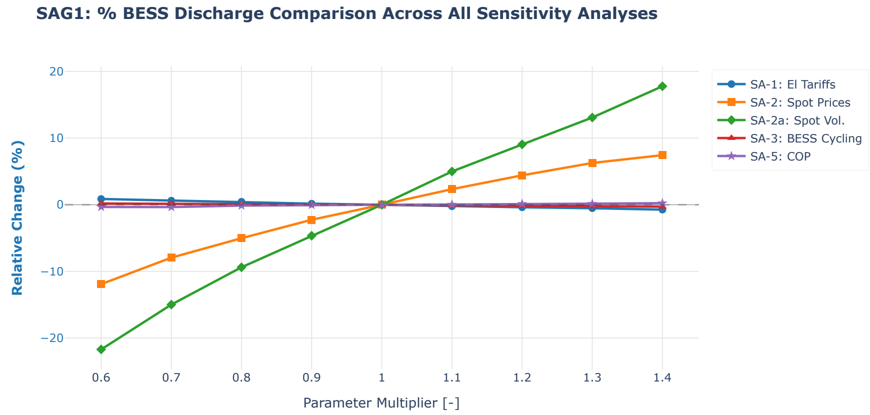

Figure 4.8: SAG1: relative change in BESS discharge across all sensitivity parameters. Reference scenario: S-18.

4.6 Complete LEC Operation Scenarios

The Phase 4 scenarios extend the S-18 configuration to the two-building LEC boundary, adding the secondary store and scaling PV and BESS capacity to community level. In addition to the inter-building energy sharing connection, these scenarios test expanded PV and BESS capacities at the community level. Table 4.5 summarises the KPIs for S-24, the best-performing scenario in Phase 4, pairing a 5,000 m^2 (1,000 kWp) PV array with a 771 kWh BESS rated at 257 kW.

Table 4.5: S-24 performance KPIs, Phase 4 best scenario.

KPI	Value	Units
SC	100	%
SS	10.5	%
Electricity Import Reduction	5.7	%
Electricity Cost Reduction	5.6	%
Annual Savings	1.3	MSEK
CAPEX	11.4	MSEK
NPV	3.4	MSEK
PBP	11.1	years

Relative to the two-building base scenario (S-01a), S-24 achieves a 5.6% reduction in total electricity costs and a 5.7% reduction in energy imports, maintaining a SC ratio of 100 %. After doubling the installed PV capacity and tripling the BESS capacity relative to S-08, the scenario yields a PBP of 11.1 years and a positive NPV of 3.4 MSEK, with annual savings of 1.3 MSEK.

4.7 EV Charging Integration Pathways

EV charging introduces additional electrical demand whose magnitude depends on the number of charging points and sessions, but most critically on the charging mode. The final nine scenarios (Phase five) build on S-24 to assess three charging modes: DC, V1G , and V2G across three charging point densities (10, 20, and 30 CPs). Table 4.6 reports the KPIs for S-27, S-30, and S-33, corresponding to the 30 CP configuration in each mode, selected to enable direct mode comparison at maximum fleet size. Reducing the number of charging points produces a near-linear scaling of all reported metrics, the full results across all nine scenarios are provided in Appendix B. All three modes increase grid imports relative to S-24, reflected in negative import reduction values, as the EV fleet adds net electrical demand regardless of dispatch flexibility. However, the cost and savings outcomes diverge across modes: DC (S-27) incurs the highest import increase (3.6 %) and the largest cost penalty (2.2 %) relative to S-24, while V2G (S-33) limits the cost impact to 0.2 % and achieves the lowest annual cost increase of 24 kSEK.

Table 4.6: S-27, S-30, and S-33 performance KPIs, Phase 5 - 30 CP.

KPI	**S-27**	**S-30**	**S-33**	**Units**
Charging Mode	DC	V1G	V2G	-
Self-Consumption	100	100	100	%
Self-Sufficiency	10	10.3	10.2	%
Electricity Import Increase	3.6	2.5	2.7	%
Electricity Cost Increase	2.2	1	0.2	%
Annual Savings (S-24)	-289	-104	-24	kSEK

Figures 4.9 to 4.11 illustrate the flexibility asset dispatch on the same representative summer day across the three charging modes. In S-27 (DC), EV charging is uncontrolled and distributed relatively uniformly throughout store opening hours. In S-30 (V1G), the optimiser redistributes EV charging away from the evening hours towards the lower-price morning and midday window, visibly reducing the orange V2G charging contribution during the late afternoon peak. In S-33 (V2G), bidirectional operation introduces discharge events below zero: EVs inject power back into the LEC during the late-evening spot price peak (around 20:00), supplementing BESS discharge.

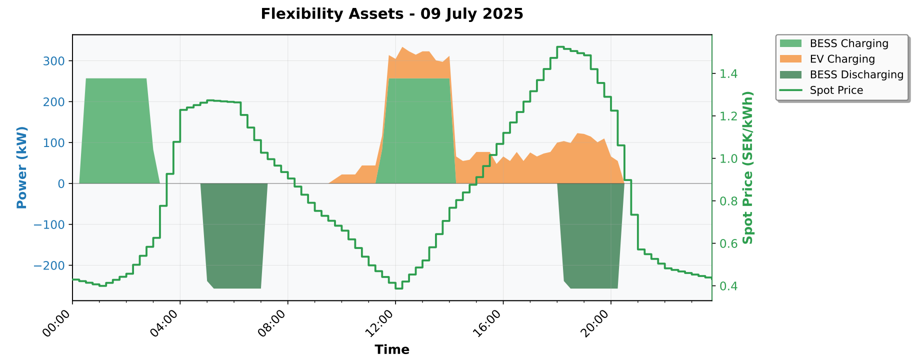

Figure 4.9: DC behaviour on a representative summer day, S-27 (DC, 30 CP).

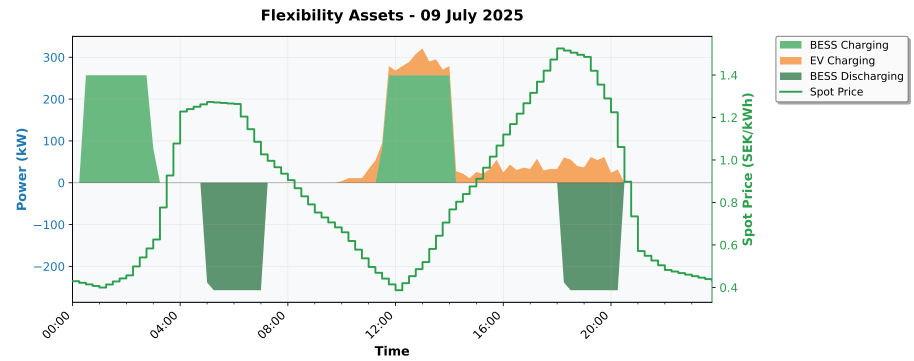

Figure 4.10: V1G behaviour on a representative summer day, S-30 (V1G, 30 CP).

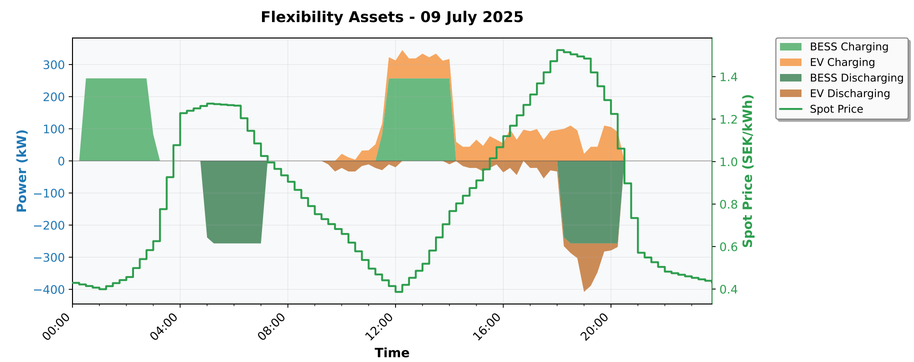

Figure 4.11: V2G behaviour on a representative summer day, S-33 (V2G, 30 CP).

4.8 Sensitivity Analysis on LEC with EV Charging

S-31 is the complete LEC configuration with V2G charging at 5 charging points, and serves as the reference scenario for the second sensitivity analysis group (SAG2). As defined in Section 3.6, SAG2 covers three market and tariff parameters only: electricity tariffs (SA-1), spot price level (SA-2), and spot price volatility (SA-2a). Each parameter is varied independently across 0.6×–1.4× its baseline value. An additional stand-alone analysis (SAG2-3) examines the effect of V2G charger power rating across discrete CP rating values of 5, 11, 22, and 50 kW. Figures 4.12 to 4.14 report the relative change in total energy cost, energy imports, and BESS discharge across the three multiplier-based parameters. Figure 4.15 reports the response to CP rating variation.

Total Energy Cost

Spot price level (SA-2) is the dominant driver of total cost in SAG2, producing a near-linear response ranging from approximately −17 % at 0.6× to +16 % at 1.4×, while electricity tariffs (SA-1) and spot price volatility (SA-2a) both remain within ±1.5 % across the full range, with their responses overlapping closely throughout.

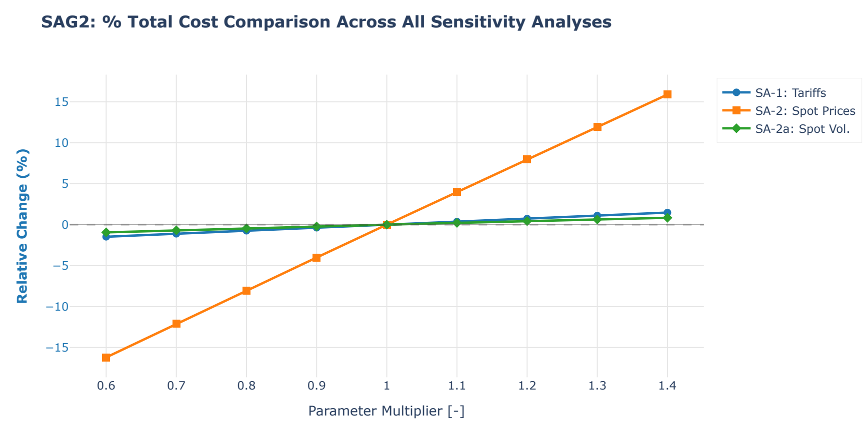

Figure 4.12: SAG2: relative change in total energy cost across sensitivity parameters. Reference scenario: S-31.

Electricity Imports

Spot price level (SA-2) produces a quasi-linear decreasing import response, from approximately +1.3 % at 0.6× to −0.9 % at 1.4×.Furthermore, spot price volatility (SA-2a) follows a similar trend at a slightly reduced magnitude, reaching approximately +0.5 % at 0.6× and −0.3 % at 1.4×. Electricity tariffs (SA-1) show negligible variation throughout.

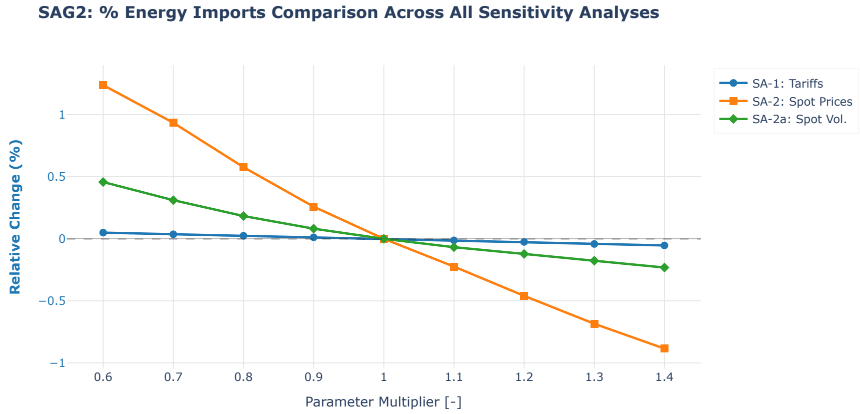

Figure 4.13: SAG2: relative change in electricity imports across sensitivity parameters. Reference scenario: S-31.

BESS Discharge

Spot price volatility (SA-2a) is the dominant driver of BESS discharge, ranging from approximately −22 % at 0.6× to +17 % at 1.4×. Additionally, spot price level (SA-2) produces a secondary response of similar shape but smaller magnitude, reaching approximately −12 % and +7 % at the respective extremes. Electricity tariffs (SA-1) remain within ±1 % .

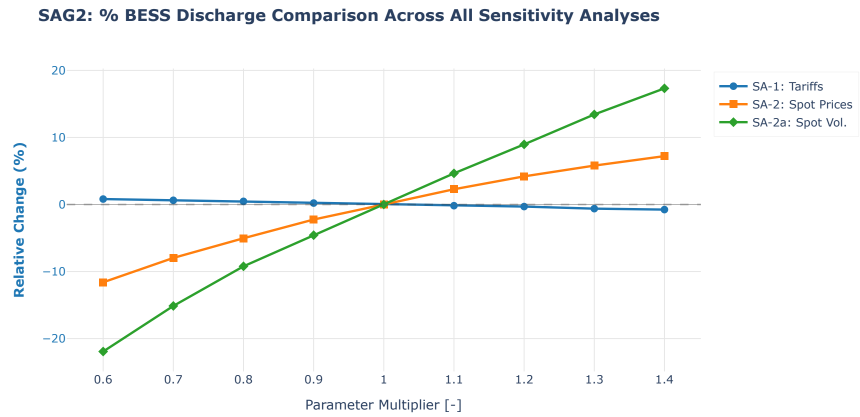

Figure 4.14: SAG2: relative change in BESS discharge throughput across sensitivity parameters. Reference scenario: S-31.

Charging Point Power Rating

Figure 4.15 reports the effect of CP power rating on the three metrics for S-31. Total cost decreases as CP rating increases, falling by approximately 0.6 % at 50 kW relative to the 11 kW baseline. Energy imports and BESS discharge both increase with higher CP ratings, reaching approximately +0.25 % and +0.175 % respectively at 50 kW. At the lowest rating of 5 kW, total cost rises slightly above baseline while imports fall marginally, reflecting the reduced V2G discharge capacity available at lower power ratings.

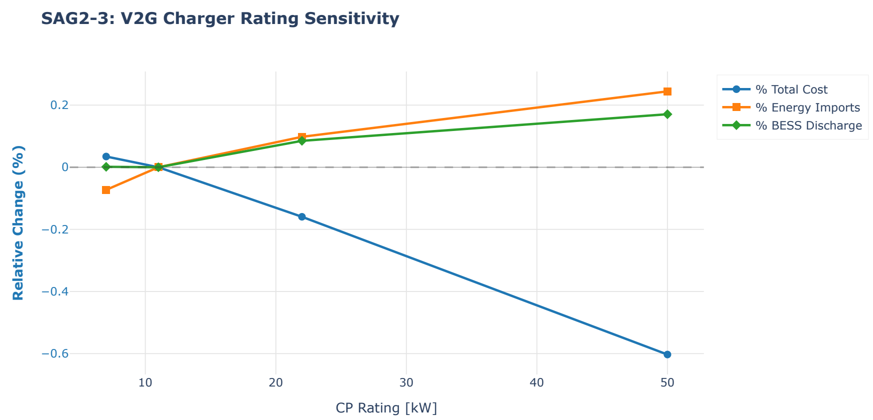

Figure 4.15: SAG2: relative change in total cost, energy imports, and BESS discharge as a function of V2G charger power rating. Reference scenario: S-31 11 kW baseline rating).

5

Discussion

This chapter interprets the results presented in Chapter 4, evaluating the techno-economic and environmental performance of each technology phase against the research questions defined in Section 1.3.1. The discussion follows the same progressive structure as the scenario matrix, moving from solar-only configurations through full LEC operation with EV charging integration, before addressing the GSHP investment case and the implications of the sensitivity analysis. Complete scenario and sensitivity results for all 34 scenarios are reported in Appendix B.

5.1 Techno-Economic Performance

Adding solar PV to the main building naturally displaces electricity imports during daytime hours, shifting residual grid dependency towards the morning and evening periods when irradiance is absent. Reviewing the results of the solar-only scenarios (S-02 to S-06), reported in Appendix B.1.2, larger installed capacities progressively increase generation volume and drive SS consistently upward. SC follows a different trajectory: the ratio increases up to the solar tax threshold at 500 kWp, beyond which it declines. Once this threshold is crossed, every kilowatt-hour of solar generation that is self-consumed becomes subject to the full electricity tax. The optimiser must therefore weight self-consumption against grid export on a time-step basis: when the spot price is sufficiently high, selling to the grid yields a net profit, making export the preferred option over self-consumption. This price-dependent dispatch behaviour explains the decline in SC beyond the threshold, and is confirmed by the electricity cost breakdown, where income from the transmission health incentive grows by approximately one order of magnitude between S-03 and S-04 (see Table B.2), while electricity supply costs decrease as grid imports are progressively displaced.

Considering only SC, SS, and operational costs, larger systems would appear unconditionally attractive. However, when economic performance is assessed, exceeding the 500 kWp threshold is not financially viable. The deterioration is not driven by electricity costs, which continue to fall, but by the compounding effect of higher CAPEX, O&M costs, and tax penalties that increasingly erode the NPV and push the PBP close to the assumed system lifetime of 30 years for PV. This establishes a clear economic optimum precisely below the solar tax threshold (S-02), where financial performance is maximized. However, if SS is factored into the decision, a gain of 4% justifies an increased PBP of 0.1 years, making S-03 the preferred option.

As established in Section 4.2, a solar-only configuration captures daytime import displacement but leaves morning and evening demand peaks, which coincide with the highest spot prices, unaddressed. BESS closes this gap by charging during low-price midday hours and discharging into the high-price periods that solar generation alone cannot reach, directly addressing the first research question regarding the economic and operational value of integrating BESS with on-site solar PV.

Reviewing the results of scenarios S-07 to S-15, reported in Appendix B.1.3, SS and SC follow a similar pattern to the solar-only cases with respect to installed PV capacity. An interesting divergence appears, however, when examining the transmission health incentive income across equivalent PV capacities with and without BESS. Below the 500 kWp threshold, scenarios with BESS report lower incentive income than their solar-only counterparts, as the optimiser preferentially dispatches stored energy during high-price evening periods rather than exporting it. Above the threshold, the relationship inverts: with the full electricity tax applying to every kilowatt-hour of SC, the optimiser identifies additional arbitrage opportunities through storage, holding energy to maximise export revenue at peak price moments, which increases incentive income relative to the solar-only equivalent.

A notable operational pattern emerges around midday, when spot prices are at their lowest and direct PV generation covers most of the store demand. The BESS charges during this window, drawing additional power from the grid and transiently increasing electricity import peaks relative to the base case. Crucially, these peaks remain below the contracted capacity threshold, avoiding DSO peak power penalties. The net effect is a reduction in total electricity costs, driven not by peak shaving but by the cost-effective dispatch of stored energy into high-price evening hours.

Across the scenario matrix, larger PV and BESS capacities generally yield greater grid import reductions (see Table B.3), directly addressing the second research question on self-sufficiency and grid import reduction. However, when BESS capacity is varied at a fixed PV array size and power rating, grid import reductions remain unchanged, indicating that the binding constraint is the power rating rather than the energy capacity. From a cycling perspective, larger BESS capacities exhibit lower cycle counts over the simulation period than smaller ones. For example, a 771 kWh system completes up to 980 full equivalent cycles, compared to approximately 1,130 for a 514 kWh system and 1,260 for a 257 kWh system. This inverse relationship between capacity and cycling intensity is expected, as a larger battery distributes the same daily energy throughput across a greater usable capacity. In all cases, annual cycle counts remain well within the threshold assumed for battery lifetime estimation.

Regarding economic performance, the pattern established in the solar-only analysis repeats, costs decrease up to the 500 kWp threshold, rise above it, and fall again at higher capacities, this time driven by price arbitrage and increased export revenue rather than import avoidance. The best-performing economically viable scenario remains S-08, positioned precisely at the solar tax threshold, achieving a PBP of 12.4 years (approximately one year longer than the best solar-only scenario) reflecting the additional BESS CAPEX. S-09, with double the battery capacity, delivers meaningfully higher annual savings but also doubles the CAPEX and O&M costs, extending the PBP to 13.7 years. Combined with no improvement in grid import reduction and marginally higher cycle wear, S-09 underperforms S-08 in the overall techno-economic assessment.

A key strategic objective for the main store is to reduce its dependency on the DH network, whose equivalent CO_2 emissions are tied to the DSO's fuel mix and cannot be directly controlled by the company, limiting the scope for further improvements in carbon accounting. Scenarios S-16 to S-19, with complete results reported in Table B.4, address this directly, providing the evidence base for the third research question: whether replacing DH with a GSHP is economically attractive under Swedish market conditions. Testing increasing GSHP capacities as a means of displacing DH supply, the results show that this substitution carries both an environmental and an economic incentive: since a heat pump delivers COP times more thermal energy per unit of electricity consumed than DH, displacing it with GSHP reduces overall energy costs provided the electricity tariff is sufficiently low relative to the DH tariff. It should be noted that electricity-related emissions are not accounted for in this analysis, as the company holds mechanisms to offset these, effectively achieving carbon neutrality on the electricity side.

Integrating a GSHP increases the site's total electricity consumption, driving electricity costs up to approximately 98% of the base case level for the largest 700 kW system, almost completely offsetting the gains achieved by PV and BESS in earlier phases. However, this is not the complete picture as DH costs fall by up to 35% relative to the S-08 configuration for the largest GSHP assessed, translating to a reduction of approximately 14% against the base case and around 6% against S-08 in total energy cost terms.

The mechanism behind these savings lies in the GSHP's operational role, rather than serving the base thermal load, the GSHP is dispatched to cover demand peaks, pushing DH back to a continuous base load. This avoids the peak tier of the two-part DH tariff structure in most operating hours, which accounts for the substantial cost reduction. On the electrical side, the optimiser consistently approaches the contracted capacity threshold without exceeding it, deploying the GSHP selectively during intervals where the incremental compressor load does not trigger a DSO peak power penalty. This constraint explains why total energy savings grow considerably up to a GSHP capacity of 300 kW (S-17), but plateau beyond that point, as larger capacities cannot operate at full load for proportionally more hours without breaching the electrical peak limit, dampening the marginal gain in thermal displacement and energy savings.

From an economic standpoint, S-17 delivers the lowest PBP of 9.5 years across all scenarios assessed to this point, lower even than the best solar-only configuration, driven by the volume of combined electricity and DH savings. However, when CO_2 emission avoidance is brought into the assessment, S-18 emerges as the preferred configuration in direct response to the third research question. While it does not achieve the largest absolute savings, it avoids approximately 12% more emissions than S-17, at a trade-off of only 0.1 years increase in PBP. At this capacity, the system avoids approximately 66.7% of baseline emissions while remaining the most economically attractive configuration when both financial and environmental performance are considered jointly, confirming that GSHP integration is not only environmentally justified but economically compelling under the Swedish market and DH tariff conditions of this case study.

With all static flexibility measures implemented and evaluated for the main store, the analysis is extended to a two-building LEC comprising the main store and its higher-load neighbouring facility, returning to the first research question to assess how LEC participation shapes the benefits already established at single-building level. Scenarios S-20 to S-24, with complete results reported in Appendix B.1.5, not only assess the operational and economic impact of connecting both buildings under a shared energy management framework, but also explore expanded PV array and BESS configurations (including higher power ratings) to ensure that the flexibility potential of the larger combined load is not left unrealised. The two-building baseline for this phase is S-01a, which simulates both stores operating independently without any flexibility technologies.

The extension to a two-building LEC raises the solar self-consumption tax threshold to 1,000 kWp, and the scenarios are designed to explore PV and BESS combinations up to this limit. Given the lessons from the first two phases, exceeding the threshold yields economically unattractive results, so these scenarios focus instead on expanding BESS configurations within the feasible range. CO_2 emissions remain unchanged across this phase, as the GSHP capacity is fixed from S-18. SC remains at 100% throughout, as virtually all on-site generation is consumed within the community. SS decreases relative to the single-building cases, as the secondary store's additional load dilutes the impact of larger PV and BESS systems.

As expected from earlier phases, higher BESS power ratings yield greater SS and higher cycling, with cycle counts remaining well within the annual threshold assumed for battery lifetime preservation. Higher power ratings also increase total system electricity peaks, as the BESS can exchange energy at a faster rate, producing more pronounced but short-duration import spikes during charging intervals.

In terms of energy performance, total electricity imports are reduced by up to 5.7% in S-24, the configuration with the highest installed PV and BESS capacities, contributing to the second research question at community scale. S-20, which connects both buildings without expanding flexibility resources, reduces imports by only 0.7%, confirming that the inter-building connection alone provides limited benefit and that additional flexibility capacity is needed to realise the community's potential. Annual energy cost savings range from approximately 6% to 10% across the five scenarios relative to S-01a, which is lower than the reductions achieved in the single-building configurations. This reflects the higher absolute cost base introduced by the secondary store, but the LEC framework nonetheless delivers a net benefit to the combined system that neither building could achieve independently.

From an economic standpoint, connecting the secondary building without additional flexibility (S-20) already reduces the system PBP slightly, confirming a baseline benefit from coordinated operation. Expanding to larger PV and BESS capacities increases the PBP by approximately one year for the smallest LEC configurations and up to 1.5 years for the largest, relative to S-18. Critically, these costs are shared across both participants: by jointly owning and benefiting from the expanded infrastructure, both stores can split CAPEX and O&M obligations, making the investment considerably more attractive than if either building pursued the same configuration independently.

The best-performing scenario across the combined set of metrics is S-24. While it carries one of the longer PBP within this phase, it achieves the highest total energy cost savings and maintains a SS ratio of approximately 10.5% (higher than all other LEC configurations) making it the recommended configuration for the complete two-building system prior to EV integration.

The progressive electrification of road transport introduces a double-edged challenge for building energy systems: while EVs represent a growing source of flexible storage capacity, an uncontrolled charging fleet imposes additional and often poorly-timed electricity demand that can erode the cost savings achieved by on-site generation and storage, and in dense deployment scenarios, risk triggering DSO peak power penalties. Managing how and when EVs charge is therefore not merely an optimisation opportunity, it is an operational necessity as fleet sizes grow.

With the complete LEC configuration established in S-24, scenarios S-25 to S-33 assess how three EV charging modes across three CP densities affect the operational economics of the system (full results are reported in Appendix B.1.6). Since EV charging increases energy imports and costs regardless of mode, these scenarios are benchmarked against S-24 rather than the baseline S-01a, isolating the net impact of EV integration on an already optimised system.

Direct Charging (S-25 to S-27)

In uncontrolled DC mode, EVs draw power from the grid as soon as they connect, with no coordination with system dispatch. Electricity imports increase from 0.6% at the lowest CP density to 3.6% at the highest, reducing annual savings relative to S-24 by between 4% and 23%. The net EV charging cost ranges from 106 to 630 kSEK depending on CP density. EV energy demand as a share of total system consumption ranges from 0.7% to 3.9%. These results illustrate the risk of unmanaged charging: at high CP densities, the coincidence of EV demand with building peaks can substantially deteriorate system economics and, if the contracted capacity threshold were approached, trigger peak power penalties.

A notable consequence of uncontrolled DC charging is its effect on CO_2 avoidance. As EV load scales up, the inflexible and simultaneous nature of DC charging saturates the system, pushing total demand towards the contracted capacity threshold. To avoid peak penalty charges, the optimiser is forced to curtail the GSHP dispatch, reducing its utilisation rate to as low as 60% at 30 charging points compared to 66.7% in the GSHP-only reference (see Table B.6). This creates a direct trade-off between EV charging scale and thermal decarbonisation, as the GSHP is partially displaced by district heating to accommodate the additional electrical load within the capacity constraint.

This limitation is effectively resolved by smart and bidirectional charging modes. Under V1G and V2G, the optimiser redistributes charging demand away from peak-risk periods, preserving sufficient headroom for full GSHP operation. As a result, DH displacement remains at 67% across all V1G and V2G scenarios regardless of fleet size, recovering the CO_2 avoidance performance lost under DC charging and reinforcing the case for controllable EV flexibility as a complement to thermal electrification.

Smart Charging (S-28 to S-30)

Introducing demand-responsive V1G allows the optimiser to shift EV charging towards low-price, low-demand intervals, avoiding the cost penalties of uncontrolled coincident demand. Electricity imports increase from only 0.4% at the lowest CP density to 2.5% at the highest, and annual savings are reduced by just 1% to 8% relative to S-24, a marked improvement over DC at every density level. The net EV charging cost falls to between 60 and 360 kSEK, and EV energy as a share of total demand ranges from 0.4% to 2.3%, reflecting the more efficient temporal allocation of charging load.

Vehicle-to-Grid (S-31 to S-33)

V2G extends the smart charging logic by enabling bidirectional energy exchange: EV batteries charge beyond their immediate session requirement during low-price intervals and discharge a portion of that energy back into the system during high-price periods, in exactly the same way a stationary BESS would. Approximately 34% of the energy charged is subsequently discharged back into the LEC, performing price arbitrage and reducing grid imports at the most expensive hours. This mechanism brings the net EV charging cost to between 60 and 360 kSEK (identical to V1G), but achieves the lowest system cost impact of any charging mode, reducing annual savings relative to S-24 by only 0.3% to 2%. Electricity imports increase from 0.5% to 2.7% across CP densities, and EV energy as a share of total demand ranges from 0.6% to 3.8%.

Conceptually, V2G transforms the EV fleet into a distributed, mobile battery system that participates in community-level energy management. Unlike a stationary BESS, however, EV batteries are not always available, their dispatch is constrained by session presence, departure deadlines, and the need to respect minimum departure SoC requirements. This intermittency limits the degree to which V2G can replicate stationary storage, but the results demonstrate that even with a modest fleet at low CP densities, the flexibility contribution is meaningful and the cost impact of integrating EVs into the LEC can be reduced to near-negligible levels.

Taken together, these scenarios provide a direct answer to the first research question: integrating BESS with solar PV and progressive EV charging flexibility delivers measurable and scalable economic and operational benefits. V2G in particular converts what would otherwise be a cost burden into an active flexibility resource, one that becomes increasingly valuable as both EV penetration and electricity price volatility continue to rise.

5.2 Sensitivity Analysis Implications

5.2.1 SA on Main Store Operation

The first sensitivity analysis group (SAG1) evaluated five parameters against the full single-store configuration S-18, which integrates PV, BESS, and GSHP. The results reveal a clear hierarchy of influence across the three tracked metrics, with spot price level and volatility emerging as the dominant drivers, and GSHP COP producing a meaningful but secondary effect. Full results are reported in Appendix B.

Spot Price Level

Spot price level produces the largest response in total system cost across all parameters tested, with a near-linear relationship across the full multiplier range. This is an expected but important finding: a higher market price level directly inflates the cost of every kilowatt-hour imported from the grid, and Sweden, despite its high share of low-cost hydropower and nuclear generation, is not insulated from sustained price increases. Prolonged dry years reducing reservoir levels, exceptionally cold periods driving demand spikes, and increasing cross-border electricity trade with higher-price markets are all plausible mechanisms through which the average price level could shift upward over the system's lifetime. Under such conditions, the optimiser responds by reducing grid imports and increasing BESS dispatch, widening the arbitrage margin and shaving more expensive peak demand. The secondary positive effect on BESS discharge confirms that higher price levels not only raise costs but also improve the economic case for storage utilisation, partially offsetting the cost increase.

Spot Price Volatility

Spot price volatility, while leaving the mean price unchanged, produces the largest response of any parameter on BESS discharge, with discharge increasing by approximately 18% at the highest volatility factor and decreasing by almost 22% at the lowest. The mechanism is the following: wider price spreads create deeper and more frequent arbitrage opportunities, incentivising the optimiser to charge more aggressively at price troughs and discharge more at peaks. The dampening effect on energy imports under high volatility is consistent with this behaviour, when electricity prices spike, the optimiser partially substitutes GSHP operation with district heating where the DH tariff is more stable and cost-competitive, reducing electricity consumption at the added price of increasing CO_2 emissions. Conversely, under low volatility, the price spread narrows, arbitrage becomes less rewarding, BESS discharge falls, and the GSHP is used more consistently given the more predictable electricity cost. This increase in GSHP utilisation drives energy imports up, as more electricity is consumed for heat supply rather than displaced by stored energy. Despite the large swing in BESS behaviour, total system cost is relatively insensitive to volatility changes, suggesting that the optimiser successfully adapts its dispatch strategy to extract value under both flat and volatile price regimes, largely preserving economic performance.

From a forward-looking perspective, the direction of travel in the Swedish electricity markets points towards greater volatility rather than less, as variable renewable generation displaces dispatchable capacity and introduces greater temporal imbalances between supply and demand. The results indicate that the S-18 configuration is well-positioned to benefit from this trend, with BESS utilisation increasing substantially as price spreads widen.

GSHP Coefficient of Performance

GSHP COP variation produces a moderate but non-linear effect on both total system cost and energy imports. Below the baseline COP, the system progressively substitutes GSHP operation with district heating, as a less efficient heat pump requires more electricity per unit of heat delivered, eroding the cost advantage of electrified thermal supply. At a multiplier of 0.6, the efficiency loss is sufficient to make DH the preferred thermal source for a significant share of operating hours, causing energy imports to rise sharply, a non-linear response driven by the discrete nature of the GSHP dispatch decision. At a multiplier of 0.9, however, energy imports remain marginally positive, indicating that the GSHP retains a cost advantage even at slightly below-reference efficiency, and that the substitution threshold lies somewhere between the 0.6 and 0.9 multiplier values. Above the baseline COP, energy imports decrease consistently, as less electricity is required to deliver the same thermal output, and total system costs fall accordingly. The numerical results are available for reference in Appendix B.1.4. Notably, BESS discharge is unaffected by COP variation across the full range, confirming that the electrical and thermal subsystems operate largely independently, in terms of storage dispatch strategy.

The COP sensitivity is particularly relevant given that the Carnot-based model adopted in this work has not been validated against measured heat pump performance data. The results show that the system economics are meaningfully sensitive to COP assumptions, reinforcing the importance of accurate heat pump characterisation in future work.

Electricity Tariffs and BESS Cycling Cost

Electricity tariff level and BESS cycling cost both produce negligible variation across all three output metrics throughout the full multiplier range. The insensitivity to electricity tariffs reflects the fact that the variable consumption-based components subject to the multiplier represent a relatively small share of total electricity costs, with capacity-based and spot prices (held constant in this analysis) dominating the bill structure. The insensitivity to cycling cost confirms that, at the reference degradation cost, BESS dispatch in S-18 is driven primarily by arbitrage and peak shaving incentives rather than by the marginal penalty on cycling, and that moderate changes to this parameter do not materially alter the optimiser's storage utilisation strategy.

5.2.2 Sensitivity Analysis on LEC with EV Charging

The second sensitivity analysis group (SAG2) evaluated three parameters against the complete LEC configuration with V2G charging at five charging points, S-31. Spot price level and volatility remain the dominant drivers of system cost and BESS behaviour, consistent with the findings of SAG1, while the charging point power rating introduces a dimension specific to the V2G-enabled LEC that has no equivalent in the single-store analysis. Full results are reported in Appendix B.

Spot Price Level

As in SAG1, spot price level produces the largest and most linear response in total system cost across all parameters tested in SAG2. A higher market price level raises the cost of every grid-imported kilowatt-hour across both buildings, and total costs increase near-linearly with the multiplier. Energy imports follow a quasi-linear decreasing trend, as the optimiser reduces grid consumption in response to higher prices by increasing storage dispatch. BESS discharge increases as a secondary effect, reflecting wider arbitrage margins. The presence of V2G in S-31 provides additional flexible storage capacity relative to S-18, meaning the LEC has a broader set of dispatch options through which to respond to price level changes, though this does not fundamentally alter the nature of the relationship observed in SAG1.

Spot Price Volatility

Spot price volatility produces the largest response on BESS discharge in SAG2, consistent with SAG1. Higher volatility factors widen the price spread, deepening arbitrage opportunities and incentivising more aggressive storage dispatch, reflected in the substantial increase in BESS discharge at elevated multipliers. Energy imports decrease under high volatility, consistent with the same GSHP–DH substitution mechanism identified in SAG1: when electricity price spikes become more pronounced, the optimiser partially shifts thermal supply towards district heating to avoid expensive electricity consumption, reducing overall imports. Total system cost remains relatively insensitive to volatility across the full range, confirming that the combined dispatch flexibility of the LEC, (spanning PV, BESS, GSHP, and the V2G-capable EV fleet) is sufficient to preserve economic performance under both flat and volatile price regimes.

Under low volatility, the compressed price spread reduces BESS discharge and increases energy imports, as more consistent electricity prices make continuous GSHP operation more attractive relative to storage-mediated peak avoidance. As with SAG1, the forward-looking implication favours the S-31 configuration: rising renewable penetration and the associated increase in price volatility are likely to enhance the value of combined stationary and vehicle-based storage over the system's operational lifetime.

Charging Point Power Rating

The CP power rating analysis evaluates four discrete ratings: 7.4, 11, 22, and 50 kW with 11 kW as the reference baseline, and is reported separately from the multiplier-based parameters. The CP rating sets the maximum power exchange per session, directly bounding the rate at which EV batteries can contribute to or draw from the system within any given time-step.

At the lowest rating of 7.4 kW, the constrained per-session power limits the system's overall bidirectional flexibility, and total system cost rises marginally above the 11 kW baseline. Energy imports increase slightly, as the reduced discharge capacity leaves more high-price demand intervals uncovered by stored energy. BESS discharge also increases at this rating, suggesting that the BESS compensates partially for the reduced V2G contribution by increasing its own discharge, though not sufficiently to fully offset the flexibility loss.

As the CP rating increases to 22 and 50 kW, total system cost decreases progressively and energy imports fall, reflecting the greater discharge capacity available to the system per session. BESS discharge increases alongside, consistent with higher CP ratings enabling more pronounced price arbitrage windows that the stationary BESS also exploits. However, the marginal benefit of increasing the CP rating diminishes at higher values, as the binding constraint shifts from per-session power availability towards the number of active charging points and the duration of EV sessions: with only five charging points, the total flexible energy capacity available at any time-step is inherently limited regardless of the individual power rating.

This has a direct practical implication, higher CP power ratings deliver diminishing returns unless accompanied by an increase in CP density or fleet size. The combination of CP density and power rating therefore represents a key infrastructure design variable for retail LEC configurations seeking to maximise the flexibility value of an integrated V2G fleet.

5.3 Model Limitations

Several simplifications bound the scope and interpretability of the results presented in this thesis.

The GSHP thermal model relies on a Carnot-based COP formulation with a fixed empirical efficiency factor and a linear heating curve (Appendix A.1). Cooling is not modelled as a separate operating mode, and no measured heat pump performance data are available to validate it, as no GSHP is currently installed at the site. Results involving GSHP scenarios should therefore be interpreted as model-consistent projections rather than empirically validated forecasts. Additionally, the district heating return water temperature reimbursement mechanism is not captured in the model, resulting in a systematic overestimation of DH costs identified during cost reconciliation(Appendix A.1.2).

The BESS degradation model captures cycle wear through a linear cycling cost and a minimum SoC floor, but omits calendar ageing, temperature effects, and non-linear depth-of-discharge wear mechanisms. The same limitation applies to EV batteries: the current formulation does not account for degradation costs incurred during V2G discharge, which may systematically overstate the economic attractiveness of bidirectional charging.

EV charging scenarios rely on synthetically generated session data with deterministic arrival and departure times constrained to store operating hours (Appendix A.4.4). The absence of real charging records means that EV-related scenarios can only be assessed for internal consistency rather than empirical accuracy. Real-world charging behaviour exhibits significant variability in session timing, initial SoC, and energy demand that the current session model does not capture.

Finally, all building loads are treated as aggregated, non-controllable inputs. The absence of sub-meter data for individual end-use circuits means that explicit demand-side management is not modelled, and the full flexibility potential of the retail buildings is not represented.

5.4 Future Lines of Research

Several directions emerge naturally from the modelling choices and simplifications adopted in this thesis. They are grouped below by the component or system level they address.

Thermal system refinement

Future work should implement a dedicated GSHP cooling mode and validate the thermal model against measured performance data. Incorporating district heating return water temperature as a modelled variable would remove the systematic cost overestimation identified in Appendix A.1.2. Including thermal energy storage (TES) as a dispatchable asset alongside the GSHP would further enhance the thermal flexibility dimension, enabling heat load shifting in response to price signals in a way the current model does not capture.

Battery and storage modelling

A more physics-informed degradation model incorporating calendar ageing, temperature effects, and non-linear DoD wear would improve lifetime estimates and the reliability of NPV projections. Extending the cycling cost framework to EV batteries, differentiated by vehicle model and chemistry, would bring the cost-benefit analysis of V2G into closer alignment with real operator incentives.

Electric vehicle data and flexibility

Future research should incorporate real session data where available, or stochastic session generators calibrated to empirical distributions, including a broader range of EV models with heterogeneous battery capacities and charging power ratings. A more realistic session model would also provide the basis for a rigorous analysis of V2G revenue allocation between the store operator and EV owners, a contractual and economic dimension that the current framework does not address.

Demand-side management and load granularity

Replacing store-level aggregate meter data with sub-meter data for individual end-use circuits such as refrigeration, HVAC zones, and lighting would enable explicit DSM modelling, where controllable loads participate in the optimisation alongside storage and generation assets, representing the full flexibility potential of retail buildings.

Community scale and heterogeneity

Extending the LEC to include a more diverse set of participants such as residential prosumers, service buildings, or light industrial units would test whether the benefits observed here would scale and intensify with greater profile diversity. A larger, mixed-use LEC would also raise open questions of cost and benefit allocation across participants with different consumption patterns and asset ownership structures.

6
Conclusions

This thesis investigated whether retail stores can be transformed into active energy assets through the joint optimisation of distributed flexibility technologies within a local energy community framework, using a two-building retail site in Sweden as a case study. A MILP model was developed and validated against real 2025 billing data, simulating 34 scenarios of progressive technology integration spanning solar PV, battery storage, ground-source heat pump, and electric vehicle charging across three modes over a three-year rolling horizon at 15-minute resolution.

The results demonstrate that integrated flexibility delivers substantial and scalable value. Solar PV alone, sized at the 500 kWp regulatory threshold that avoids the Swedish solar tax, reduces electricity costs while achieving full self-consumption: a configuration that simultaneously maximises economic and technical performance. The addition of a BESS enables price arbitrage against day-ahead spot prices, converting morning and evening demand peaks from a cost liability into a managed resource. GSHP integration proves to be the most impactful single addition: by displacing the peak tier of the district heating tariff, it reduces total energy cost by 14%, avoids 66.7% of baseline CO_2 emissions, and yields a net present value of 3.2 MSEK with a payback period of approximately 9.6 years. Expanding to the full two-building LEC configuration (S-24) builds on this foundation through community-level energy sharing, achieving annual savings of 1.25 MSEK and an NPV of 3.38 MSEK. Sensitivity analysis confirms that economic performance is most sensitive to spot price level and volatility, and secondarily to GSHP coefficient of performance, both of which reinforce rather than undermine the investment case as Nordic electricity markets become progressively more volatile.

The principal contribution of this work is a validated, transferable MILP framework for the techno-economic optimisation of a retail LEC under Nordic tariff and market conditions, with simultaneous treatment of PV, BESS, GSHP, and three EV charging modes. Existing literature has concentrated on residential and Southern European contexts, while this thesis provides a directly applicable reference for the commercial retail sector operating under capacity-based DSO tariffs, tiered district heating structures, and the specific Swedish solar production tax regime.

Investment Recommendation

The immediate priority (Horizon 1), is investment in PV and BESS within the S-18 configuration. This combination is commercially actionable today: it requires no regulatory novelty, no coordination beyond standard grid connection agreements, and no changes to building operations. It delivers a robust business case under all but the most pessimistic spot price scenarios and should be treated as the baseline against which all further investment is measured. Alongside this, the GSHP represents a compelling near-term addition as its economics would strengthen with rising district heating tariffs and its CO_2 avoidance performance is decisive for retailers with Scope 1 and 2 decarbonisation targets. S-18, which integrates a 500 kWp solar PV array, a 257 kWh/125 kW BESS, and a 500 kW GSHP at the main store, is the recommended first investment horizon.

Full LEC formalisation, as assessed in S-24, belongs to Horizon 2. The techno-economic case is sound, but operationalising energy sharing between co-located commercial buildings raises regulatory and commercial questions that are not yet resolved in the Swedish context: cost allocation between participants, the contractual relationship with the DSO under shared metering, and potential grid reinforcement implications as distributed flexibility assets proliferate. These are not impossible obstacles, but they require deliberate engagement with the regulatory process and demonstration project experience before full deployment. Horizon 2 is therefore best pursued once the Horizon 1 investment is operational and the LEC regulatory environment matures.

On EV Charging

From a pure energy cost standpoint, not installing charging points is the cheapest choice as every charging mode tested adds net electricity cost relative to the non-EV baseline. However, this ignores a practical commercial reality: customers with electric vehicles increasingly choose where to shop based on charging availability, and the additional time spent at the store while charging tends to increase spending. Whether to invest in charging infrastructure is therefore not purely an energy question, and the operational cost increase should be weighed against the expected commercial benefit.

If charging points are installed, how they are operated matters significantly. Uncontrolled direct charging can increase annual costs by up to 2.2% relative to full LEC operation (S-24) and should be avoided. Beyond cost, at high fleet densities DC charging was found to constrain GSHP dispatch and reduce CO_2 avoidance from 66.7% to as low as 60%, an interaction fully eliminated by V1G and V2G. Smart charging recovers most of that loss and is achievable with off-the-shelf hardware today. V2G offers additional value by allowing parked EVs to discharge back into the building during peak price periods, complementing the BESS, but it depends on bidirectional chargers and vehicle compatibility that are not yet widely available. The recommended approach is to install V1G-capable hardware as standard, designed to be upgradeable to V2G when the technology becomes more accessible.

Bibliography

[1] IEA. "Sweden - countries & regions," IEA. (2026), [Online]. Available: https://www.iea.org/countries/sweden (visited on 05/28/2026).

[2] H. Jonker and R. J. M. Niessink, "Breaking down the energy use into energy applications for dutch retail buildings," TNO, 2022. [Online]. Available: https://repository.tno.nl/SingleDoc?docId=55353.

[3] H. Li, Z. Wang, T. Hong, and M. A. Piette, "Energy flexibility of residential buildings: A systematic review of characterization and quantification methods and applications," *Advances in Applied Energy*, vol. 3, p. 100 054, Aug. 25, 2021, ISSN: 2666-7924. DOI: 10.1016/j.adapen.2021.100054.

[4] IEA, "Energy flexible buildings towards resilient low carbon energy systems (annex 82)," International Energy Agency, 2025. [Online]. Available: https://annex82.iea-ebc.org/.

[5] S. Huang, Y. Ye, D. Wu, and W. Zuo, "An assessment of power flexibility from commercial building cooling systems in the united states," *Energy*, vol. 221, p. 119 571, Apr. 15, 2021, ISSN: 0360-5442. DOI: 10.1016/j.energy.2020.119571.

[6] U.S. Department of Energy, "Grid-interactive efficient buildings: Projects summary," U.S. Department of Energy, 2020. [Online]. Available: https://www.energy.gov/eere/buildings/articles/grid-interactive-efficient-buildings-projects-summary.

[7] *Directive (EU) 2024/1275 of the european parliament and of the council of 24 april 2024 on the energy performance of buildings (recast)*, Apr. 24, 2024. [Online]. Available: http://data.europa.eu/eli/dir/2024/1275/oj.

[8] P. E. Campana *et al.*, "Li-ion batteries for peak shaving, price arbitrage, and photovoltaic self-consumption in commercial buildings: A monte carlo analysis," *Energy Conversion and Management*, vol. 234, p. 113 889, Apr. 15, 2021, ISSN: 0196-8904. DOI: 10.1016/j.enconman.2021.113889.

[9] A. Bergström, "Techno-economic analysis of commercial battery storage systems in northern europe," Master's thesis, Uppsala University, 2020. [Online]. Available: https://urn.kb.se/resolve?urn=urn:nbn:se:uu:diva-404320.

[10] V. Papadopoulos, J. Knockaert, C. Develder, and J. Desmet, "Peak shaving through battery storage for low-voltage enterprises with peak demand pricing," *Energies*, vol. 13, no. 5, 2020, ISSN: 1996-1073. DOI: 10.3390/en13051183.

[11] M. I. Azim, M. Khorasany, R. Razzaghi, M. Jalili, L. Meegahapola, and X. Yu, "Feasibility assessment of behind-the-meter batteries under typical tariff structures for commercial and industrial customers," *Journal of Energy Storage*,

vol. 90, p. 111 817, Jun. 15, 2024, ISSN: 2352-152X. DOI: 10.1016/j.est.2024.111817.

[12] U. S. Department of Energy, "Vehicles-to-grid integration assessment report," U. S. Department of Energy, Washington, DC, Assessment Report, 2025. [Online]. Available: https://www.energy.gov/eere/vehicles/articles/vehicle-grid-integration-assessment-report.

[13] I. Rodrig Dekordevi, "Business models for vehicle-grid integration: A literature review and european case studies," Master's thesis, Politecnico di Milano, Apr. 3, 2025. [Online]. Available: https://www.politesi.polimi.it/handle/10589/234689.

[14] T. Meelen, H. Budnitz, and T. Schwanen, "Advantages of electric vehicle adoption and vehicle-to-grid charging in the fleet market: Lessons from the v2go project," Transport Studies Unit, University of Oxford, Oxford, Policy Briefing, 2020. [Online]. Available: https://www.tsu.ox.ac.uk/sites/default/files/2023-01/V2GO-Policy-Brief-TSU.pdf.

[15] F. Roudet, D. Clement, and J. Robb, "Electric vehicle charging infrastructure (EVCI) for commercial buildings: How onsite renewable power generation and battery storage can mitigate the costs of EVCI for commercial buildings," Eaton, White Paper, 2021. [Online]. Available: https://www.eaton.com/content/dam/eaton/markets/buildings/buildings-as-a-grid/assets/Commercial%20building%20and%20EV%20opportunities.pdf.

[16] N. Rossetto, "Beyond individual active customers: Citizen and renewable energy communities in the european union," *IEEE Power and Energy Magazine*, vol. 21, no. 4, pp. 36–44, Jul. 2023, ISSN: 1558-4216. DOI: 10.1109/MPE.2023.3269541.

[17] T. Bauwens *et al.*, "Conceptualizing community in energy systems: A systematic review of 183 definitions," *Renewable and Sustainable Energy Reviews*, vol. 156, p. 111 999, Mar. 1, 2022, ISSN: 1364-0321. DOI: 10.1016/j.rser.2021.111999.

[18] *Directive (EU) 2018/2001 of the european parliament and of the council of 11 december 2018 on the promotion of the use of energy from renewable sources (recast) (text with EEA relevance.)* Dec. 11, 2018. [Online]. Available: http://data.europa.eu/eli/dir/2018/2001/oj.

[19] *Directive (EU) 2019/944 of the european parliament and of the council of 5 june 2019 on common rules for the internal market for electricity and amending directive 2012/27/EU (recast) (text with EEA relevance.)* Jun. 5, 2019. [Online]. Available: http://data.europa.eu/eli/dir/2019/944/oj.

[20] E. Tarpani *et al.*, "Energy communities implementation in the european union: Case studies from pioneer and laggard countries," *Sustainability*, vol. 14, no. 19, p. 12 528, Jan. 2022, ISSN: 2071-1050. DOI: 10.3390/su141912528.

[21] S. Ahmed, A. Ali, and A. D'Angola, "A review of renewable energy communities: Concepts, scope, progress, challenges, and recommendations," *Sustainability*, vol. 16, no. 5, p. 1749, Jan. 2024, ISSN: 2071-1050. DOI: 10.3390/su16051749.

[22] B. Bonfert, "'we like sharing energy but currently there's no advantage': Transformative opportunities and challenges of local energy communities in europe," *Energy Research & Social Science*, vol. 107, p. 103 351, Jan. 1, 2024, ISSN: 2214-6296. DOI: 10.1016/j.erss.2023.103351.

[23] G. Yiasoumas *et al.*, "Key aspects and challenges in the implementation of energy communities," *Energies*, vol. 16, no. 12, p. 4703, Jan. 2023, ISSN: 1996-1073. DOI: 10.3390/en16124703.

[24] Svenska Kraftnät. "Operations and electricity markets." (Apr. 26, 2024), [Online]. Available: https://www.svk.se/en/national-grid/operations-and-electricity-markets/ (visited on 03/05/2026).

[25] P. Shinde. "Increasing volatility & negative prices: The swedish flexibility need," Montel Energy. (May 16, 2024), [Online]. Available: https://montel.energy/commentary/increasing-volatility-negative-prices-the-swedish-flexibility-need (visited on 03/05/2026).

[26] Nord Pool. "Transition to 15-minute market time unit (MTU)." (2025), [Online]. Available: https://www.nordpoolgroup.com/en/trading/transition-to-15-minute-market-time-unit-mtu/ (visited on 03/05/2026).

[27] P. Holmberg and T. P. Tangerås, "The swedish electricity market – today and in the future," Research Institute of Industrial Economics (IFN), 2022. [Online]. Available: https://www.riksbank.se/globalassets/media/rapporter/pov/artiklar/engelska/2023/230512/2023_1-the-swedish-electricity-market--today-and-in-the-future.pdf.

[28] Energimarknadsinspektionen (Ei). "Elnätsavtal med effektavgift." (Mar. 7, 2025), [Online]. Available: https://ei.se/konsument/anvand-el-smartare/elnatsavtal-med-effektavgift (visited on 03/05/2026).

[29] M. M. Wagner and B. J. Höyer, "Investigating the integration of vehicle-to-grid (v2g) technology in energy communities with private solar panels and electric vehicles," Bachelor's thesis, Technical University of Denmark, 2024. [Online]. Available: https://ev4eu.eu/wp-content/uploads/2024/08/2024_BSC_Mikkel-Morkeberg-Wagner-and-Bjorn-Jacobi-Hoyer_DTU.pdf.

[30] N. Pezzati, E. Innocenti, L. Berzi, and M. Delogu, "Scalable energy management model for integrating v2g capabilities into renewable energy communities," *World Electric Vehicle Journal*, vol. 16, no. 8, p. 450, Aug. 2025, ISSN: 2032-6653. DOI: 10.3390/wevj16080450.

[31] C. Silva, P. Faria, R. Barreto, and Z. Vale, "Fair management of vehicle-to-grid and demand response programs in local energy communities," *IEEE Access*, vol. 11, pp. 79 851–79 860, 2023, ISSN: 2169-3536. DOI: 10.1109/ACCESS.2023.3299500.

[32] G. Barone *et al.*, "How smart metering and smart charging may help a local energy community in collective self-consumption in presence of electric vehicles," *Energies*, vol. 13, no. 16, p. 4163, Jan. 2020, ISSN: 1996-1073. DOI: 10.3390/en13164163.

[33] G. G. Zanvettor, M. Casini, A. Giannitrapani, S. Paoletti, and A. Vicino, "Optimal management of energy communities hosting a fleet of electric vehicles," *Energies*, vol. 15, no. 22, p. 8697, Jan. 2022, ISSN: 1996-1073. DOI: 10.3390/en15228697.

[34] G. Angrisani, M. Canelli, C. Roselli, and M. Sasso, "Microcogeneration in buildings with low energy demand in load sharing application," *Energy Conversion and Management*, vol. 100, pp. 78–89, Aug. 1, 2015, ISSN: 0196-8904. DOI: 10.1016/j.enconman.2015.04.065.

[35] E. Marrasso, C. Roselli, M. Sasso, A. Picallo-Perez, and J. M. Sala Lizarraga, “Dynamic simulation of a microcogeneration system in a spanish cold climate,” *Energy Conversion and Management*, vol. 165, pp. 206–218, Jun. 1, 2018, ISSN: 0196-8904. DOI: 10.1016/j.enconman.2018.03.052.

[36] F. Ceglia, E. Marrasso, C. Roselli, and M. Sasso, “Small renewable energy community: The role of energy and environmental indicators for power grid,” *Sustainability*, vol. 13, no. 4, p. 2137, Jan. 2021, ISSN: 2071-1050. DOI: 10.3390/su13042137.

[37] F. Ceglia, P. Esposito, A. Faraudello, E. Marrasso, P. Rossi, and M. Sasso, “An energy, environmental, management and economic analysis of energy efficient system towards renewable energy community: The case study of multi-purpose energy community,” *Journal of Cleaner Production*, vol. 369, p. 133 269, Oct. 1, 2022, ISSN: 0959-6526. DOI: 10.1016/j.jclepro.2022.133269.

[38] B. Fina, C. Monsberger, and H. Auer, “Simulation or estimation?—two approaches to calculate financial benefits of energy communities,” *Journal of Cleaner Production*, vol. 330, p. 129 733, Jan. 1, 2022, ISSN: 0959-6526. DOI: 10.1016/j.jclepro.2021.129733.

[39] P. Huang, M. Lovati, J. Shen, J. Chai, and X. Zhang, “Investigation of the peer-to-peer energy trading performances in a local community under the future climate change scenario in sweden,” *Energy Reports*, vol. 8, pp. 989–1001, 2022, ISSN: 2352-4847. DOI: 10.1016/j.egyr.2021.12.032.

[40] D. Cirone, R. Bruno, P. Bevilacqua, S. Perrella, and N. Arcuri, “Techno-economic analysis of an energy community based on PV and electric storage systems in a small mountain locality of south italy: A case study,” *Sustainability*, vol. 14, no. 21, p. 13 877, Jan. 2022, ISSN: 2071-1050. DOI: 10.3390/su142113877.

[41] V. Caballero, A. Briones, A. Coca-Ortegón, A. Pérez, B. Barrios, and M. de la Mano, “Analysis and simulation of an urban-industrial sustainable energy community: A use case in san juan de mozarrifar using photovoltaic energy,” *Energy Reports*, vol. 9, pp. 1589–1605, Dec. 1, 2023, ISSN: 2352-4847. DOI: 10.1016/j.egyr.2022.12.059.

[42] F. Ceglia, E. Marrasso, C. Martone, G. Pallotta, C. Roselli, and M. Sasso, “Towards the decarbonization of industrial districts through renewable energy communities: Techno-economic feasibility of an italian case study,” *Energies*, vol. 16, no. 6, p. 2722, Jan. 2023, ISSN: 1996-1073. DOI: 10.3390/en16062722.

[43] R. Peeren, D. Dabhi, and J. Dalton, “Levelling the playing field for smart renewable energy community in the electricity market through the high street electricity market model,” *Applied Energy*, vol. 377, p. 124 660, Jan. 1, 2025, ISSN: 0306-2619. DOI: 10.1016/j.apenergy.2024.124660.

[44] S. Abouebeid *et al.*, “Urban building energy modelling and multi-objective optimization for PED transition in an existing neighbourhood in sweden,” *Energy and Buildings*, vol. 352, p. 116 783, Feb. 1, 2026, ISSN: 0378-7788. DOI: 10.1016/j.enbuild.2025.116783.

[45] J. Wang and L. Wang, “Industrial energy organizations: Cost sharing, grid effect, and storing energy development,” *Energy*, vol. 328, p. 136 411, Aug. 1, 2025, ISSN: 0360-5442. DOI: 10.1016/j.energy.2025.136411.

[46] M. Mazidi *et al.*, "Evaluating the potential for developing local energy communities in sweden: Case studies at jättesten and chalmers campus," in *Energy Informatics*, I. Martinac, B. N. Jørgensen, Z. G. Ma, R. Unnþórsson, and C. Bordin, Eds., Cham: Springer Nature Switzerland, 2026, pp. 173–186, ISBN: 978-3-032-03098-6. DOI: 10.1007/978-3-032-03098-6_12.

[47] F. Ceglia, E. Marrasso, C. Roselli, and M. Sasso, "A micro-trigeneration geothermal plant for a smart energy community: The case study of a residential district in ischia," *IOP Conference Series: Earth and Environmental Science*, vol. 690, no. 1, p. 012 051, Mar. 2021, ISSN: 1755-1315. DOI: 10.1088/1755-1315/690/1/012051.

[48] R. Wu, G. Mavromatidis, K. Orehounig, and J. Carmeliet, "Multiobjective optimisation of energy systems and building envelope retrofit in a residential community," *Applied Energy*, vol. 190, pp. 634–649, Mar. 15, 2017, ISSN: 0306-2619. DOI: 10.1016/j.apenergy.2016.12.161.

[49] E. Fabrizio *et al.*, "Monitoring and managing of a micro-smart grid for renewable sources exploitation in an agro-industrial site," *Sustainable Cities and Society*, vol. 28, pp. 88–100, Jan. 1, 2017, ISSN: 2210-6707. DOI: 10.1016/j.scs.2016.08.026.

[50] M. Thebault and L. Gaillard, "Optimization of the integration of photovoltaic systems on buildings for self-consumption – case study in france," *City and Environment Interactions*, vol. 10, p. 100 057, Apr. 1, 2021, ISSN: 2590-2520. DOI: 10.1016/j.cacint.2021.100057.

[51] G. Pontes Luz and R. Amaro e Silva, "Modeling energy communities with collective photovoltaic self-consumption: Synergies between a small city and a winery in portugal," *Energies*, vol. 14, no. 2, p. 323, Jan. 2021, ISSN: 1996-1073. DOI: 10.3390/en14020323.

[52] E. Dal Cin, G. Carraro, G. Volpato, A. Lazzaretto, and P. Danieli, "A multi-criteria approach to optimize the design-operation of energy communities considering economic-environmental objectives and demand side management," *Energy Conversion and Management*, vol. 263, p. 115 677, Jul. 1, 2022, ISSN: 0196-8904. DOI: 10.1016/j.enconman.2022.115677.

[53] J. McCarty, C. Waibel, and A. Schlueter, "Multi-period optimisation of district-scale building integrated photovoltaic deployment," *IOP Conference Series: Earth and Environmental Science*, vol. 1196, no. 1, p. 012 015, Jun. 2023, ISSN: 1755-1315. DOI: 10.1088/1755-1315/1196/1/012015.

[54] G. Ansari and R. Keypour, "Optimizing the operation of shopping malls using commercial demand response aggregator to reduce consumption in the day-ahead market," *Smart Grids and Sustainable Energy*, vol. 10, no. 1, p. 12, Jan. 18, 2025, ISSN: 2731-8087. DOI: 10.1007/s40866-024-00237-x.

[55] F. Guo, L. Gomes, L. Ma, Z. Tian, Z. Vale, and S. Pang, "Optimizing battery storage for sustainable energy communities: A multi-scenario analysis," *Sustainable Cities and Society*, vol. 118, p. 106 030, Jan. 1, 2025, ISSN: 2210-6707. DOI: 10.1016/j.scs.2024.106030.

[56] F. Mattana, R. Ricciu, G. Sitzia, and E. Ghiani, "Optimizing the trade-off among comfort, electricity use, and economic benefits in smart buildings within

renewable electricity communities," *Energies*, vol. 19, no. 2, p. 547, Jan. 2026, ISSN: 1996-1073. DOI: 10.3390/en19020547.

[57] D. Curto *et al.*, "Multi-carrier based optimization of renewable energy communities in small non-interconnected islands," *Energy*, vol. 347, p. 140 469, Mar. 15, 2026, ISSN: 0360-5442. DOI: 10.1016/j.energy.2026.140469.

[58] I. Pizzuti and G. Delibra, "Integration of battery energy storage systems in renewable energy communities: Optimal configurations and strategies," *Journal of Energy Storage*, vol. 153, p. 120 857, Apr. 1, 2026, ISSN: 2352-152X. DOI: 10.1016/j.est.2026.120857.

[59] T. Huld, R. Müller, and A. Gambardella, "A new solar radiation database for estimating PV performance in europe and africa," *Solar Energy*, vol. 86, no. 6, pp. 1803–1815, Jun. 1, 2012, ISSN: 0038-092X. DOI: 10.1016/j.solener.2012.03.006.

[60] S. Ø. Jensen *et al.*, "IEA EBC annex 67 energy flexible buildings," *Energy and Buildings*, vol. 155, pp. 25–34, Nov. 15, 2017, ISSN: 0378-7788. DOI: 10.1016/j.enbuild.2017.08.044.

[61] W. E. Hart, J.-P. Watson, and D. L. Woodruff, "Pyomo: Modeling and solving mathematical programs in python," *Mathematical Programming Computation*, vol. 3, no. 3, pp. 219–260, Sep. 1, 2011, ISSN: 1867-2957. DOI: 10.1007/s12532-011-0026-8.

[62] M. L. Bynum *et al.*, *Pyomo — Optimization Modeling in Python* (Springer Optimization and Its Applications). Cham: Springer International Publishing, 2021, vol. 67, ISBN: 978-3-030-68927-8 978-3-030-68928-5. DOI: 10.1007/978-3-030-68928-5.

[63] Gurobi Optimization, LLC, *Gurobi optimizer reference manual*, 2026. [Online]. Available: https://www.gurobi.com.

[64] T. p. d. team, *Pandas-dev/pandas: Pandas*, Mar. 30, 2026. DOI: 10.5281/zenodo.19340003.

[65] A. Grimaldi, F. D. Minuto, A. Perol, S. Casagrande, and A. Lanzini, "Ageing and energy performance analysis of a utility-scale lithium-ion battery for power grid applications through a data-driven empirical modelling approach," *Journal of Energy Storage*, vol. 65, p. 107 232, Aug. 15, 2023, ISSN: 2352-152X. DOI: 10.1016/j.est.2023.107232.

[66] P. Zippenfenig, *Open-meteo.com weather API*, Dec. 31, 2024. DOI: 10.5281/zenodo.14582479.

[67] L. Hirth, J. Mühlenpfordt, and M. Bulkeley, "The ENTSO-e transparency platform – a review of europe's most ambitious electricity data platform," *Applied Energy*, vol. 225, pp. 1054–1067, Sep. 1, 2018, ISSN: 0306-2619. DOI: 10.1016/j.apenergy.2018.04.048.

[68] Mälarenergi AB, "Priser mälarenergi elnät företag 2025," Mälarenergi AB, Sep. 1, 2025. [Online]. Available: https://www.malarenergi.se/globalassets/dokument/elnat/priser/prislista_elnat_2025-09-01_foretag_a4.pdf.

[69] Energimyndigheten. "Marknadsstatistik," Energimyndigheten. (2026), [Online]. Available: https://www.energimyndigheten.se/energisystem-och-analys/styrmedel-for-produktion-av-el-gas-varme-och-kyla/

elcertifikatsystemet/marknadsstatistik/?currentTab=1 (visited on 05/14/2026).

[70] Skatteverket. "Skatt på el." (2026), [Online]. Available: https://www.skatteverket.se/foretag/skatterochavdrag/punktskatter/energiskatter/skattpael.4.15532c7b1442f256bae5e4c.html (visited on 05/28/2026).

[71] S. Liljeroth, "A techno-economic study of commercial and industrial PV systems in sweden," Master's thesis, Uppsala University, Jun. 2025. [Online]. Available: https://www.diva-portal.org/smash/record.jsf?pid=diva2%3A1980349&dswid=-9739.

[72] SUNGROW. "Powerstack - ST255cs-2h," SUNGROW. (2026), [Online]. Available: https://www.sungrowpower.com/eu/en/products/c-i-energy-storage-system/st255cs-2h (visited on 05/13/2026).

[73] NextG Power. "The LFP battery life cycle: Understanding 8000 cycles and 70% SOH - battery energy storage system manufacturer NextG power." (Jan. 21, 2026), [Online]. Available: https://nextgpower.com/the-lfp-battery-life-cycle-understanding-8000-cycles-and-70-soh/ (visited on 03/31/2026).

[74] C. Kost, P. Müller, J. Sepúlveda Schweiger, V. Fluri, and J. Thomsen, "Levelized cost of electricity renewable energy technologies," Fraunhofer Institute for Solar Energy Systems (ISE), Jul. 2024. [Online]. Available: https://www.ise.fraunhofer.de/en/publications/studies/cost-of-electricity.html.

[75] M. Ahouad, A. Sunjaq, E. Wikner, and T. Thiringer, "Economic assessment of battery energy storage for frequency regulation in the nordic power systems," in *2024 20th International Conference on the European Energy Market (EEM)*, ISSN: 2165-4093, Jun. 2024, pp. 1–5. DOI: 10.1109/EEM60825.2024.10608974.

[76] A. Ban and C. Bungău, "Estimation of the initial investment cost in systems equipped with heat pumps using regression analysis," *Journal of Engineering Sciences and Innovation*, 3rd ser., vol. 7, 2022. DOI: 10.56958/jesi.2022.7.3.293.

[77] T. Arghand, S. Javed, and J.-O. Dalenbäck, "Combining direct ground cooling with ground-source heat pumps and district heating: Energy and economic analysis," *Energy*, vol. 270, p. 126 944, May 1, 2023, ISSN: 0360-5442. DOI: 10.1016/j.energy.2023.126944.

[78] SUNGROW. "AC22-01," SUNGROW. (2026), [Online]. Available: https://www.sungrowpower.com/eu/en/products/ev-charger/ac22-01 (visited on 05/13/2026).

[79] EV Database. "Tesla model 3 RWD (highland)," EV Database. (2026), [Online]. Available: https://ev-database.org/car/3403/Tesla-Model-3-RWD (visited on 05/28/2026).

[80] B. Couraud, S. Norbu, M. Andoni, V. Robu, H. Gharavi, and D. Flynn, "Optimal residential battery scheduling with asset lifespan consideration," in *2020 IEEE PES Innovative Smart Grid Technologies Europe (ISGT-Europe)*, Oct. 2020, pp. 630–634. DOI: 10.1109/ISGT-Europe47291.2020.9248889.

[81] F. Witte and P. Schönfeldt, *Oemof workshop on modeling of heat pumps*, May 6, 2026. [Online]. Available: https://github.com/oemof/heat-pump-tutorial (visited on 05/15/2026).

[82] H. Pieper, I. Krupenski, W. Brix Markussen, T. Ommen, A. Siirde, and A. Volkova, “Method of linear approximation of COP for heat pumps and chillers based on thermodynamic modelling and off-design operation,” *Energy*, vol. 230, p. 120 743, Sep. 1, 2021, ISSN: 0360-5442. DOI: 10.1016/j.energy.2021.120743.

[83] VICUS Software. “Heating curves - fundamentals and application.” (2026), [Online]. Available: https://vicus-software.com/en/knowledge/plant-engineering/heating-curves/ (visited on 05/15/2026).

[84] I. Bokne and C. Elf, “Model predictive control for ground source heat pumps: Reducing cost while maintaining comfort,” Master’s thesis, Linköping University, Department of Electrical Engineering, Automatic Control, 2023, 79 pp. [Online]. Available: https://urn.kb.se/resolve?urn=urn:nbn:se:liu:diva-195982.

[85] O. Ruhnau, L. Hirth, and A. Praktiknjo, “Time series of heat demand and heat pump efficiency for energy system modeling,” *Scientific Data*, vol. 6, no. 1, p. 189, Oct. 1, 2019, ISSN: 2052-4463. DOI: 10.1038/s41597-019-0199-y.

[86] M. Wetter, W. Zuo, T. S. Nouidui, and X. Pang, “Modelica buildings library,” *Journal of Building Performance Simulation*, vol. 7, no. 4, pp. 253–270, 2014. DOI: 10.1080/19401493.2013.765506.

[87] T. Brudermueller, U. Potthoff, E. Fleisch, F. Wortmann, and T. Staake, “Estimation of energy efficiency of heat pumps in residential buildings using real operation data,” *Nature Communications*, vol. 16, no. 1, p. 2834, Mar. 22, 2025, ISSN: 2041-1723. DOI: 10.1038/s41467-025-58014-y.

A

Assumptions, Data, and Component Models

A.1 Modelling Assumptions

This section documents the principal numerical and mathematical simplifications embedded in the optimisation formulation. Where assumptions introduce uncertainty or may overestimate achievable flexibility, implications for result interpretation are noted.

A.1.1 Numerical and Parametric Assumptions

Symmetric Round-Trip Efficiency

All battery systems (EV and BESS) use symmetric round-trip efficiency $\eta^2 = 0.865$ [65] applied equally to charging and discharging paths, regardless of power level, temperature, or SoC. Temperature-dependent and non-linear efficiency effects are neglected. Real batteries exhibit efficiency curves that vary with operating conditions; this simplification may underestimate true losses during rapid charging/discharging or temperature extremes.

Battery Degradation Representation

Battery wear is modelled via (1) a minimum SoC floor ($\sigma^{\min} = 0.20$) limiting usable depth of discharge to 80 %, and (2) a linear cycling cost that penalizes battery throughput to account for degradation wear. However, this approach does not capture calendar ageing, temperature effects, or non-linear cycle-depth-dependent wear mechanisms. As a result, estimated battery lifetimes may not accurately reflect real degradation, particularly for batteries operated frequently at high depths of discharge or in harsh thermal conditions.

Asset Performance Constancy

All performance parameters (PV efficiency, BESS efficiency, GSHP COP) are held constant over 2023–2025. Seasonal variations are partially captured through temperature-dependent parametrization (e.g., GSHP heating curve), but long-term performance drift and degradation trajectories are not modelled. This assumption is reasonable over a 3-year horizon but would require re-parametrization for studies spanning decades.

No Minimum On/Off Time or Ramp-Rate Constraints

Controllable assets (BESS, GSHP, EV chargers) may change operating mode at every 15-minute time step with no minimum on/off duration or rate-of-change constraints. In reality, equipment often exhibits minimum run times, ramp limitations, and mode-transition delays. This assumption may overestimate short-term operational flexibility and optimize dispatch patterns that are physically infeasible for real equipment.

A.1.2 Market and Grid Assumptions

Rolling-Horizon Optimisation

The optimisation operates on a 24-hour rolling horizon with 36-hour foresight, where the knowledge of spot prices, solar generation, EV sessions, and building loads is limited to this window. This design represents an upper bound on achievable cost savings, while real-time or forecast-driven implementations with shorter lookahead would incur additional costs due to prediction errors.

Lossless Intra-Community Distribution

Electrical losses within the LEC are neglected, meaning all generation and storage discharge is fully available at any metering point. This conservative assumption overstates the economic value of inter-building power exchange, since real distribution networks incur losses proportional to current and distance. As a result, inter-building power sharing may appear more economically attractive in optimisation results than physically realizable.

Linear Cost Structure (with Exception for Non-linear Tariffs)

Most tariff components (spot prices, transmission fees, energy taxes, subscription fees) are linear functions of power or energy. Two non-linear elements are explicitly modelled: (1) Swedish solar production tax (Appendix A.2.3) and (2) district heating two-tier capacity pricing (Appendix A.2.3). Quantity-based rebates and other non-linear pricing structures are excluded. One notable omission is the district heating return water temperature reimbursement, a contractual credit applied by the supplier when return temperatures fall below a specified threshold, which introduces a systematic overestimation of district heating costs.This simplification enables efficient MILP formulation but may misrepresent cost-minimization incentives in real tariff structures with complex rebate or volume-discount schemes.

Static Regulatory Environment

Electricity market rules, grid tariffs, solar taxation thresholds, transmission fees, and subsidy structures are assumed static over 2023–2025. Future regulatory or policy changes are not anticipated. This assumption allows for stable year-long optimisations but would require re-parametrization if major policy reforms (e.g., solar tax threshold changes, tariff restructuring) occur.

A.1.3 Data and Input Assumptions

Deterministic EV Availability

EV session parameters (arrival time, departure time, initial SoC, desired SoC) are treated as fixed and known in advance. The synthetic EV data generator produces deterministic sessions constrained to store operating hours (9:30–20:30 weekdays, 9:30–18:30 weekends) with same-day parking. Stochastic variations in driver behaviour, unplanned arrivals, or charging request changes are not modelled. This assumption may overestimate achievable V2G flexibility, as real-world EV availability and charging requirements exhibit significant day-to-day and hour-to-hour variability.

Fixed Load Profiles

Electrical and thermal demand at both buildings are treated as exogenous, non-negotiable constraints. Demand adaptation in response to price signals, energy interventions, or comfort trade-offs is not modelled. This conservative assumption represents current operational practice but may understate the potential for demand-side flexibility. Real customers may adjust consumption patterns in response to strong price signals or energy management campaigns.

Weather and Climate Data Representativeness

Weather data (temperature, solar irradiance) are sourced from historical observations and reanalysis for 2023–2025. Long-term climate variability, decadal climate trends, and extreme weather scenarios beyond this period are not captured. Solar generation data are available only for 2023, thus these data are looped for subsequent years. This approach may introduce bias if 2023 was atypical for solar resources in the case study location, or if climate trends shift significantly within the analysis period. Results should be interpreted as representative of recent historical conditions rather than long-term averages or future climate scenarios.

A.2 Data Acquisition

This section describes the data sources and acquisition methods used to parametrise the simulation model, organised into five categories corresponding to the subsections below.

A.2.1 Energy Load & Cost Data

Operational data were obtained directly from the store, covering aggregate energy consumption and cost records for both buildings. The dataset includes:

- Aggregated electrical load profile at 15-minute resolution
- Aggregated heat load profile at hourly resolution
- Historical electricity and heating costs

Data were available for both buildings for the years 2023, 2024, and 2025. As the heat load profile is provided at hourly resolution, it is upsampled to 15-minute resolution using linear interpolation to match the temporal resolution of the electrical load data and the model, as described in Section A.3.

A.2.2 Weather & PV Production Data

Weather and PV production data were obtained from publicly available sources. Outdoor air temperature at 2 m above ground was retrieved from the Open-Meteo ERA5 reanalysis archive via its open-access API [66], providing hourly historical records aligned with the operational data period. Solar PV production was obtained from PVGIS [59], using a normalised $1\,\mathrm{kW}_p$ system as a reference, which was subsequently scaled to the installed capacity defined in each scenario.

The air temperature dataset covers the years 2023, 2024 and 2025, while the PV generation dataset only covers 2023, due to data availability. Both sets are specific to the geographic coordinates of the case study sites. As the model operates at 15-minute resolution, the hourly weather and PV production data are upsampled accordingly using linear interpolation (see Section A.3).

A.2.3 Energy Market & Tariff Data

The electricity and district heating cost structures applied in this study reflect the full cost stack faced by a commercial energy consumer at the case study sites. The data was obtained from multiple sources and is described below.

Electricity Spot Prices

Hourly day-ahead spot prices from 2023 until the 29th of September 2025, followed by 15-minute resolution until the end of the year, were obtained for the SE3 bidding zone via the European Network of Transmission System Operators RESTful API [67]. The hourly data is upsampled via linear interpolation to meet the 15-minute model resolution, as described in Section A.3.

Grid Tariffs

The tariff rates correspond to the 6-10 kV connection category as defined by the DSO and apply to both buildings. The grid subscription fee, variable transmission fee, subscribed power fee, and transmission health incentive, were obtained directly from the DSO electricity tariff schedule [68]. The energy certificate cost is not explicitly listed in the tariff schedule and were instead estimated based on [69]. All applicable rates for 2025 are listed in Table A.1.

Taxes

The energy tax and VAT rates were obtained from the Swedish Tax Agency [70], and apply to all electricity consumed on site. The applicable rates are assumed constant over the simulation horizon, consistent with the modelling assumptions outlined in Section 1.4, and are listed in Table A.2.

Table A.1: DSO grid tariff rates for 2025 (6-10 kV category)

Component	2025	Unit
Grid subscription fee	3,000	SEK/month
Variable transmission fee	0.04	SEK/kWh
Subscribed power fee	35.84	SEK/kW/month
Transmission health incentive	0.04	SEK/kWh
Energy certificate*	0.005	SEK/kWh

* Estimated value; not directly provided by the DSO.

Table A.2: Tax rates

Component	Value	Unit
Energy tax	0.439	SEK/kWh
VAT	25	%

The treatment of energy tax on self-consumed solar electricity depends on the total installed PV capacity. If the installed capacity is under 500 kW per building, a tax exemption exists. Contrary, if the capacity is over that limit, the full electricity tax rate is applied to every unit of energy consumed.

District Heating Tariffs

The district heating tariff structure was obtained directly from the DSO, district heating supplier serving both case study sites. However, as heat supply does not participate in the LEC, the district heating tariff is only applied to the main store, consistent with the scope defined in Section 1.4.The tariff applicable to the case study sites falls under the large property category, which applies to consumers with a subscribed capacity exceeding 499 kW. It comprises five components that distinguish between base and peak consumption tiers, as well as seasonal pricing. The rates applicable to the simulation period are summarised in Table A.3.

Table A.3: DSO district heating tariff rates for 2025 (large properties, subscribed capacity over 499 kW)

Component	2025	Unit
Fixed annual fee	169,615	SEK/year
Base capacity charge	441	SEK/kW/year
Maximum capacity charge	685	SEK/kW/year
Base energy rate – summer	188	SEK/MWh
Base energy rate – non-summer	458	SEK/MWh
Peak energy rate	1,200	SEK/MWh

The tariff distinguishes between a summer and a non-summer period, with higher base energy rates applying outside the summer months. Peak consumption surcharges are exclusively applied during the non-summer period, so no peak energy rates are charged during summer regardless of consumption level. Additionally, DH has a CO_2 intensity of 40.1 g/kWh, reported yearly by the DSO.

A.2.4 Technology and Cost Data

Technical and cost parameters for each modelled technology were compiled from a combination of industry reports, peer-reviewed literature, and manufacturer data sheets. CAPEX and fixed O&M costs are included for PV, BESS, and GSHP, and are used in the post-simulation techno-economic assessment. For EV charging, no CAPEX or O&M costs are assigned, as the charging infrastructure is only assessed from an operational point of view. The parameters used as model inputs are summarised in Table A.4. Additionally, a constant exchange rate of 11.1 SEK/EUR is used when required.

Table A.4: Technology and cost parameters used in the model

Parameter	Value	Unit	Source
Solar PV			
CAPEX	8,000	SEK/kW$_p$	[71]
Fixed O&M	2	% of CAPEX/year	[71]
BESS			
Capacity	257–771	kWh	[72]
Power	125–257	kW	[72]
Round-trip efficiency	86.5	%	[65]
SoC bounds	20–100	%	[73]
Rated cycles	6,000	–	[73]
CAPEX	400	EUR/kWh	[9, 74]
Fixed O&M	2	% of CAPEX/year	[9, 75]
Geothermal			
CAPEX	$2{,}485P^{0.6094}$	EUR/kW$_h$	[76]
Fixed O&M	2	% of CAPEX/year	[77]
V2G			
Charging point power	11	kW	[78]
Charging efficiency	93	%	[65]
Vehicle battery capacity	60	kWh	[79]

Note: Where P is the GSHP capacity no higher than 1,7 MW$_h$.

Vehicle battery capacities and the number of vehicles, charging sessions, and availability windows were not directly available and were instead generated as synthetic inputs based on store operating hours and representative EV specifications. The method used to construct these inputs is described in Section A.4.4.

A.2.5 Building and Site Data

Site-specific data was collected for both sites through a combination of an on-site visit and Google Maps imagery. The following information was obtained:

- Available area for solar PV installation, including rooftop, ground-mounted, and carport configurations over parking spaces
- Number of available parking slots
- Store operating schedule

A.3 Data Pre-Processing

All datasets were processed in Python using pandas [64] prior to model input, to ensure temporal consistency, completeness, and compatibility with the 15-minute model resolution. The steps applied to each data type are described below.

Electrical Load Profiles

The aggregated electrical load profiles were provided at 15-minute resolution and required no resampling. Missing values caused by metering errors or data gaps were identified and filled using linear interpolation.

Heat Load Profiles

The aggregated heat load profiles were provided at hourly resolution. Missing values were first identified and filled using linear interpolation, after which the complete profiles were upsampled to 15-minute resolution, also via linear interpolation. Each hourly value was subsequently scaled by a factor of $\frac{1}{4}$ so that the per-time-step energy quantity represents MWh per 15-minute interval, preserving the correct energy total upon summation.

Weather & PV Production Data

Outdoor air temperature and PV generation profiles were obtained at hourly resolution and upsampled to 15-minute resolution using linear interpolation. PV generation timestamps follow a centre-of-hour convention (e.g. 00:11 representing the 00:00 interval) and were floored to the nearest hour boundary prior to upsampling. Both datasets use UTC-referenced timestamps.

Electricity Spot Prices

Spot prices were available at hourly resolution from 2023 until the 30th of September 2025, and at 15-minute resolution thereafter. Timestamps were first standardised to UTC to avoid ambiguities introduced by daylight saving time transitions. The hourly segment was then upsampled to 15-minute resolution using linear interpolation, producing a consistent price series across the full simulation period.

District Heating Tariff

The district heating rate profiles are derived from the DSO's published 2025 annual tariff schedules. Rather than back-calculating rates from historical invoices, the approach applies published energy rates that vary seasonally throughout the year.

The district heating tariff distinguishes between two seasonal periods:

- **Summer (June–August):** A flat, single energy rate applies uniformly to all heat consumption.
- **Non-summer (September–May):** A two-tier rate structure applies, where consumption up to the subscribed base capacity threshold (P_{base}) is billed at the lower base rate, and consumption above this threshold is billed at the higher peak rate.

Additionally, three fixed daily capacity charges are applied year-round, derived from the DSO's published tariff terms.

The published energy rates and fixed daily charges are assembled into a time-series profile at 15-minute resolution. This profile captures the seasonal variation in rates and provides the optimizer with accurate pricing information for each time-step without making assumptions about demand patterns or back-calculating implicit rates. This approach avoids inferring rates from historical invoices, which may be affected by billing anomalies, and directly reflects the published tariff schedule.

Temporal Alignment and Multi-Year Profile Extension

Following individual preprocessing, all datasets were aligned to a common UTC-based 15-minute time index covering the full 2023–2025 period, ensuring consistency across all model inputs.

All input profiles were extended to cover three years of simulation (2023–2026) using two complementary approaches. Profiles based on measured or market data (electricity demand, heat demand, electricity spot prices, and outdoor temperature) were created by horizontally concatenating individual year files into continuous time-series, preserving year-to-year variations in observed conditions. DH rates and solar generation profiles were extended by temporal cycling: a year (2025 for the first and 2023 for the latter) was repeated cyclically across the full three-year horizon.

The repeating approach maintains consistent tariff and generation assumptions across the simulation period and accounts for the unavailability of multi-year tariff histories, while the concatenation approach preserves actual inter-annual variability in market prices, demand, and weather.

A.4 Component Modelling & Sizing

Each asset in the LEC is characterised by a physical sub-model and a fixed set of sizing parameters. All component models are pre-parametrised before each daily solve and enter the MILP as fixed-coefficient linear expressions, therefore no endogenous capacity decisions are made within the optimiser. The mathematical representation of each component (i.e. state-of-charge dynamics, power-limit constraints, and cost contributions) is fully stated in the MILP formulation (Section 3.1). This section focuses on the physical basis and the methodology used to determine the upper bounds of component capacities.

A.4.1 Solar Photovoltaic

This section describes how the solar PV generation profile is constructed and how peak capacity is assigned to each scenario.

Generation Profile

The output of the rooftop PV installation at building b is computed as a parameter profile $G_{b,t}$ [kW] before each simulation run by scaling a pre-computed normalised generation profile by the installed peak capacity:

$$G_{b,t} = P_b^{\mathrm{pv}} \cdot \tilde{g}_t \tag{A.1}$$

where $\tilde{g}_t$ [kW/kWp] is the normalised AC output of a 1 kWp reference system, sourced from PVGIS, and P_b^{pv} [kWp] is the installed peak capacity of building b. The normalised profile is pre-processed to the 15-minute model resolution before the simulation.

The installed peak capacity is derived from the physical installation parameters:

$$P_b^{\mathrm{pv}} = \eta_{\mathrm{PV}} \cdot A_b \cdot g_{\mathrm{STC}} \quad \text{[kWp]} \tag{A.2}$$

where η_{PV} is the panel conversion efficiency, A_b is the effective area [m^2], and $g_{\mathrm{STC}} = 1$ kW/m^2 is the standard test condition irradiance. This capacity governs both the generation scaling and the applicability of the Swedish solar production tax, as defined in Section 3.1.6 of the MILP formulation.

Sizing Across Scenarios

PV capacity is treated as a scenario parameter, reflecting investment decisions made prior to the operational horizon. Installed areas range from 0 to 5,000 m^2 across the scenario matrix (Section 3.5), corresponding to peak capacities of 0–1,000 kWp. The 500 kWp threshold is explicitly represented to isolate the step-change in solar production tax liability. The key sizing parameters used across all scenarios are listed in Table A.5.

Table A.5: Solar PV sizing parameters.

Symbol	Value	Description
η_{PV}	0.20	Panel conversion efficiency
g_{STC}	1.0 kW/m^2	Standard Test Condition irradiance
A_b	0–5,000 m^2	Installed aperture area (scenario-dependent)
P_b^{pv}	0–1,000 kWp	Corresponding peak capacity range

A.4.2 Battery Energy Storage System

This section presents the physical model adopted for the lithium-ion battery energy storage system, derives the cycling cost coefficient that enters the objective function, and describes the load-duration curve analysis used to determine the installed capacity.

Physical Description

The BESS is modelled with symmetric round-trip efficiency. The SoC dynamics, mutual-exclusion constraint on simultaneous charge and discharge, minimum SoC floor, and the cycling cost contribution to the objective function are stated in Section 3.1.6 of the MILP formulation.

Degradation Cost Coefficient

The cycling cost coefficient c_{cyc} [SEK/kWh discharged/kWh capacity] is derived from the battery's techno-economic specification by spreading the total capital cost evenly over the rated energy throughput, instead of using an exact half-cycle depth-of-discharge (DoD) scheme [80]:

$$c_{\text{cyc}} = \frac{\text{CAPEX}}{N \cdot \text{DoD}_{\text{rated}}} \cdot r_{\text{EUR}\to\text{SEK}} \quad \text{[SEK/kWh discharged/kWh capacity]} \tag{A.3}$$

where CAPEX [EUR/kWh] is the specific capital cost, N is the manufacturer-rated cycle life at the design depth-of-discharge, and $\text{DoD}_{\text{rated}} = 1 - \sigma^{\text{min}}$ is the permissible depth of discharge. This formulation ensures that the optimiser implicitly internalises battery ageing: a discharge event is only economically justified when the resulting electricity cost saving exceeds the marginal degradation charge. The parameter values used to compute c_{cyc} are given in Table A.6.

Sizing Methodology

BESS capacity is sized using a load-duration curve (LDC) exceedance analysis applied to the main building's electricity load profiles for 2023–2025 at 1h resolution (unprocessed data). A peak-shaving threshold of $P_{\text{thr}} = 600$ kW ($\sim 200\,\text{h}$) is selected as the target limit. For each continuous period during which the building load exceeds the threshold, two sizing quantities are derived:

Table A.6: BESS degradation cost parameters.

Symbol	Value	Description
CAPEX	250 EUR/kWh	Specific capital cost
N	6,000	Rated cycle life at $\mathrm{DoD}_{\mathrm{rated}}$
$\mathrm{DoD}_{\mathrm{rated}}$	0.80	Maximum permissible depth of discharge
$r_{\mathrm{EUR}\rightarrow\mathrm{SEK}}$	11.1	EUR–SEK conversion rate

$$P^{\mathrm{bess,req}} = \max_{t\in\mathrm{event}} \Big(L_{b,t} - P_{\mathrm{thr}} \Big) \tag{A.4}$$

$$E^{\mathrm{bess,req}} = \sum_{t\in\mathrm{event}} \Big(L_{b,t} - P_{\mathrm{thr}} \Big) \cdot \Delta t \tag{A.5}$$

These represent, respectively, the instantaneous power headroom and the energy buffer required to suppress that exceedance event entirely. The two metrics are evaluated across all events identified in the three-year dataset, and the 95th-percentile values are selected as the upper bound. This approach avoids over-dimensioning for isolated worst-case events, with the residual 5% of extreme peaks managed by accepting a temporary exceedance or relying on V2G discharge. The resulting sizing specification is approximately 220 kW / 750 kWh. The nearest commercially available system [72] is adopted as the upper bound in the scenario matrix; lower tiers (514 kWh / 125 kW) represent partial storage coverage. The scenario matrix (Section 3.5) then independently varies both the energy capacity and the rated power according to commercially available systems (Appendix A.2.4) to assess the marginal value of additional storage across all combinations.

A.4.3 Ground Source Heat Pump

This section describes the three-step pre-processing procedure used to compute the GSHP electrical intensity parameter $\alpha_{b,t}$ from outdoor temperature data, and the heat demand analysis used to determine the installed thermal capacity.

Physical Description

The GSHP extracts low-grade heat from a vertical borehole field and upgrades it via a vapour-compression cycle to meet the building's space-heating demand. All COP-related calculations are performed as a pre-processing step before the optimisation; the results enter the MILP as fixed, time-varying parameters, preserving its linear structure [81, 82].

Step 1: Supply temperature (heating curve). The required supply temperature is set by a linear heating curve that raises the set-point as outdoor temperature falls [83–85]:

$$T_t^{\mathrm{sup}} = T_{\mathrm{set}} - k_{\mathrm{hc}} \cdot T_t^{\mathrm{out}} \quad [\mathrm{K}] \tag{A.6}$$

where T_{set} [K] is the design supply temperature at $T^{\mathrm{out}} = 0\,\mathrm{K}$ and k_{hc} [K/K] is the heating curve slope. The outdoor temperature time series T_t^{out} is taken from the processed 15-minute temperature dataset.

Step 2: Time-varying COP (Carnot model). A Carnot-based COP is computed at each time step using the supply temperature and a fixed ground temperature as the source and sink, respectively [82, 86]:

$$\mathrm{COP}_t = \eta_{\mathrm{Carnot}} \cdot \frac{T_t^{\mathrm{sup}}}{T_t^{\mathrm{sup}} - T_{\mathrm{ground}}} \tag{A.7}$$

where η_{Carnot} [-] is the Carnot efficiency factor accounting for real-cycle irreversibilities. The result is clipped to $\mathrm{COP}_t \geq 1$ as a physical lower bound.

Step 3: Electrical intensity parameter. The ratio of electrical input to thermal output, including auxiliary consumption (circulation pumps, controls), is:

$$\alpha_{b,t} = \frac{f_{\mathrm{aux}}}{\mathrm{COP}_t} \quad [\mathrm{kW_{el}/kW_{th}}] \tag{A.8}$$

where $f_{\mathrm{aux}} \geq 1$ scales up the electrical draw to account for auxiliary loads [87]. The full time series $\alpha_{b,t}$ is passed to the MILP as a fixed parameter, so that the GSHP electricity consumption $P_{b,t}^{\mathrm{gshp}} = \alpha_{b,t} \cdot Q_{b,t}^{\mathrm{gshp}}$ remains a linear expression in the thermal output variable.

The GSHP and district heating operate as complementary heat sources: their combined output must satisfy the building thermal demand at every time step (MILP formulation, Section 3.1). The optimiser dispatches the cheaper source at each time step, where the GSHP marginal cost is $\alpha_{b,t} \cdot \lambda_{b,t}$ and the district heating marginal cost is given by the applicable tariff tier.

Table A.7: GSHP pre-processing parameters.

Symbol	**Value**	**Description**
T_{set}	55 °C	Supply temperature at $T^{\mathrm{out}} = 0\,°\mathrm{C}$
k_{hc}	1.0	Heating curve slope
T_{ground}	8 °C	Ground/borehole source temperature
η_{Carnot}	0.50	Carnot efficiency factor
f_{aux}	1.10	Auxiliary consumption factor

Sizing Methodology

The GSHP thermal capacity $Q_b^{\text{gshp,max}}$ is derived from the heat demand load duration curve of the main building, using heat load profiles for 2023–2025 at hourly resolution. The upper bound is the 95th percentile of the heat load curve across all non-zero operating hours in the three-year dataset:

$$Q_b^{\text{gshp,max}} = Q_{p95}^{\text{th}} \tag{A.9}$$

This choice ensures that the GSHP covers approximately 95% of operating hours autonomously; the comparatively few high-demand hours above $Q_b^{\text{gshp,max}}$ are supplied by the district heating top-up. Sizing to the full peak demand would require a significantly larger and more costly heat pump for only marginal incremental coverage, which is unlikely to be economically justified given the relatively low per-unit cost of district heating at peak conditions.

The analysis yields a reference thermal capacity of 700 kW ($\sim$ 200 h). To assess the results as a function of heat pump sizing, the scenario matrix (Section 3.5) also includes lower capacity variants, representing partial GSHP coverage relative to the heat demand distribution.

A.4.4 Electric Vehicles

This section characterises the EV charging infrastructure, covering the three charging control modes available in the scenario matrix, the stochastic session generation model used to produce synthetic charging data, and the vehicle fleet specifications.

Charging Modes

Three EV charging control modes are examined in the scenario matrix (Section 3.5). The mode parameter m^{ev} is set at the scenario level and applies uniformly to all charging points; the three modes are defined in Section 2.2.2.

The battery dynamics, power-limit mutual-exclusion constraint, minimum SoC floor, and departure SoC requirement for all three modes are stated in MILP formulation Section 3.1.7.1.

Session Generation Model

Real EV session data for the study period were not available; charging sessions are therefore generated stochastically using a purpose-built data generator calibrated to represent retail parking behaviour at the store site. In this study, 50 sessions per month and charging point have been generated, amounting to 1,800 sessions per CP over the simulation period. All sessions are constrained to occur within store operating hours (Monday–Friday 10:00–20:00 $\pm$ 30 min buffer; Saturday–Sunday 10:00–18:00 $\pm$ 30 min buffer) and must begin and end on the same calendar day, reflecting the short-stay nature of customer parking. Session durations are drawn from a truncated normal distribution:

$$d \sim \mathcal{N}(\mu_d,\, \sigma_d^2), \quad d \in [d_{\min},\, d_{\max}] \tag{A.10}$$

with $\mu_d = 3.0$ h, $\sigma_d = 0.8$ h, $d_{\min} = 0.5$ h, $d_{\max} = 5.5$ h. Arrival SoC values are drawn uniformly from $[\sigma^{\min},\, 1.0]$; desired departure SoC is drawn uniformly from $[\sigma^{\mathrm{arr}}_{c,e},\, 1.0]$. Each generated session is checked for power feasibility: if the energy needed to reach the desired departure SoC cannot be delivered at the rated power $P^{\mathrm{ev,max}}$ within the available parking window, the desired departure SoC is reduced to the maximum value achievable at $P^{\mathrm{ev,max}}$, ensuring all sessions in the dataset are feasible by construction.

Vehicle Specifications

A homogeneous fleet is assumed, representative of mid-range battery electric vehicles equipped with standard AC on-board chargers. The specifications are summarised in Table A.8; the corresponding parameter definitions used within the optimization are given in Section 3.1.4.3 of the MILP formulation.

Table A.8: EV fleet specifications.

Parameter	Value	Description
$E^{\mathrm{ev}}_{c,e}$	60 kWh	Usable battery capacity
$P^{\mathrm{ev,max}}_{c,e}$	11 kW	Maximum charging/discharging power
η	0.93	One-way charging efficiency
$\sigma^{\min}$	0.20	Minimum SoC (battery health floor)
μ_d	3.0 h	Mean session duration

B

Complete Scenario and Sensitivity Analysis Results

B.1 Scenarios

This appendix presents the complete numerical results for all scenarios analysed in this thesis, as well as the sensitivity analysis. The scenarios are organised by development phase, following the same structure as Chapter 4. Each table consolidates scenario characteristics, system operation and performance metrics, operation costs, and investment economics to facilitate cross-scenario comparison.

B.1.1 Baseline Scenarios

Table B.1 presents the operational cost breakdown for the baseline scenarios S-01 and S-01a, which represent the main store and LEC operating without any on-site energy assets. These scenarios serve as the reference case against which all subsequent scenarios are evaluated, as discussed in Section 4.1. All absolute cost figures, Nätnytta income, and electricity imports are reported for the full three-year simulation period unless otherwise stated.

Table B.1: Baseline scenarios results summary

	Units	**S-01**	**S-01a**
System Operation & Performance			
Electricity Imports	GWh	8.3	27.8
Operation Costs			
Electricity Cost	MSEK	10.0	32.6
DH Cost	MSEK	5.8	5.8
Total Cost	MSEK	15.8	38.4

B.1.2 Phase 1: Solar only Scenarios

Table B.2 summarises results for scenarios S-02 to S-06, which evaluate the installation of rooftop PV systems ranging from 400 kWp to 1,600 kWp with no additional flexibility assets. A detailed discussion of these results is provided in Section 4.2.

Table B.2: Solar only results summary

	Units	S-02	S-03	S-04	S-05	S-06
Scenario Characteristics						
PV Capacity	kWp	400	500	800	1,200	1,600
System Operation & Performance						
SC	%	100	100	89	72	60
SS	%	14	18	25	31	34
Electricity Imports	%	-14	-17	-25	-31	-34
Operation Costs						
Nätnytta Income	kSEK	0.2	0.9	10.6	38.6	73.9
Electricity Cost	MSEK	9.0	8.8	9.0	8.5	8.0
Total Cost	MSEK	14.8	14.5	14.8	14.3	13.7
Investment Economics						
CAPEX	MSEK	3.2	4.0	6.4	9.6	12.8
O&M	kSEK/yr	64	80	128	192	256
Annual Savings	MSEK/yr	0.35	0.43	0.35	0.53	0.70
Net Benefit	MSEK	0.28	0.35	0.22	0.33	0.44
NPV	MSEK	1.12	1.37	-2.98	-4.47	-5.96
PBP	yr	11.4	11.5	28.8	28.8	28.8

B.1.3 Phase 2: Solar with Battery Storage Scenarios

Table B.3 presents results for scenarios S-07 to S-15, which pair rooftop PV with a battery energy storage system (BESS). All BESS units share the same power rating of 125 kW; capacity and PV size are varied to assess their combined effect on self-sufficiency, cost reduction, and investment viability. A full analysis is presented in Section 4.3.

Table B.3: Solar and BESS results summary

	Units	**S-07**	**S-08**	**S-09**	**S-10**	**S-11**	**S-12**	**S-13**	**S-14**	**S-15**
Scenario Characteristics										
PV Capacity	kWp	400	500	500	800	800	1,200	1,200	1,600	1,600
BESS Capacity	kWh	257	257	514	257	514	514	771	514	771
System Operation & Performance										
SC	%	100	100	100	87	86	72	72	60	60
SS	%	14	18	18	24	24	30	30	34	34
Electricity Imports	%	-14	-17	-17	-24	-23	-29	-29	-33	-33
BESS Cycles	-	1,258	1,261	1,100	1,264	1,136	1,137	980	1,136	980
Operation Costs										
Nätnytta Income	kSEK	0.1	0.4	0.5	12.1	13.1	39.7	39.8	74.4	74.5
Electricity Cost	MSEK	8.9	8.6	8.6	8.9	8.8	8.3	8.2	7.7	7.7
Total Cost	MSEK	14.7	14.4	14.3	14.6	14.5	14.0	14.0	13.5	13.4
Investment Economics										
CAPEX	MSEK	3.9	4.7	5.4	7.1	7.8	11.0	11.7	14.2	14.9
O&M	kSEK/yr	78.3	94.3	108.5	142.3	156.5	220.5	234.8	284.5	298.8
Annual Savings	MSEK/yr	0.39	0.48	0.51	0.40	0.43	0.60	0.62	0.78	0.80
Net Benefit	MSEK	0.31	0.38	0.40	0.25	0.27	0.38	0.39	0.49	0.50
NPV	MSEK	0.55	0.80	0.00	-3.56	-4.34	-5.83	-6.78	-7.32	-8.27
PBP	yr	12.5	12.4	13.7	28.1	28.8	28.8	30.1	28.8	29.8

B.1.4 Phase 3: GSHP Integration Scenarios

Table B.4 summarises results for scenarios S-16 to S-19, which integrate a GSHP into the base system consisting of a fixed 500 kWp PV array, and a 257 kWh/125 kW BESS. The BESS cycles at approximately 1,262 per year across all four scenarios and is therefore not reported per-column. Only GSHP capacity varies, ranging from 100 kW to 700 kW, with the objective of partially displacing district heating demand. Since CO_2 emissions savings are directly proportional to district heating displacement in this system, both metrics are numerically equivalent and only DH Displacement is reported. Results are discussed in Section 4.4.

Table B.4: GSHP integration results summary

	Units	**S-16**	**S-17**	**S-18**	**S-19**
Scenario Characteristics					
GSHP Capacity	kW	100	300	500	700
System Operation & Performance					
SC	%	100	100	100	100
SS	%	18	18	18	18
Electricity Imports	%	-11	-5	-2	-1
BESS Cycles	-	1,262	1,262	1,262	1,262
DH Displacement	%	27	55	67	71
CO_2 Avoided	%	27	55	67	71
Operation Costs					
Electricity Cost	MSEK	9.1	9.6	9.8	9.9
DH Cost	MSEK	4.9	4.1	3.8	3.7
Total Cost	MSEK	14.0	13.7	13.6	13.6
Investment Economics					
CAPEX	MSEK	5.2	5.6	5.9	6.2
O&M	kSEK/yr	103.4	112.1	118.6	124.2
Annual Savings	MSEK/yr	0.60	0.70	0.74	0.74
Net Benefit	MSEK	0.50	0.59	0.62	0.62
NPV	MSEK	2.14	3.13	3.22	2.98
PBP	yr	10.4	9.5	9.6	10.0

B.1.5 Phase 4: LEC Integration Scenarios

Table B.5 presents results for scenarios S-20 to S-24, which explore LEC configurations built on the Phase 3 base system. The GSHP is fixed at 500 kW across all LEC scenarios; PV capacity, BESS size, and BESS power rating are varied to assess the impact of increased flexibility on community-level performance and economics. A detailed discussion is provided in Section 4.6.

Table B.5: LEC integration results summary

	Units	**S-20**	**S-21**	**S-22**	**S-23**	**S-24**
Scenario Characteristics						
PV Capacity	kWp	500	700	1,000	700	1,000
BESS Capacity	kWh	257	514	514	771	771
BESS Power	kW	125	125	257	125	257
System Operation & Performance						
SC	%	100	100	100	100	100
SS	%	5	7	10	7	10
Electricity Imports	%	-1	-3	-6	-3	-6
BESS Cycles	-	1,249	1,127	1,127	973	1,213
DH Displacement	%	66	67	67	67	67
CO_2 Avoided	%	66	67	67	67	67
Operation Costs						
Electricity Cost	MSEK	32.4	31.8	31.0	31.7	30.8
Total Cost	MSEK	36.2	35.6	34.8	35.5	34.7
Investment Economics						
CAPEX	MSEK	5.9	8.2	10.6	9.0	11.4
O&M	kSEK/yr	118.6	164.9	212.9	179.1	227.1
Annual Savings	MSEK/yr	0.74	0.94	1.22	0.96	1.25
Net Benefit	MSEK	0.62	0.78	1.00	0.79	1.03
NPV	MSEK	3.25	3.04	4.10	2.09	3.38
PBP	yr	9.6	10.6	10.6	11.4	11.1

B.1.6 Phase 5: EV Integration Pathways

Table B.6 presents results for scenarios S-25 to S-33, which evaluate three EV charging strategies (DC, V1G, and V2G), at 5, 15, and 30 charging points. All scenarios share the same underlying energy system, which is the outcome from Phase 4: a 1,000 kWp PV array, a 771 kWh/257 kW BESS, and a 500 kW GSHP. The impact of charging mode and scale on grid interaction, and costs is discussed in Section 4.7.

Table B.6: EV integration pathways results summary

	Units	S-25	S-26	S-27	S-28	S-29	S-30	S-31	S-32	S-33
Scenario Characteristics										
EV Charging Mode	-	DC	DC	DC	V1G	V1G	V1G	V2G	V2G	V2G
Charging Points	-	5	15	30	5	15	30	5	15	30
System Operation & Performance										
SC	%	100	100	100	100	100	100	100	100	100
SS	%	10	10	10	10	10	10	10	10	10
Electricity Imports	%	-5	-4	-2	-5	-4	-3	-5	-4	-3
BESS Cycles	-	1,017	676	429	1,213	1,213	1,212	1,213	1,214	1,215
DH Displacement	%	65	62	60	67	67	67	67	67	67
CO_2 Avoided	%	65	62	60	67	67	67	67	67	67
Operation Costs										
Electricity Cost	MSEK	30.9	31.2	31.5	30.9	31.0	31.2	30.9	30.9	30.9
EV Charging Cost	kSEK	106	317	630	60	180	360	60	180	361
DH Cost	MSEK	3.8	4.0	4.0	3.8	3.8	3.8	3.8	3.8	3.8
Total Cost	MSEK	34.8	35.1	35.5	34.7	34.8	35.0	34.7	34.7	34.7
Investment Economics										
Annual Savings	MSEK/yr	1.21	1.10	0.96	1.24	1.20	1.15	1.25	1.24	1.23
Net Benefit	MSEK	0.98	0.87	0.74	1.01	0.97	0.92	1.02	1.01	1.00
NPV	MSEK	2.71	1.06	-1.06	3.11	2.59	1.78	3.32	3.21	3.01
PBP	yr	11.6	13.0	15.4	11.3	11.7	12.3	11.1	11.2	11.3

B.2 Sensitivity Analysis

This section presents the complete numerical results for the two sensitivity analysis groups conducted in this thesis. SAG1 evaluates parameter sensitivity on the full store operation reference scenario S-18, while SAG2 evaluates the same on the full LEC with V2G reference scenario S-31. Results are displayed in Section 4.5 and Section 4.8 respectively.

B.2.1 SAG1: S-18

Table B.7 reports the relative change in total cost, electricity imports, and BESS discharge for SA-1, SA-2, SA-2a, SA-3, and SA-4 across the full multiplier range, with S-18 as the reference. SA-4 exhibited non-linear, thus additional absolute values are reported in Table B.8. A full discussion is provided in Chapter 5.

Table B.7: SAG1 sensitivity results (%)

Metric	SA	0.6	0.7	0.8	0.9	1.0	1.1	1.2	1.3	1.4
Total Cost	SA-1	-1.28	-0.96	-0.64	-0.32	0.00	0.32	0.64	0.96	1.28
	SA-2	-13.54	-10.04	-6.62	-3.28	0.00	3.24	6.44	9.60	12.74
	SA-2a	-1.25	-0.90	-0.58	-0.28	0.00	0.27	0.54	0.79	1.04
	SA-3	0.00	0.00	0.00	0.00	0.00	0.00	0.00	0.00	0.00
	SA-4	3.72	2.78	1.82	0.89	0.00	-0.82	-1.59	-2.31	-2.97
Electricity Imports	SA-1	0.16	0.11	0.08	0.04	0.00	-0.04	-0.08	-0.13	-0.16
	SA-2	4.12	3.10	1.92	0.86	0.00	-0.74	-1.51	-2.25	-2.90
	SA-2a	1.70	1.15	0.66	0.30	0.00	-0.25	-0.46	-0.67	-0.88
	SA-3	0.00	0.00	0.00	0.00	0.00	0.00	0.00	0.00	0.00
	SA-4	-3.34	-1.48	-0.42	0.06	0.00	-0.22	-0.44	-0.85	-1.38
BESS Discharge	SA-1	0.87	0.61	0.45	0.16	0.00	-0.23	-0.38	-0.52	-0.74
	SA-2	-11.92	-7.94	-5.02	-2.26	0.00	2.34	4.41	6.27	7.44
	SA-2a	-21.71	-14.99	-9.39	-4.65	0.00	4.99	9.06	13.09	17.78
	SA-3	0.19	0.16	0.10	0.06	0.00	-0.07	-0.16	-0.24	-0.29
	SA-4	-0.33	-0.35	-0.13	-0.04	0.00	0.03	0.14	0.16	0.24

Table B.8 reports the absolute system response to variations in GSHP COP. The diagnostic columns reveal the underlying mechanism: at low COP multipliers the system substitutes heat supply back towards district heating, reducing GSHP utilisation and producing a non-monotonic cost response. This behaviour is discussed in Chapter 5.

Table B.8: SA-4 GSHP COP sensitivity

Metric	**Unit**	**0.6**	**0.7**	**0.8**	**0.9**	**1.0**	**1.1**	**1.2**	**1.3**	**1.4**
Electricity Imports	MWh	7,844	7,995	8,081	8,120	8,115	8,098	8,079	8,046	8,003
Total Cost	SEK	4.71	4.67	4.62	4.58	4.54	4.50	4.47	4.44	4.41
$P_{\text{el,GSHP}}$	kWh	3,830	4,432	4,777	4,934	4,913	4,844	4,770	4,638	4,466
Q_{GSHP}	kWh	8,176	11,009	13,600	15,780	17,416	18,824	20,128	21,105	21,827
Q_{DH}	kWh	17,949	15,115	12,524	10,344	8,708	7,300	5,997	5,019	4,297
GSHP Ratio	%	31	42	52	60	67	72	77	81	84

B.2.2 SAG2: S-31

Table B.9 reports the relative change in total cost, electricity imports, and BESS discharge for SA-1, SA-2, and SA-2a across the full multiplier range, with S-31 as the reference. The CP power rating analysis is reported separately in Table B.10 as it uses discrete values rather than a continuous multiplier. A full discussion is provided in Chapter 5.

Table B.9: SAG2 sensitivity results (%)

Metric	**SA**	**0.6**	**0.7**	**0.8**	**0.9**	**1.0**	**1.1**	**1.2**	**1.3**	**1.4**
Total Cost	SA-1	-1.48	-1.11	-0.74	-037	0.00	0.37	0.74	1.11	1.48
	SA-2	-16.21	-12.11	-8.05	-4.01	0.00	3.99	7.98	11.94	15.89
	SA-2a	-0.94	-0.69	-0.45	-0.22	0.00	0.22	0.43	0.64	0.84
Electricity Imports	SA-1	0.05	0.04	0.02	0.01	0.00	-0.01	-0.02	-0.04	-0.05
	SA-2	1.24	0.93	0.58	0.26	0.00	-0.22	-0.46	-0.68	-0.88
	SA-2a	0.46	0.31	0.18	0.08	0.00	-0.07	-0.12	-0.18	-0.23
BESS Discharge	SA-1	0.81	0.63	0.47	0.21	0.00	-0.18	-0.31	-0.62	-0.76
	SA-2	-11.6	-7.97	-5.04	-2.24	00.0	2.27	4.20	5.80	7.21
	SA-2a	-21.93	-15.13	-9.22	-4.58	0.00	4.64	8.97	13.43	17.32

Table B.10 reports the relative system response to variations in CP power rating for S-31. A power rating of 11 kW serving as the reference value consistent with Section 3.6.

Table B.10: SAG2-3 CP power rating sensitivity (%)

Metric	**7.4 kW**	**11 kW**	**22 kW**	**50 kW**
Total Cost	0.03	0.00	-0.16	-0.60
Electricity Imports	-0.07	0.00	0.10	0.24
Bess Discharge	0.00	0.00	0.09	0.17

C

ISO Country Codes Used in Table 1.1

The following ISO 3166-1 alpha-2 country codes appear in Table 1.1, listed in alphabetical order:

AT	Austria
CH	Switzerland
DK	Denmark
ES	Spain
FR	France
IE	Ireland
IR	Iran
IT	Italy
NO	Norway
PT	Portugal
SE	Sweden

DEPARTMENT OF ELECTRICAL ENGINEERING
CHALMERS UNIVERSITY OF TECHNOLOGY
Gothenburg, Sweden
www.chalmers.se

CHALMERS
UNIVERSITY OF TECHNOLOGY